UNIVERSITY OF CALIFORNIA

Los Angeles

Optimal Integration of Battery Energy Storage and Transportation Electrification in Distribution Grids

A dissertation submitted in partial satisfaction
of the requirements for the degree
Doctor of Philosophy in Mechanical Engineering

by

Behnam Khaki

2019

ABSTRACT OF THE DISSERTATION

Optimal Integration of Battery Energy Storage and Transportation Electrification in Distribution Grids

by

Behnam Khaki
Doctor of Philosophy in Mechanical Engineering
University of California, Los Angeles, 2019
Professor Rajit Gadh, Chair

Two pioneer states, California and New York, have set their ambitious targets to get 100% and 70% of their electricity from renewable energy resources by 2045 and 2030, respectively. Aligned with these endeavors, currently 19.2% of the electricity in California is coming from the solar energy where the utilities are expected to add an additional 60% solar energy in the next five years. To achieve this goal, *Electrification*- the transition from non-electric end-use energy consumers to the electric consumers is a trend in the energy sector, as it facilitates to have access to sustainable and clean energy infrastructure. The fact that 28% of the energy in the USA is consumed by the transportation sector where 92% is provided by the fossil fuel energy motivates *Electrification* strongly. This revolution is specifically happening in the California state where 50% of the electric vehicle (EV) owners are living.

The increasing penetration of renewable energies, such as solar energy, as well as *Electrification* in the electrical grids introduce new challenges for system operation and planning. Solar energy, inherently, is intermittent and shows stochastic behavior which makes it a non-dispatchable source of electricity. Therefore, the conventional models to capture its generation profile are no longer applicable. Also according to a new report by National Renewable Energy Laboratory (NREL) [MJL18], EVs are introduced as one of the most influential elements of *Electrification*. EVs can drastically change the load pattern, thus their integration in the power grids is carefully observed by the electric utilities.

To mitigate the stochastic behavior of solar energy and make it a dispatchable resource, the energy storage can be utilized to capture its intermittency through the coordinated charging and discharging sequences. That is one reason why the California and New York states plan to integrate an additional 1.3 GW and 3.0 GW energy storage in their power grids by 2024 and 2030, respectively. Moreover, EVs are controllable loads that provide the flexibility and opportunity to shift their consumption profile according to the operating conditions of the power grids. Nevertheless, the deployment of energy storage is challenging as the generation profile of the solar energy should be modeled accurately, and an effective and optimal controller should be designed to coordinate the charging and discharging of the energy storage. Also designing an efficient charging load management system for EVs is a difficult task since all the involved entities in the load management decision making, such as the system operator, load aggregators, and the end customers, must be satisfied, and the safe and stable operation of the grid should be guaranteed. Accordingly, the optimal load management is a large scale problem, especially when it should be solved and repeated every several minutes for the whole power grid.

The models proposed in the literature for the solar energy generation, load, and EV charging demand modeling either can not capture their stochasticity accurately or are not computationally efficient. Therefore, the coordination methods for energy storage as well as EV loads are not effective in accommodating renewable energies and *Electrification* in the power grids. In addition, the energy storage and load coordination methods are not scalable and suffer from a considerable computation burden when the number of energy resource units and controllable loads in the optimal decision-making increases.

In this dissertation, (1) modeling of the solar generation, load demand, and EV charging load, (2) the integration of battery energy storage system (BESS) in the power grids, and (3) the large scale accommodation of EV loads are addressed. For the modeling, a probability model based on kernel density estimator (KDE) is proposed which, comparing to the previous models, provides a low-computation precise stochastic model. For the integration of BESS in the electrical grids, a mobile BESS (MBESS) is prototyped to capture the random behavior of the EV charging profile, reduce the charging demand cost and improve the

reliability and resiliency of the charging service. The performance of MBESS is validated through the experiments in the Civic Center parking structure, in the City of Santa Monica, and it is shown that MBESS can effectively shave the peak load of the EV charging demand. To address the lack of scalability in the previous load management methods, the distributed optimization methods are used so that the optimal EV load coordination is solved through an iterative negotiation procedure. The scalability of the proposed methods is coming from the fact that each agent solves its desired problem locally while it exchanges the insensitive limited information with the others. The proposed methods satisfy all the agents and guarantee the power grid operation in the stability and safe region.

The proposed probability model is shown to improve the accuracy of the solar energy profile up to 36.7%, the load demand profile up to 5.9%, and the EV charging parameters, including the arrival time, required charging energy, and the departure time up to 26.6%, 49.3%, and 41.21%, respectively. In addition, the experiments with MBESS verifies that it not only reduces the charging cost but also provides the emergency power to the charging system in the case of failure in the power grid, which is called islanded operation. Moreover, through the numerical simulations using real data, it is validated that the distributed multi-agent based methods for the load coordination can approximately decrease the convergence time and the communication overhead by 94% while the computation burden for the distribution system operator and the load aggregators reduces significantly. Also the load coordination results validate the efficacy of the proposed frameworks in accommodating the large populations of EV loads in the distribution grids by improving the voltage profile from 45% up to 93% and reducing the peak load from 50% up to 66%. The results show that an efficient load management system is a necessity for *Electrification* integration without any investment on the grid capacity expansion.

The dissertation of Behnam Khaki is approved.

Robert M'Closkey

Xiaochun Li

Deepak Rajagopal

Rajit Gadh, Committee Chair

University of California, Los Angeles

2019

To my parents, Mohammad Reza and Susan,

and my grandmother, Talat.

TABLE OF CONTENTS

LIST OF FIGURES

LIST OF TABLES

ACKNOWLEDGMENTS

First, I would like to express my gratitude to Prof. Rajit Gadh for involving me in various research projects throughout my years spent in the Smart Grid Energy Research Center (SMERC) at UCLA, where I have had the unique opportunity to improve my soft and technical skills, conduct independent research, and build my future direction.

I would like to thank Prof. Robert M'Closkey, Prof. Xiaochun Li, and Prof. Deepak Rajagopal for having served on my committee.

I would also like to express my deepest appreciation to Prof. Robert S. Shaefer who was by my side during all these years for academic and personal support. His support has been tremendous, and I am so grateful for every moment I spent with him. I have learned from him quality work, discipline, generosity, humbleness, and most importantly how to be a better person.

I would like to thank Dr. Peter Chu for his help in designing and prototyping the battery energy storage which is presented in Chapter 4 of this dissertation. I am also grateful for my lab-mates in SMERC for providing a friendly and collaborative research environment: Dr. ChingYen Chung, Dr. Bin Wang, Dr. Yubo Wang, Dr. Hamidreza Nazaripouya, Dr. Tianyang Zhang, Dr. Yingqi Xiong, Zhiyuan Cao, Shashank Gowda,and specifically Yu-Wei Chung with whom I have done lots of fruitful collaboration and research.

I want to thank my dearest friends, Dr. Mehrdad Shahabi, Mehdi Shahbazi, and Wadie Chalgham who have been always by my side, and whom I had the most memorable moments with. Last but not least, my appreciation goes especially to my parents, Mohammad Reza and Susan, my grandmother, Talat, my sisters, Bahareh and Mansoureh, my brother, Mahziyar, my uncles and aunt, and Shayesteh, for their consistent and priceless support, guidance, and love.

This work has been sponsored in part by grants from the California Energy Commission (CEC) entitled "Demonstrating Plug-in Electric Vehicles Smart Charging and Storage Supporting the Grid", award number EPC-14-056, the University of California Office of the

President (UCOP) initiative S-00098, and the American Power Power Association through the Demonstration of Energy & Efficiency Development (DEED) scholarship, student research grant number CS-2186.

Chapter 3 is a version of Khaki, Behnam,Yu-Wei Chung, Chicheng Chu, and Rajit Gadh. "Nonparametric user behavior prediction for distributed ev charging scheduling." 2018 IEEE Power & Energy Society General Meeting (PESGM). IEEE, 2018.

Chapter 4 is a version of Khaki, Behnam,Yu-Wei Chung, Chicheng Chu, and Rajit Gadh. "Stochastic EV and Battery Storage Control for Charging stations." in preparation.

Chapter 5 is a version of Khaki, Behnam, Chicheng Chu, and Rajit Gadh. "A hierarchical admm based framework for ev charging scheduling." 2018 IEEE/PES Transmission and Distribution Conference and Exposition (T&D). IEEE, 2018.

Chapter 6 is a version of Khaki, Behnam, Chicheng Chu, and Rajit Gadh. "Hierarchical distributed framework for EV charging scheduling using exchange problem." Applied energy 241 (2019): 461-471.

Chapter 7 is a version of Khaki, Behnam, Yu-Wei Chung, Chicheng Chu, and Rajit Gadh. "Probabilistic Electric Vehicle Load Management in Distribution Grids." 2019 IEEE Transportation Electrification Conference and Exp, Novi, Michigan, 2019.

Chapter 8 is a version of Khaki, Behnam, Yu-Wei Chung, Chicheng Chu, and Rajit Gadh. "Hierarchical Distributed EV Charging Scheduling in Distribution Grids." 2019 IEEE Power & Energy Society General Meeting (PESGM). IEEE, 2019.

VITA

2015–2018 M.Sc. in Mechanical Engineering, University of California, Los Angeles.

2013–2015 M.Sc. in Electrical Engineering, West Virginia University.

2006–2009 M.Sc. in Electrical Engineering- Power Systems, Amirkabir University of Technology (Formerly Tehran Polytechnic).

2001–2006 B.Sc. in Electrical Engineering, Chamran University of Ahvaz (Formerly Jundishapur University).

PUBLICATIONS

Journal Articles:

- **Khaki, Behnam**, Chicheng Chu, and Rajit Gadh. "Hierarchical distributed framework for EV charging scheduling using exchange problem." Applied energy 241 (2019): 461-471.
- Chung, Yu-Wei, **Behnam Khaki**, Chicheng Chu, and Rajit Gadh. "Ensemble machine learning-based algorithm for electric vehicle user behavior prediction." *Accepted to Applied energy* (2019).
- Azar, Armin Ghasem, Hamidreza Nazaripouya, **Behnam Khaki**, Chi-Cheng Chu, Rajit Gadh, and Rune Hylsberg Jacobsen. "A non-cooperative framework for coordinating a neighborhood of distributed prosumers." IEEE Transactions on Industrial Informatics 15.5 (2018): 2523-2534.

Conference Papers:

- **Khaki, Behnam**, Yu-Wei Chung, Chicheng Chu, and Rajit Gadh. "Hierarchical distributed EV charging scheduling in distribution grids." ***Selected as one of the Best Papers***, 2019 IEEE Power & Energy Society General Meeting (PESGM). IEEE, 2019.

- **Khaki, Behnam**, Yu-Wei Chung, Chicheng Chu, and Rajit Gadh. "Probabilistic electric vehicle load management in distribution grids." 2019 IEEE Transportation Electrification Conference and Exp, Novi, Michigan, 2019.

- Reeh, Devin, Francisco Cruz Tapia, **Behnam Khaki**, Yu-Wei Chung, Chicheng Chu, and Rajit Gadh. "Vulnerability analysis and risk assessment of EV charging system under cyber-physical threats." 2019 IEEE Transportation Electrification Conference and Exp, Novi, Michigan, 2019.

- Chung, Yu-Wei, **Behnam Khaki**, Chicheng Chu, and Rajit Gadh. "Electric vehicle user behavior prediction using hybrid kernel density estimator." 2018 IEEE International Conference on Probabilistic Methods Applied to Power Systems (PMAPS). IEEE, 2018.

- **Khaki, Behnam**,Yu-Wei Chung, Chicheng Chu, and Rajit Gadh. "Nonparametric user behavior prediction for distributed ev charging scheduling." 2018 IEEE Power & Energy Society General Meeting (PESGM). IEEE, 2018.

- Xiong, Yingqi, **Behnam Khaki**, Chicheng Chu, and Rajit Gadh. "Real-time bidirectional electric vehicle charging control with distribution grid implementation." 2018 IEEE/PES Transmission and Distribution Conference and Exposition (T&D). IEEE, 2018.

- **Khaki, Behnam**, Chicheng Chu, and Rajit Gadh. "A hierarchical admm based framework for ev charging scheduling." 2018 IEEE/PES Transmission and Distribution Conference and Exposition (T&D). IEEE, 2018.

CHAPTER 1

Introduction

1.1 Motivation

The integration of renewable energy sources (RESs) in the electrical power grids is increasing at a fast pace. Two main reasons support this revolution in the energy industry: (1) increasing the electricity demand dramatically is pushing the power grid operation close to its capacity margins; (2) the traditional power generation stations located far from the end consumers have a low efficiency and crucial contribution to the environment pollution. In the United States, along with many other countries and industrial leaders in the world, strict plans are mandating the replacement of the traditional sources of electricity with sustainable and environment-friendly resources. Two major examples are the California and New York states. Until April 2019, the data released by U.S. Energy Information Administration (EIA) [eia] shows that approximately 35% of the electricity generation in California is coming from the non-hydro RESs, and this number in New York is 7.5%. The two states have mandated ambitious goals to supply 100% and 70% of their electricity sector with RESs by 2045 and 2030, respectively.

To meet the RES integration targets, not only the generation, but also the mix of energy consumption is of vital importance. In addition to replacing the electricity end-consumers with energy efficient technologies, the transition from non-electric to the electric end-consumers, introduced as *Electrification* is a key factor for success. According to the national renewable energy laboratory (NREL) report [MJL18], *Electrification* is mostly happening in two sectors, transportation and building, where the most influential elements are the electric vehicles (EVs) and electric heat pumps (HPs). According to the EIA report re-

leased in May 2019 [eia], one in four homes was all-electric in 2015, which shows a growth of 6% compared to 2005. To make it more clear that *Electrification* will be dominated by HPs, let us have a look at the mix of electricity consumption in the residential and commercial sectors in 2008 [eia], keeping in mind that these two sectors together consume 74.7% of the total electricity in the United States. In the residential sector, 49.8% of the total electricity, and in the commercial sector, 39.9% is consumed for heating, cooling, and ventilation. These numbers verify the importance of HP loads in the future of energy and electricity consumption.

In the transportation sector, however, there is still a considerable room for *Electrification*. By 2018, 29% of the total energy is absorbed by the transportation sector [eia], 92% and 3% of which are supplied by petroleum products and natural gas, and only 1% is provided by electricity. In the USA, only 1 million EVs have been sold until September 2018 [doe, ins], where 50% belongs to California [gre]. To meet the environment pollution reduction and sustainable energy infrastructure goals, *Electrification* in the transportation sector needs more investment certainly. California is a leading state in this field, where the government has already passed the bills mandating petroleum use in cars and trucks to be cut by 50% by 2030, and accommodating up to 1.5 million EVs by 2025.

1.2 Challenges

The integration of RESs, EVs, and HPs in the power grids introduces new challenges which must be addressed otherwise the safe and efficient operation of the power grids is degraded. The first challenge relates to the intermittent and stochastic behavior of the renewable energies, specifically solar, electricity load demand as well as the EV charging load Fig. 1.1. The balance between the generation and demand must be always guaranteed in the power grids. The solar energy, however, is available only during the day, and its peaks happen around noon when the load demand is low. That is, a considerable discrepancy is observed between the solar generation and load demand, which is known as Duck Curve Fig. 1.2. Duck Curve can become worse by more penetration of solar energy in the power grid. In the electricity

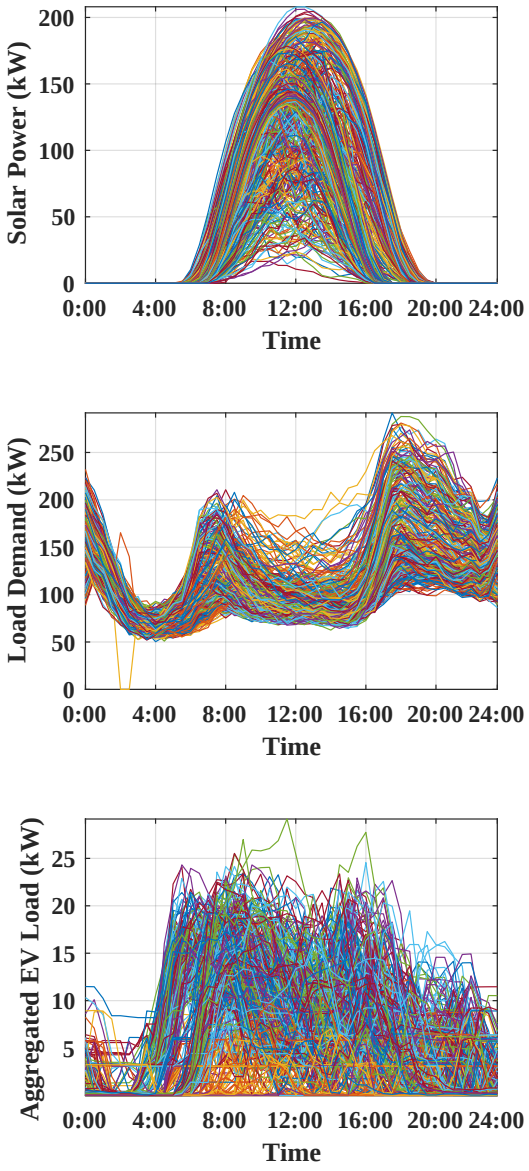

Figure 1.1: The stochastic behavior of solar energy (top), load demand (middle), and aggregated EV charging load (bottom).

sector, solar energy is introduced as a non-dispatchable energy resource.

The EV charging load, depending on the user, can have different profiles. For the EV chargers located in the residential sector, the charging demand starts in the evening and ends in the morning, while in the commercial locations, the EV charging demand starts in the morning and lasts until the afternoon. As discussed by NREL [MJL18], EV charging

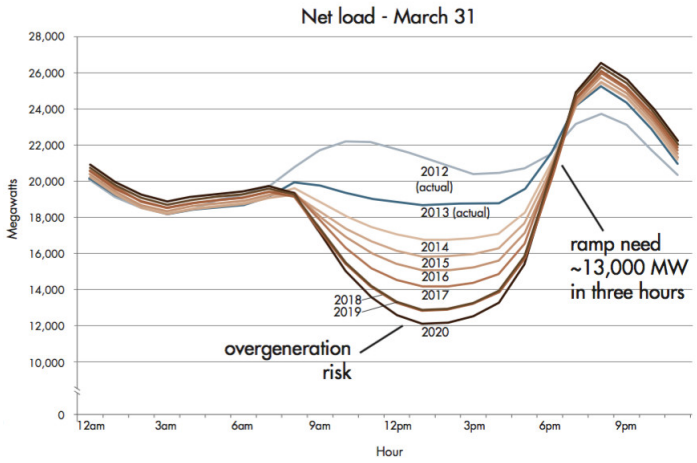

Figure 1.2: California Duck Curve [CAD].

load can drastically change the aggregated load demand profile which should be investigated by the utilities.

To eliminate the discrepancy between the solar generation and load demand in the power grids with rich integration of RESs and EVs, the first solution is to utilize energy storage. The charging and discharging coordination of the energy storage, however, is challenging as a reliable model is required to emulate the behavior and availability of RESs as well as the fluctuations of the load, specifically EVs. This model can be used by the utilities or other beneficiary entities to optimally coordinate the operation of the energy storage and provide different grid or customer-side services.

Although energy storage can mitigate the intermittency and non-dispatchability of the solar energy as well as the EV charging load fluctuations, relying on it as the only solution is not practical. Studying the EV load profiles shows that they are often plugged-in for long periods of time, which reveals their flexibility to participate in demand-side management program where the load is shifted to the periods with more available energy from RESs, and the power grid is not working close to its capacity boundaries. Nonetheless, there are three challenges for EV load management implementation which should be addressed through designing an effective load management system:

- **Entities' satisfaction:** the benefit of the grid operator, load aggregators, and end-use

customers should be considered in and satisfied by the load management.

- **Computation burden:** load management involves all the entities' control and variable parameters as well as the power grid constraints, which make it a large scale optimization problem with significant computation effort.

- **Entities' privacy:** each entity has its own constraints and variables which should not be shared with others, otherwise its privacy might not be preserved. For example, the EV's arrival time, required charging energy, and departure time as well as building's occupancy are the private information of the grid customers which are used for optimal load management.

1.3 Background

1.3.1 Solar Generation Modeling

Solar generation forecasting and modeling is a critical step for effective integration of photovoltaic (PV) solar panels in the power grids. The methods found in the literature provide either deterministic [DDL13, WCC15, WYP17] or probabilistic models. However, as the management of solar generation uncertainty is possible only with the stochastic optimization methods, probabilistic methods are of interest. The probabilistic methods can be classified into the statistical time-series, physics-based, and ensemble methods [SKR18]. The statistical time-series methods use the historical observed data to find the best parameters of the probability models [ZW15, AGK18, AGK19]. These methods are featured by low computation burdens, less expensive data collection setup, and descent accuracy [IPC13]. The physics-based methods are able to forecast the solar generation by modeling the interaction between the solar irradiance and the atmosphere components [AGK18]. The physics-based methods, however, are relatively expensive as they need a comprehensive measurement system and careful calibration [NRF93]. The ensemble methods benefit from the combination of the single-predictor methods to achieve a better accuracy [GPG16, BCD17, LZC18, ZLL19, WAM19], nonetheless their computation burden is higher than the single-predictor statistical methods,

and they need data collected for various parameters.

Due to less complexity and lower data measurement cost, the focus of this dissertation is on the statistical time-series methods. In [ZW15], the authors use k-nearest neighbor and kernel density estimation (KDE) to model the probability of solar power generation. Using k-nearest neighbor, the closest historical data are found for training, and KDE is applied to calculate the probability density function (p.d.f) of the solar generation. In [AGK18], the correlation between different solar farms is utilized to improve the accuracy of the prediction. Afterward, a spatio-temporal linear model is applied which its coefficients are calculated by minimizing the residual sum of the squares method. Another spatio-temporal method is proposed by the same authors in [AGK19], where they improve the scalability and speed of their method by using an efficient feature selection approach. As using the neighboring power plant production data raises the dimensionality and over-fitting issues, the authors solve the quantile regression with least absolute shrinkage and selection operator (LASSO).

1.3.2 EV User Behavior Modeling

In the literature, a variety of methods have been proposed to model the stochasticity of EV charging load demand [CTL12, ASD14, MQC15, WHQ15, LLY15, WWN17, LLL19]. In [CTL12], Gaussian distribution is used to model the arrival time and initial energy of the EVs, while the authors in [ASD14] assume that the charging behavior underlays Poisson distribution. In [MQC15], the authors evaluate and compare the performance of several methods including k-nearest neighbor, lazy-learning, and pattern sequence-based forecasting to estimate the aggregated EV charging demand. Autoregressive integrated moving average is proposed in [WHQ15] to predict the week-ahead aggregated EV charging load of the University of California, Los Angeles (UCLA) campus. It should be noticed that the aggregated load estimation is applicable to the situations when there is no control on the EV charging load, and the purpose is to coordinate the energy resources supplying the charging system. In other words, aggregated EV load modeling is not practical when the purpose is to coordinate the individual EV charging scheduling. KDE is used for EV charging estimation and control

in [LLY15], where the authors calculate the probability model of the traveling distance and end-time of the last trip for individual EVs. In [WWN17], KDE is proposed to estimate the expected stay duration and charging energy of the individual EVs according to their arrival time. The authors show the estimation accuracy using the data collected on the UCLA campus, and apply the models to the optimal individual EV charging control problem. The authors in [LLL19] propose to use Gaussian mixture model (GMM) to estimate both the individual EV user behavior and the aggregated charging load. They validate the estimated model using real EV data collected from the California Institute of Technology (CalTech) campus and Jet Propulsion Lab (JPL) facilities.

In this dissertation, the focus is on the individual EV charging load demand, while the proposed model is applicable to the aggregated EV load demand estimation as well.

1.3.3 EV Load Coordination

In the literature, there are two different structures for the integration of EV management system (EVMS) in the distribution management system (DMS). In the first structure, EVMS is introduced as a separate module which interacts with DMS [WCL15] to receive the information about the available grid capacity for the EV charging load and to send the aggregated EV load demand back to DMS after optimal scheduling. In the second structure, EVMS problem, i.e. optimal scheduling of the EV charging demand and its corresponding constraints, is integrated with the optimal control and management of the distribution system as a unified structure, and it is solved with the consideration of the power grid model. In the following, these two structures are reviewed separately.

1.3.3.1 EVMS- A Separate Network Application

There is a rich body of literature proposing a variety of approaches for EVMS which fall into two categories: centralized and distributed. In the former, a central aggregator (CA) receives all the required data over the communication system from the dispersed EVs and coordinates their charging demand. Then, the optimal charging profiles are sent back to

EVs. In [CHD10], it is shown that the uncoordinated EV charging increases power loss and voltage deviation, therefore the authors propose a centralized method where the EV owners have no control over the charging profile, and their charging demand is controlled by CA; a model predictive based algorithm is proposed in [TZ17] for total charging cost reduction (CR), where the authors use the truncated sample average approximation to reduce the complexity of their centralized method at the cost of performance degradation; the authors in [WHW16] introduce a centralized event-triggered receding horizon (RH) method to reduce EV charging cost in a charging infrastructure located in the UCLA campus parking; an optimal strategy for vehicle-to-grid (V2G) aggregator is designed in [PZL17] to maximize the economic benefit of EV aggregators by participation in frequency regulation while satisfying EV owners' load demand; a centralized algorithm is designed by the authors in [BNE18] to flatten the netload fluctuations due to RESs using EV charging control; in [ZSS18], a real-time EV charging scheduling is proposed where the computational complexity is reduced by introducing a capacity margin and the charging priority indices; a centralized mechanism is proposed in [PGM18] where a third-party entity coordinates a day-ahead bidding system to optimize the global bid; a transactive EV charging management is presented in [LWS18] to maximize the real-time profit based on the net electricity exchange with the grid; and a two-layer centralized EV charging control (EVCS) is proposed by [MVS19] where each aggregator optimizes active power of the EVs in the first layer, and the second layer provides reactive power management for loss reduction in the power grid. Despite the effective EV charging results, the centralized approaches have several issues: (I) they can not preserve the EV owners' privacy as sensitive charging information (e.g. arrival and departure times as well as their battery energy level and capacity) must be communicated with CA, (II) they suffer from the curse of dimensionality when EV penetration increases in the power grid, and (III) they are vulnerable to a single point failure, i.e. if CA faces any problem, the whole system breaks down. In the distributed approaches, which address the above issues, CA coordinates the EV charging demand through communication with the EV charger agents or EV aggregators (EVAs). Instead of solving the large-scale scheduling problem centrally, it is solved through a distributed and iterative procedure in collaboration with the EVA and

EV agents.

Among the distributed methods, two different EV charging infrastructures (ECIs) are considered: (I) bilayer structure which consists of either EVA and EVs or CA and EVAs, and (II) trilayer structure which includes CA, EVAs, and EVs. Considering the bilayer structure, the authors in [GTL13] propose a distributed charging scheduling which is solved using the projected gradient descent and provides valley filling; in [RGJ17], the EVCS problem is formulated as the *exchange problem* which is efficiently solved by the alternating direction method of multipliers (ADMM) [BPE11] for the valley filling and CR; the authors in [XWC18] use a water filling algorithm incentivizing the EV owners to shift their charging demand to the off-peak hours; a mean-field game theory-based method is proposed in [TK18] to provide valley filling and reduce the battery degradation cost; the work is further expanded in [SK19] by considering the plug-in hybrid EVs, in which the propulsion provided by gasoline gives more flexibility to EVs for participation in V2G services [KT05]; in[LRK19], a distributed method is proposed where each EV communicates only with its neighbors to reduce the communication overhead, and the optimal charging problem is addressed by the full Nash Folk theorem; in [YZW13], the authors propose a bi-level programming-based hierarchical decomposition EVCS where the objective is to reduce the generation unit cost for CA; the authors in [MGT14] propose three algorithms based on the projected gradient descent [GTL13] and ADMM, where EVAs communicate with their neighbors, and each EVA centrally calculates the optimal charging profiles of EVs which it supplies; the proposed distributed bilayer EVCS in [CLY18] reduces the charging cost and increases EV owners' convenience, where EVAs update their aggregated charging load sequentially, not in parallel; the authors in [SSG18] propose a decentralized method where the EVAs will be notified by CA if their aggregated charging load results in the transmission line congestion. EVAs reschedule all the EVs' load demands and recalculate the available V2G capacity to relieve the congestion. Considering the on-site uncertain wind generation, a distributed method is proposed in [YJD18] to increase the local wind energy utilization and satisfy the EV load demand through penalizing energy purchase from the grid.

Considering the trilayer EV charging structure, the authors in [WCT12] use ADMM to

schedule the EV charging demand with the purpose of user convenience maximization, which is characterized by the EV battery's final state of charge; a distributed approach based on the sub-gradient method is proposed in [QXS14] to satisfy customers' charging demands and the coupled constraints relating to the EVAs' feeder capacity; the EVA constraints, however, are relaxed in [QXS14] and included in the Lagrangian of the cost function which results in sub-optimality of the coordinated charging profiles; the authors in [LLa14] design a distributed framework for V2G scheduling where EVAs' revenue is neglected, and the gradient projection method is used to solve the optimal V2G scheduling problem which is not computationally efficient, and the convergence of the method depends on the number of EVs; the hierarchical framework designed in [SWW16] includes two iterative procedures: the first procedure is between CA and EVAs, and the second one is between each EVA and its EVs; the framework suffers from considerable communication overhead and computational burden, and it does not provide flexibility for the agents to have their desired objective function; in [LBM16], the EVCS problem is modeled as a weakly concave function which is solved iteratively between the agents by the projected gradient method; to have a fully distributed EVCS, the authors use the Lagrangian to consider the coupled constraints in the optimization problem which leads to sub-optimal results; in addition, their framework does not consider EVAs' objective function, and there is a strict assumption on CA's objective function; in [CLL18], the framework proposed in [LLa14] is expanded to a generic V2G scheduling framework which includes several layers of EVAs; there is, however, no flexibility in the method to include any other desired scheduling objective, the optimization solved by EVAs to calculate the V2G capacity depends on the number of EVs, and the agents update their optimization variable sequentially; the authors in [ZHM18] develop a sequential trilayer structure, where the transformers as EVA agents reach a consensus price minimizing the generation cost in the first iterative procedure of the method, and EVs maximize their payoff function according to their transformers' price signal in the second procedure; the convergence of the method, however, is based on the strict assumptions on the objective function.

In this dissertation, to address the issues discussed above, two trilayer fully distributed

frameworks are proposed. In the proposed methods, the strict assumptions considered in the literature on the objective functions are relaxed. Furthermore, the feeder capacity constraints are introduced as the local EVAs' constraints, thus the charging scheduling results are not sub-optimal.

1.3.3.2 EVMS- An Integrated Network Application

Similar to EVMS as a separate application, there are two approaches for the consideration of the distribution grids' constraints in EVCS problem: centralized and distributed. In the centralized approaches, the distribution system operator (DSO) coordinates the distributed energy resources (DERs) such as the energy storage and the controllable loads of all customers with taking the power flow model and grid operation constraints (i.e. nodal voltages and feeders' loading capacity) into consideration [STS19, WBP19, HW18, MSK18, KMY19, HST19]. To this end, the EV owners send their information about the arrival and departure times as well as required charging energy to DSO. After calculating the optimal individual EV charging profiles, DSO transmits them to the customers. Considering the centralized approach, the authors in [STS19] propose a method based on the model predictive control, where the optimization problem is reformulated as a semi-definite problem, solved by a non-smooth algorithm; in [WBP19], EVs are considered as not only the active power load but also as a source of the reactive power injection/absorption which can provide power factor correction and voltage regulation services; to mitigate the grid congestion, a locational pricing mechanism is designed in [HW18] which incentivizes the customers with controllable loads to shift their energy profile to the time periods without grid congestion possibility; two charging strategies for public parking stations are proposed in [MSK18], for total charging cost reduction and load leveling, where the EVCS problem is solved by DSO using a heuristic method; the centralized method introduced in [KMY19] aims at minimizing the electricity cost for the customers by coordinating EV load; the purpose is to minimize solar energy curtailment, while the nodal voltages are within the acceptable range; in this method, the EV load is controlled by the customers according to the constraints defined by DSO; in [HST19], a methodology for the participation of EV aggregators in the day-ahead and real-time energy

markets is proposed, which not only maximizes the aggregators' benefit, but also minimizes the effect of EV load uncertainty on the power grid operation. The centralized methods, however, have two main drawbacks: the curse of dimensionality when DSO has to coordinate a large population of DERs and controllable loads, and non-privacy preserving as the customers have to share their sensitive information with DSO which makes it vulnerable to data manipulation by an eavesdropper.

To address the drawbacks of the centralized approaches, the researchers have proposed distributed demand control where the load coordination problem is solved in a distributed manner between the involved entities. There are two structurally different distributed approaches depending on the interaction between the entities. Within the first approach, the customers are not actively involved in load coordination procedure; instead, the load aggregators collect the information relating to the customers which they supply and communicate with DSO [YZW13, WSW17, HMC18, MML19]. In this approach, the load coordination problem is solved through an iterative procedure between DSO and the aggregators. In the second approach, either DSO communicates directly with the customers and the load coordination problem is solved between them iteratively [LPS19], or DSO is in communication with the aggregators only, and each aggregator exchanges information with its own customers. In this approach, the load coordination problem is solved through two iterative procedures between (1) DSO and the aggregators, and (2) each aggregator and its customers [ZKG17, XYF19].

Considering the first load coordination approaches, a bi-level programming method is proposed in [YZW13] for optimal EVCS problem where DSO minimizes the energy resources' cost subjected to the power flow constraints, and the aggregators are responsible for finding the optimal charging schedules reducing the EVs' battery degradation cost; the authors in [WSW17] benefit from the separable objective function which minimizes the resistive loss and electricity cost, and they apply ADMM to find the optimal load and BESS charging/discharging profiles through an iterative procedure between DSO and the aggregators; in [HMC18], a distributed optimization between DSO and the aggregators based on the dual decomposition method is proposed to coordinate the thermostatically controllable loads con-

sidering the power flow model as well as the uncertainty of the solar energy. The authors model the load as a lumped aggregated one located at each grid bus. Similar to the distributed method in [WSW17], a robust distributed optimization is proposed in [MML19] where the optimal load control problem is formulated as a mixed-integer linear program and solved by ADMM between DSO and the aggregators; the authors, however, do not provide the details on how the integer variables are relaxed. Considering the second distributed load control approaches, the authors in [LPS19] propose a novel shrunken primal-dual subgradient method for valley-filling/load leveling problem, where DSO considers the linearized power flow model and communicates directly with the residential customers; consequently, the aggregators are excluded from the load coordination problem; in [ZKG17], a two-layer framework is proposed where the first layer between DSO and the aggregators is solved using ADMM based on the *consensus problem*, and the second layer which is defined between each aggregator and its customers is solved using the distributed Frank-Wolf method; a similar two-layer framework is introduced in [XYF19] where the first layer is solved by ADMM, and the second layer of optimal load control problem between the aggregators and their customers is solved using the gradient-based dual ascend already proposed in [GTL13].

In this dissertation, a distributed framework is proposed where the load control problem is solved through an iterative procedure between DSO and the aggregators based on the *consensus problem*. In this method, DSO regulates the voltage by controlling the aggregated loads, and the aggregators minimize the load profile variance and electricity cost of their customers. The formulated load control is further exploited mathematically to derive a fully distributed two-layer framework where the customers are directly involved in the load management problem. In this framework, the iterative procedure between the aggregators and their customers is formulated as the *sharing problem* in which the dimension of the optimization problem solved by the aggregators does not depend on their number of customers.

1.4 Objectives and Contributions

According to the literature review in the preceding section, the objectives of this dissertation are as follows.

1. **Generation and Load Modeling:** as discussed earlier, the effective integration of RESs and the *Electrification*'s elements, i.e. EVs and HPs, needs the accurate modeling of uncertainties. The first objective of this work is to propose a low-computation and accurate model for capturing the intermittency and fluctuations of the solar generation profile, load demand, EV charging load.

2. **Optimal BESS Control for EV and Solar Integration:** As mentioned earlier, a practical solution to integrate the solar energy and EV loads in the power system is realized through the optimal BESS control. Accordingly, the second objective of this work is to experiment with the BESS deployment in an EV charging system for load leveling and mitigating the solar energy and EV charging uncertainties.

3. **Scalable Load Coordination:** According to the computational burden of the proposed methods in the literature and the privacy-preserving issue in the centralized and semi-distributed approaches for the optimal load coordination, the third objective of this dissertation is to provide a fully scalable load management system where the grid entities (e.g. DSO, aggregators and EVs) do not need to share their sensitive information with others.

To meet the objectives of this dissertation, the contributions of this work are defined as follows.

1. A non-parametric time-series based probability model is proposed for modeling the solar energy, load demand, and EV charging load (both aggregated and individual). The proposed model is based on KDE, which compared to the methods proposed in the literature, it is adaptive to the history data, and therefore it improves the accuracy of the estimated model. Comparing to the spatio-temporal methods, the proposed

method needs only the time-series data history of the estimated parameter, therefore it does not require a costly data acquisition system.

2. An experimental setup is prototyped to integrate BESS in an EV charging infrastructure. The setup provides EV load leveling and emergency power to decrease the charging cost and increase the reliability of the charging system. The performance of the prototyped BESS is validated by executing various services such as peak load shaving and islanded operation, in which the emergency power is provided to the charging infrastructure.

3. Two scalable and privacy-preserving frameworks are proposed for EVMS, which can be included as a separate application in DMS. Both frameworks are designed based on the multi-agent systems, in which the EVMS problem is solved using the distributed optimization methods. Specifically, ADMM is used to solve EVMS through the iterative negotiation procedures between the involved entities, i.e. CA, load aggregators, and EV customers.

4. A semi-distributed method is proposed for EVMS as an integrated application in DMS, where DSO and load aggregators negotiate to improve the nodal voltage profiles of the distribution grid, minimize the load profile variance of the aggregators, and reduce the charging cost for the EV customers. In this method, the EVMS problem formulated as the *consensus problem*, and it is solved by ADMM.

5. A fully distributed and scalable framework is proposed to coordinate the EV and HP loads in the distribution grids. The proposed method has a hierarchical structure in which DSO negotiates with the load aggregators, and each aggregator negotiates with its residential customers. The iterative negotiation procedure between DSO and the aggregators is formulated as the *consensus problem*, and the iterative negotiation between the aggregators and the customers is written in the form of the *sharing problem*. The feature of the proposed method is that the dimension of the aggregators' optimization problem does not depend on the number of their customers. In this method, both negotiation procedures are solved by ADMM.

1.5 Organization

The rest of the dissertation is organized as follows:

Chapter 2- In this chapter, the models for BESS, EV, HP, and the distribution power grids are introduced. As the distributed optimization method used in the dissertation is applicable to the convex optimization problems, the models provided in this chapter are convex.

Chapter 3- In this chapter, an adaptive KDE based on diffusion is proposed to model the p.d.f of solar generation, load demand, and EV charging load. To improve the accuracy of the estimated models for solar generation and load demand, the k-means clustering method is introduced to cluster the corresponding historical data.

Chapter 4- In this chapter, we first describe the prototyped BESS which provides load leveling, cost reduction and emergency power to the EV charging system. Afterward, we propose a stochastic optimization method to coordinate the charging/discharging of BESS using the Monte Carlo Simulation (MCS) and adaptive KDE model developed in Chapter 3.

Chapter 5- A hierarchical distributed framework is proposed in this chapter to optimally control EV charging loads considering the capacity constraints of the aggregators' feeders. The framework consists of two layers of the *sharing problem* which are solved by ADMM.

Chapter 6- To improve the convergence time and reduce the communication overhead of the method proposed in Chapter 5, the mathematical properties of the optimal EVCS problem is exploited to rewrite the problem in the form of the *exchange problem*. The new formulation eliminates the dual variable of the system agents, therefore the convergence time and communication overhead are reduced considerably.

Chapter 7- In this chapter, an EVMS framework is proposed to consider the power grid constraints including the voltage limitation. The proposed method aiming at regulating

the nodal voltage and reducing EV charging cost is written in the form of the *consensus problem*. The EVMS is then solved by ADMM through an iterative procedure between DSO and the load aggregators.

Chapter 8- As the load aggregators of the proposed EVMS in Chapter 7 solve the optimal charging problem for their customers, it results in a considerable computation burden. Also, the customers have to share their sensitive information with the aggregators. To mitigate those issues, a fully distributed load coordination method is proposed in this chapter where each customer solves its problem locally and exchanges limited information with the aggregators. In this chapter, the customers participate in the optimal load management with controlling their EV as well as HP loads.

Chapter 9- The dissertation is concluded in this chapter, and possible future directions for BESS control and load coordination in the distribution grids are discussed.

CHAPTER 2

System Modeling

In this chapter, the model of BESS, EV, HP as well as the distribution grid are introduced, respectively. In addition to the difference and differential equations which define the discrete-time dynamics of the system, the inequalities forcing the power grid and its components to operate within the acceptable domain are included in the models. Those equations and inequalities guaranteeing the proper operation of the distribution grid and its components build the set of equality and inequality constraints of optimal system control and management problem. More details are provided in the following sections.

2.1 Battery Energy Storage System

The BESS installed at the ith node of the distribution system is indicated by BES_i, and it is modeled by a discrete-time linear time-invariant system as follows:

$$c_i^{bs}(t+1) = \alpha_i^{bs} c_i^{bs}(t) + T_d\big(\eta_i^{bs^+} p_i^{bs^+}(t) + p_i^{bs^-}(t)/\eta_i^{bs^-}\big) \tag{2.1a}$$

$$p_i^{bs}(t) = p_i^{bs^+}(t) + p_i^{bs^-}(t), \tag{2.1b}$$

for $\forall t \in \mathbb{N}$ where c_i^{bs}, $p_i^{bs^+}$, $p_i^{bs^-}$, $T_d \in \mathbb{R}$, and $(\alpha_i^{bs}, \eta_i^{bs^+}, \eta_i^{bs^-}) \in \mathbb{R}^{+3}_{\leqslant 1}$. $c_i^{bs}(t)$ is the energy stored in BESS at time t, T_d is the length of the sampling intervals and discretization in time, and $p_i^{bs^+}$ and $p_i^{bs^-}$ are the charging and discharging powers, respectively. The parameter α_i^{bs} models the self-discharging energy loss, and $\eta_i^{bs^+}$ and $\eta_i^{bs^-}$ model the energy conversion loss during charging and discharging, respectively. The energy stored in the ith BESS and its

charging and discharging powers are limited by the following constraints [ZRF19]:

$$s_i^{bs^2}(t) = p_i^{bs^2}(t) + q_i^{bs^2}(t) \leqslant \overline{s}_i^{bs^2} \tag{2.2a}$$

$$0 \leqslant p_i^{bs^+}(t) \leqslant \overline{p}_i^{bs} \tag{2.2b}$$

$$\underline{p}_i^{bs} \leqslant p_i^{bs^-}(t) \leqslant 0 \tag{2.2c}$$

$$\underline{C}_i^{bs} \leqslant c_i^{bs}(t) \leqslant \overline{C}_i^{bs}, \tag{2.2d}$$

for $\forall t \in \mathbb{N}$ where $p_i^{bs}(t)$, $q_i^{bs}(t) \in \mathbb{R}$, and $s_i^{bs}(t) \in \mathbb{C}$. $q_i^{bs}(t)$ and $s_i^{bs}(t)$ are, respectively, the reactive and apparent powers of the BESS and its bi-directional converter. $\overline{s}_i^{bs} \in \mathbb{R}$ is the apparent power rating of the bi-directional converter, and $\underline{p}_i^{bs}$ and $\overline{p}_i^{bs} \in \mathbb{R}$ are the minimum and maximum power ratings of BESS. $\underline{C}_i^{bs}(t)$ and $\overline{C}_i^{bs}(t) \in \mathbb{R}$ are the BESS energy constraints defined according to the battery manufacturer's recommendations.

The set of feasible charging and discharging trajectories of the ith BESS is defined by:

$$\mathbb{P}_i^{bs} = \left\{ \mathbf{p}_i^{bs} \in \mathbb{R}^N \mid (2.1) - (2.2)\ \forall t \in [\![t', t'+N-1]\!] \right\}. \tag{2.3}$$

In this dissertation, for the time index $t \in \mathbb{N}$ and the time horizon $N \in \mathbb{N}$, the vector notation:

$$\mathbf{y}(t) = \left(\mathbf{y}_1^T(t), \mathbf{y}_2^T(t), \ldots, \mathbf{y}_{\mathcal{N}}^T(t)\right)^T,$$

is used where $\mathbf{y}_n(t) = \left(y_n^T(t), y_n^T(t+1), \ldots, y_n^T(t+N-1)\right)^T, n \in \{1, ..., \mathcal{N}\}$, is defined component-wise.

Remark 2.1.1. The most popular BESS technologies utilized for grid applications are Li-ion, NiCd, and Lead-acid. The authors in [CCY09] compare different BESS technologies from the self-discharging and conversion loss perspectives during a day. It is discussed in [CCY09] that batteries have lower self-discharging and conversion loss comparing to the other storage technologies (e.g. flywheel, super-capacitor, fuel cell, etc.). Considering the values in Table 2.1 and a discretization of $T_d = 0.5$[h], we obtain $\alpha_i^{bs} \geqslant 0.999$ and $(\eta_i^{bs^+}, \eta_i^{bs^-}) \geqslant (0.9, 0.9)$. Therefore, the self-discharging loss can be neglected.

Table 2.1: Comparison of three BESS technologies [CCY09].

Battery Type	**Self-Discharging**	**Conversion Loss**	**Life** (cycles)	**Environmental Impact**
Li-ion	0.1-0.3%	5-10%	1000^{-}	–
NiCd	0.2-0.6%	5-10%	2000-2500	–
Lead-acid	0.1-0.3%	5-10%	500-1000	Negative

2.2 Electric Vehicle

The ith EV charger, which is supplied through the feeder connected to the jth node of the distribution grid, is indicated by $EV_{i,j}$. Similar to BESS, EV is modeled as a discrete-time linear time-invariant system as follows:

$$c^{ev}_{i,j}(t+1) = \alpha^{ev}_{i,j} c^{ev}_{i,j}(t) + T_d\big(\eta^{ev+}_{i,j} p^{ev+}_{i,j}(t) + p^{ev-}_{i,j}(t)/\eta^{ev-}_{i,j}\big) \tag{2.4a}$$

$$p^{ev}_{i,j}(t) = p^{ev+}_{i,j}(t) + p^{ev-}_{i,j}(t), \tag{2.4b}$$

for $\forall t \in \mathbb{N}$ where $c^{ev}_{i,j}$, $p^{ev+}_{i,j}$, $p^{ev-}_{i,j}$, $T_d \in \mathbb{R}$, and $(\alpha^{ev}_{i,j}, \eta^{ev+}_{i,j}, \eta^{ev-}_{i,j}) \in \mathbb{R}^{+3}_{\leqslant 1}$. $c^{ev}_{i,j}(t)$ is the energy stored in the EV's battery at time t, T_d is the discretization in time, and $p^{ev+}_{i,j}$ and $p^{ev-}_{i,j}$ are the charging and discharging powers, respectively. The parameter $\alpha^{ev}_{i,j}$ models the self-discharging energy loss, and $\eta^{ev+}_{i,j}$ and $\eta^{ev-}_{i,j}$ model the energy conversion loss during charging and discharging, respectively. The constraints on the EV charging/discharging, relating to the EV charger power rating and the EV's battery capacity, are:

$$0 \leqslant p^{ev+}_{i,j}(t) \leqslant \overline{p}^{ev}_{i,j} \tag{2.5a}$$

$$\underline{p}^{ev}_{i,j} \leqslant p^{ev-}_{i,j}(t) \leqslant 0 \tag{2.5b}$$

$$0 \leqslant \frac{p^{ev-}_{i,j}(t)}{\underline{p}^{ev}_{i,j}} + \frac{p^{ev+}_{i,j}(t)}{\overline{p}^{ev}_{i,j}} \leqslant 1, \tag{2.5c}$$

$$\underline{C}^{ev}_{i,j}(t) \leqslant c^{ev}_{i,j}(t) \leqslant \overline{C}^{ev}_{i,j}(t), \tag{2.5d}$$

for $\forall t \in \mathbb{N}$ where $\underline{p}^{ev}_{i,j}$, $\overline{p}^{ev}_{i,j} \in \mathbb{R}$ are the minimum and maximum power ratings of the EV charger, respectively, and $\underline{C}^{ev}_{i,j}(t)$, $\overline{C}^{ev}_{i,j}(t) \in \mathbb{R}$ are the EV's battery time-varying energy constraints which are defined as follows; if $EV_{i,j}$ is:

- not plugged in the charger, $\underline{C}^{ev}_{i,j}(t) = \overline{C}^{ev}_{i,j}(t) = 0$.

- plugged in the charger, but it is in idle mode, $\underline{C}^{ev}_{i,j}(t) = 0$ & $\overline{C}^{ev}_{i,j}(t) = C^{ev}_{i,j}$, where $C^{ev}_{i,j} \in \mathbb{R}$ is the EV's battery energy capacity (Assumption 2.2.1).
- plugged in the charger, and it is needed by time t, $\underline{C}^{ev}_{i,j}(t) = \overline{C}^{ev}_{i,j}(t) = C^{ev}_{i,j}$.

The constraint (2.5c) does not allow the battery to dissipate its energy surplus by avoiding charging and discharging, and it makes possible that the battery changes from charging to discharging mode and vice versa between the consecutive time steps [BFG18].

Assumption 2.2.1. All the vehicles should be fully charged before they are unplugged.

Remark 2.2.1. The EV chargers may have V2G capability to discharge EV's battery and inject power to the grid [KT05]. If the charger has V2G capability, we will set $\underline{p}^{ev}_{i,j} = -\overline{p}^{ev}_{i,j}$, otherwise $\underline{p}^{ev}_{i,j} = 0$

The set of feasible charging trajectories of $EV_{i,j}$ is defined by:

$$\mathbb{P}^{ev}_{i,j} = \left\{ \mathbf{p}^{ev}_{i,j} \in \mathbb{R}^N \mid (2.4) - (2.5)\ \forall t \in [\![t', t' + N - 1]\!] \right\}. \tag{2.6}$$

2.3 Electric Heat Pump

The model of the building for the purpose of optimal HP control is represented as a single zone where uniform air temperature is assumed in the whole zone. In this model, the building components, i.e. walls, floor, roof, and windows, are considered as lumped ones. Every lumped component is modeled by the thermal resistance and capacitance as shown in Fig. 2.1.

Although all the optimal BESS, EV, and load management methods proposed in this dissertation are built on the discrete-time variables, for consistency with the literature and better understanding, we present the continuous-time linear model of HP [KJC17]. However, for the purpose of optimal load management, the model is converted to the discrete-time linear system with the appropriate sample time (in our case, $T_d = 0.5$[h]). The superscripts z, w, o, f are used to denote, respectively, the zone, inner wall, outer wall, and floor parameters.

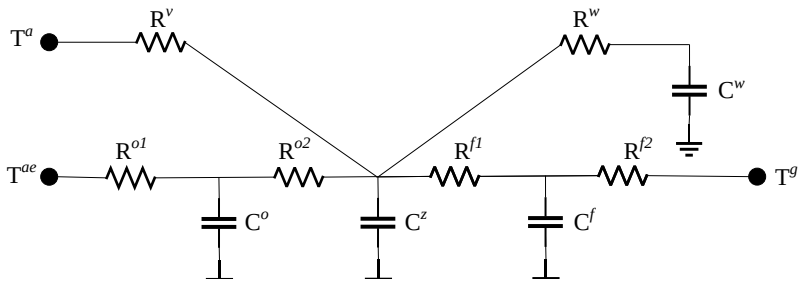

Figure 2.1: Single zone model of the building.

The heat pump located at the ith residential customer building, which is supplied through the feeder connected to the jth node of the distribution grid, is denoted by $HP_{i,j}$. The differential equations modeling the dynamic behavior of $HP_{i,j}$ are as follows:

$$\dot{T}^z_{j,i} = \tfrac{1}{R^v_{i,j}C^z_{i,j}}(T^a_{i,j} - T^z_{i,j}) + \tfrac{1}{R^w_{i,j}C^z_{i,j}}(T^w_{i,j} - T^z_{i,j}) + \tfrac{1}{R^{o1}_{i,j}C^z_{i,j}}(T^o_{i,j} - T^z_{i,j}) + \tfrac{1}{R^{f1}_{i,j}C^z_{i,j}}(T^{f1}_{i,j} - T^z_{i,j}) + \tfrac{s^z_{i,j}}{C^z_{i,j}}\varphi^{sg}_{i,j} + \tfrac{g^z_{i,j}}{C^z_{i,j}}\varphi^{ig}_{i,j} + \tfrac{f^z_{i,j}}{C^z_{i,j}}\varphi^{hp}_{i,j} \tag{2.7a}$$

$$\dot{T}^w_{i,j} = \tfrac{1}{R^w_{i,j}C^w_{i,j}}(T^z_{i,j} - T^w_{i,j}) + \tfrac{s^w_{i,j}}{C^w_{i,j}}\varphi^{sg}_{i,j} + \tfrac{g^w_{i,j}}{C^w_{i,j}}\varphi^{ig}_{i,j} + \tfrac{f^w_{i,j}}{C^w_{i,j}}\varphi^{hp}_{i,j} \tag{2.7b}$$

$$\dot{T}^o_{i,j} = \tfrac{1}{R^{o2}_{i,j}C^o_{i,j}}(T^{ae}_{i,j} - T^o_{i,j}) + \tfrac{1}{R^{o1}_{i,j}C^o_{i,j}}(T^z_{i,j} - T^o_{i,j}) + \tfrac{s^o_{i,j}}{C^o_{i,j}}\varphi^{sg}_{i,j} + \tfrac{g^o_{i,j}}{C^o_{i,j}}\varphi^{ig}_{i,j} + \tfrac{f^o_{i,j}}{C^o_{i,j}}\varphi^{hp}_{i,j} \tag{2.7c}$$

$$\dot{T}^f_{i,j} = \tfrac{1}{R^{f2}_{i,j}C^f_{i,j}}(T^g_{i,j} - T^f_{i,j}) + \tfrac{1}{R^{f1}_{i,j}C^f_{i,j}}(T^z_{i,j} - T^f_{i,j}) + \tfrac{s^f_{i,j}}{C^f_{i,j}}\varphi^{sg}_{i,j} + \tfrac{g^f_{i,j}}{C^f_{i,j}}\varphi^{ig}_{i,j} + \tfrac{f^f_{i,j}}{C^f_{i,j}}\varphi^{hp}_{i,j}, \tag{2.7d}$$

where $T^z_{i,j}$, $T^w_{i,j}$, $T^o_{i,j}$, and $T^f_{i,j} \in \mathbb{R}$ are the temperatures; $R^v_{i,j} \in \mathbb{R}$ stands for the lumped thermal bridge of the envelop area together with the ventilation and infiltration losses; $R^w_{i,j}$, $R^{o1}_{i,j}$, $R^{o2}_{i,j}$, $R^{f1}_{i,j}$, and $R^{f2}_{i,j} \in \mathbb{R}$ are the thermal resistances; $C^z_{i,j}$, $C^w_{i,j}$, $C^o_{i,j}$, and $C^f_{i,j} \in \mathbb{R}$ are the thermal capacitances; $T^{ae}_{i,j}$, $T^a_{i,j}$, $T^g_{i,j}$, $\varphi^{sg}_{i,j}$, and $\varphi^{ig}_{i,j} \in \mathbb{R}$ are defined as the equivalent ambient temperature, ambient temperature, ground temperature, solar gain through the windows, and internal gain from the occupants and devices, respectively; and $\varphi^{hp}_{i,j} \in \mathbb{R}$ is the total power of HP, and it is proportional to the compressor power $p^{hp}_{i,j} \in \mathbb{R}$ as follows:

$$\varphi^{hp}_{i,j} = \eta^{hp}_{i,j} p^{hp}_{i,j}, \tag{2.8}$$

where $\eta_{i,j}^{hp} \in \mathbb{R}_{\leqslant 1}^{+}$ is the coefficient of compressor performance. The constraints on $HP_{i,j}$ relating to the power rating of the compressor and the resident's thermal comfort are:

$$0 \leqslant p_{i,j}^{hp}(t) \leqslant \overline{p}_{i,j}^{hp} \tag{2.9a}$$

$$\underline{T}_{i,j}^{z} \leqslant T_{i,j}^{z}(t) \leqslant \overline{T}_{i,j}^{z}, \tag{2.9b}$$

where $\overline{p}_{i,j}^{hp}$ is the maximum power of the compressor, and $\underline{T}_{i,j}^{z}$ and $\overline{T}_{i,j}^{z}$ are the acceptable lower and upper zone temperatures.

The model of HP can be represented in the state-space form as:

$$\dot{x}_{i,j}^{hp} = A_{i,j}^{hp} x_{i,j}^{hp} + B_{i,j}^{hp} u_{i,j}^{hp} + D_{i,j}^{hp} w_{i,j}^{hp} \tag{2.10a}$$

$$y_{i,j}^{hp} = C_{i,j}^{hp} x_{i,j}^{hp} \tag{2.10b}$$

where $x_{i,j}^{hp} = [T_{i,j}^{z},\ T_{i,j}^{w},\ T_{i,j}^{o},\ T_{i,j}^{f}]^{T}$ is the state vector, $u_{i,j}^{hp} = \varphi_{i,j}^{hp}$ is the control variable, $w_{i,j}^{hp} = [T_{i,j}^{ae},\ T_{i,j}^{a},\ T_{i,j}^{g},\ \varphi_{i,j}^{sg}]^{T}$ is the disturbance vector, and $y_{i,j}^{hp} = T_{i,j}^{z}$ is the output or measurement vector.

The set of feasible compressor power trajectories of $HP_{i,j}$ is defined by:

$$\mathbb{P}_{i,j}^{hp} = \left\{ \mathbf{p}_{i,j}^{hp} \in \mathbb{R}^{N} \mid (2.7) - (2.9)\ \forall t \in [\![t', t' + N - 1]\!] \right\}. \tag{2.11}$$

2.4 Power Distribution Grid

The distribution grid is modeled as a connected graph shown by $\mathrm{G} = (\mathbb{N}_b, \zeta)$, where $\mathbb{N}_b$ denotes the set of the edges which are grid buses (nodes), and ζ denotes the set of the links which are the distribution grid branches (lines or transformers). $(i, j) \in \zeta$ denotes the line connecting the ith bus to the jth bus. The distribution grids are typically radial (Fig. 2.2), that is the connected graph is a tree with a root node, branches, and leaves. Accordingly, the first bus is denoted by 1, and the other buses in $\mathbb{N}_b$ are indexed by $i = 2, 3, \cdots, \mathcal{N}_b$, where $\mathcal{N}_b$ is the cardinality of $\mathbb{N}_b$.

For each branch $(i, j) \in \zeta$, we show the impedance by the complex number $z_{ij} = r_{ij} + \mathbf{i}x_{ij}$, $z_{ij} \in \mathbb{C}$, and the current by $\mathbf{i}_{ij}(t) \in \mathbb{C},\ \forall t \in \mathbb{N}$. The apparent power of the branch is shown

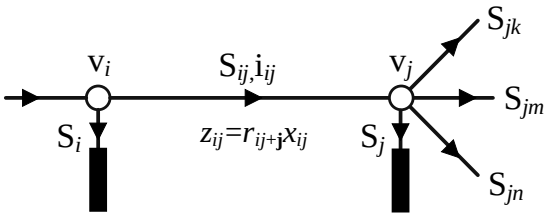

Figure 2.2: Radial distribution feeder and its corresponding parameters.

by $S_{ij}(t) \in \mathbb{C}$, $\forall t \in \mathbb{N}$, and it is obtained by $S_{ij}(t) = P_{ij}(t) + \mathbf{i}Q_{ij}(t)$, where $P_{ij}(t)$ and $Q_{ij}(t) \in \mathbb{R}$ are the active and reactive powers, respectively, flowing from the ith to the jth bus.

For each bus $i \in \mathbb{N}_b$, we show the voltage by $v_i(t) \in \mathbb{C}$, and the bus netload by $S_i(t) = P_i(t) + \mathbf{i}Q_i(t)$, $S_i(t) \in \mathbb{C}$. The netload is the total power consumption minus the generation (possibly by RESs) at the ith bus.

Given the radial distribution grid $\mathrm{G} = (\mathbb{N}_b, \zeta)$, the voltage at the root bus ($1 \in \mathbb{N}_b$), and the impedances of the grid branches ($\{z_{ij}\}_{i,j} \in \zeta$), the branch power flows and currents as well as the bus voltages should satisfy the physical power grid laws, at any time $t \in \mathbb{N}$, as follows:

- Ohm's law:

$$v_i(t) - v_j(t) = z_{ij} i_{ij}(t). \tag{2.12}$$

- Power flow:

$$S_{ij}(t) = v_i(t) {i_{ij}}^*(t). \tag{2.13}$$

- Power balance:

$$S_j(t) = S_{ij}(t) - z_{ij}|i_{ij}(t)|^2 - \sum_{(j,k)\in\zeta} S_{jk}(t). \tag{2.14}$$

Substituting (2.12) and (2.13) in (2.14), the following steady-state power flow model is

obtained [Low14a], $\forall i \;\&\; j \in \mathbb{N}_b$ and $\forall (i,j) \in \zeta$:

$$P_j(t) = P_{ij}(t) - r_{ij} I_{ij}(t) - \sum_{(j,k)\in\zeta} P_{jk}(t) \tag{2.15a}$$

$$Q_j(t) = Q_{ij}(t) - x_{ij} I_{ij}(t) - \sum_{(j,k)\in\zeta} Q_{jk}(t) \tag{2.15b}$$

$$V_i(t) - V_j(t) = 2\Big(r_{ij} P_{ij}(t) + x_{ij} Q_{ij}(t)\Big) - ({r_{ij}}^2 + {x_{ij}}^2) I_{ij}(t) \tag{2.15c}$$

$$V_i(t) I_{ij}(t) = P_{ij}^2(t) + Q_{ij}^2(t), \tag{2.15d}$$

where $I_{ij}(t) = |i_{ij}(t)|^2$ and $V_i(t) = |v_i(t)|^2$. Although the angles of bus voltages and branch currents are not directly included in (2.15a)-(2.15d), they can be uniquely determined for the radial distribution grids [Low14b].

The voltage at the root bus ($\mathbf{v}_1$) should be equal to a specific value, assuming that the distribution grids are connected to an infinite bus with infinite inertia. The other bus voltages, however, should be within the tolerance constraints to keep the distribution grids stable. That is shown by:

$$v_1(t) = v_{ref}. \tag{2.16a}$$

$$\overline{v} \leqslant |v_i(t)| \leqslant \underline{v}, \;\; \forall i \in \mathbb{N}_b \setminus \{1\}. \tag{2.16b}$$

CHAPTER 3

Non-Parametric Probabilistic Load and Solar Generation Modeling

One of the important steps in optimal load management is to estimate the generation, load demand and EV charging with acceptable accuracy. Those parameters are the stochastic random variables and the inputs to the optimal load management problem. Therefore, the accuracy of their model directly affects the optimization results. The probabilistic estimation is a strong tool to model the uncertain generation and loads. However, it is shown that the known probability density functions (i.e. Gaussian, Beta, Gamma, etc.) do not provide an accurate estimation, specifically for the load demand and EV charging.

In this chapter, the non-parametric kernel density estimation (KDE) is proposed for solar, load demand, and EV charging load estimation. To this end, the Gaussian KDE (GKDE) is first introduced, and its deficiencies are discussed. Afterward, the adaptive diffusion KDE (DKDE) is proposed to address those deficiencies [BGK10]. Before estimating the probabilistic model of the solar generation and load demand, the clustering methods should be used to only choose the data history which has more similarities with the prediction time horizon. Therefore, k-means clustering is introduced in this chapter, as well. In order to evaluate the performance of GKDE and DKDE and compare their estimation accuracy, they are applied to the real datasets, and the results are discussed.

3.1 Gaussian Kernel Density Estimation

In kernel density estimation, given an observed dataset $\mathbf{X} = [X_1, X_2, ..., X_N]$, where $X_i \in \mathbb{R}^d, \forall i \in \{1, \cdots, N\}$ and $\mathbf{X} \in \mathbb{R}^{d \times N}$, its p.d.f can be estimated as follows [Cri16]:

$$\hat{f}_x(x;t) = \frac{1}{N}\sum_{i=1}^{N} Kr(x, X_i; t), \tag{3.1}$$

where $\hat{f}_x$ is the estimated p.d.f., $Kr(\cdot)$ is the Gaussian kernel function, and $\sqrt{t}$ is its bandwidth. The kernel function is defined by:

$$Kr(x, X_i; t) = \frac{1}{\sqrt{2\pi t}} \exp(-\frac{(x - X_i)^2}{2t}). \tag{3.2}$$

The bandwidth $\sqrt{t}$ defines the shape of the kernel function, therefore it is a deterministic factor to the performance of the estimator. A large $\sqrt{t}$ oversmoothes the density function that masks the structure of data, while a small $\sqrt{t}$ generates a spiky one that makes the interpretation difficult. It is desired to find the value of t that minimizes the error between the estimated density and the actual density. However, there is a bias-variance trade-off for the bandwidth selection, which means a large bandwidth reduces the variance of $\hat{f}_x$ but increases the bias with respect to the actual density. On the other hand, a small bandwidth decreases the bias of $\hat{f}_x$ at the expense of a larger variance. Silverman's rule of thumb [Sil86], also known as the normal reference rule, provides a simple solution for the optimal bandwidth ($\sqrt{t}^*$) calculation, with the assumption that the actual density has Gaussian normal distribution:

$$\sqrt{t}^* \approx 1.06\ \sigma N^{-\frac{1}{5}}, \tag{3.3}$$

where σ is the standard deviation of N training observations. Silverman's rule usually leads to an oversmoothed p.d.f in multi-modal models as it assumes that the true density has a Gaussian normal distribution.

3.2 Diffusion Kernel Density Estimation

Different from the normal reference rule, the optimal bandwidth can be derived from the observed dataset $\mathbf{X}$ using an improved plug-in method introduced in [BGK10].

As shown by the authors in [BGK10], GKDE (3.1) is the unique solution to the Fourier heat equation as follows [BGK10]:

$$\frac{\partial}{\partial t} f'(x;t) = \frac{1}{2}\frac{\partial^2}{\partial x^2} f'(x;t), \quad x \in \mathbf{X}, \quad t > 0, \tag{3.4}$$

with initial condition:

$$f'(x;0) = \frac{1}{N}\sum_{i=1}^{N} \delta(x - X_i), \tag{3.5}$$

where $f'(x;0)$ represents the empirical density of $\mathbf{X}$, and $\delta(x - X_i)$ is the Dirac measure at X_i. The Neumann boundary condition to solve the diffusion equation (3.4) is as follows:

$$\frac{\partial}{\partial x} f'(x;t)|_{x=X_l} = \frac{\partial}{\partial x} f'(x;t)|_{x=X_u} = 0, \tag{3.6}$$

where X_l and X_u are, respectively, the lower and upper bounds of the domain. Exploiting the link between GKDE and the Fourier heat equation, finding the optimal bandwidth of (3.1) is equivalent to finding the optimal mixing time t^* of the diffusion process governed by (3.4) [Bot07]. Considering those conditions and the finite domain $[0, 1]$ (i.e. $X_l = 0$, $X_u = 1$), the analytical solution of (3.4) is obtained by:

$$\hat{f}(x;t^*) = \frac{1}{N}\sum_{i=1}^{N} \kappa(x, X_i; t^*), \quad x \in [0,1], \tag{3.7}$$

in which the kernel function is given by:

$$\kappa(x, X_i; t^*) = \sum_{k=-\infty}^{\infty} Kr(x, 2k + X_i; t^*) + Kr(x, 2k - X_i; t^*), \quad x \in [0,1]. \tag{3.8}$$

Although both estimators (3.1) and (3.7) behave similarly in the interior of the domain $[0, 1]$ for a small bandwidth, (3.7) shows a better performance near the boundaries where $x \in \{0, 1\}$. The reason is that DKDE is consistent with the true density while GKDE is inconsistent at the boundaries [BGK10]. For further clarification, two conditions are considered as follows.

1. The behavior of $\kappa(x, X_i; t)$ for the small bandwidth, $t \to 0$, $x \in [0, 1]$, is similar to the asymptotic behavior of (3.1):

$$\sum_{k=-\infty}^{\infty} Kr(x, 2k + X_i; t) + Kr(x, 2k - X_i; t) = \kappa(x, X_i; t). \tag{3.9}$$

2. For the large bandwidth, $t \to \infty,\ x \in [0,1]$, the behavior of DKDE is equivalent to:

$$\begin{aligned}\kappa\left(x, X_i; t\right) &\sim \sum_{k=-\infty}^{\infty} e^{-k^2\pi^2 t/2} cos(k\pi x) cos(k\pi X_i) \\ &\sim 1 + 2e^{-\pi^2 t/2} cos(\pi x) cos(\pi X_i),\end{aligned} \tag{3.10}$$

which means $\kappa\left(x, X_i; t\right)$ approaches the uniform density when the bandwidth becomes larger.

Accordingly, (3.8) can be approximated by:

$$\hat{f}\left(x; t\right) \approx \sum_{k=0}^{n} a_k e^{-k^2\pi^2 t/2} cos\Big(\frac{(2\mathbf{i}+1)k\pi}{2n}\Big), \tag{3.11}$$

where $n \in N$ is the number of segments which $\mathbf{X}$ is split by the bandwidth $\sqrt{t}$, and a_k is given by:

$$a_k = \begin{cases} 1 & k = 0 \\ \frac{2}{N}\sum_{i=1}^{N} cos(k\pi X_i), & k \in \{1, \cdots, n-1\}. \end{cases} \tag{3.12}$$

The coefficient a_k can be calculated by:

$$a_k = \alpha(k) \sum_{j=0}^{n-1} b(j) cos\Big(\frac{(2\mathbf{i}+1)\pi k}{2n}\Big), k \in \{1, \cdots, n-1\}, \tag{3.13}$$

where $b(j)$ denotes the probability that X_i is in the interval $[\frac{j}{n}, \frac{j+1}{n}]$, and:

$$\alpha(0) = 1,\ \alpha(k) = 2\ \forall k \in [1, \cdots, n-1]. \tag{3.14}$$

Finally, t^* using the plug-in method in [BGK10] is obtained by:

$$t^* = \left(\frac{6\sqrt{2}-3}{7}\right)^{2/5} \gamma^{[l]}(t), \tag{3.15}$$

in which [XYX15]

$$\gamma^{[l]}(t) = \gamma_1(\cdots \gamma_{l-1}(\gamma_l(t)) \cdots),\ l \geq 1, \tag{3.16}$$

and

$$\gamma_l(t) = \left(\frac{2\left(1 + (1/2)^{(l+1/2)}\right)(1 \times 3 \times \cdots (2l-1))}{3N\sqrt{\pi/2}\Big(\sum_{k=l}^{n-1}(k\pi)^{(2l+2)} a_k^2 e^{-k^2\pi^2 t}\Big)}\right), \tag{3.17}$$

where $l = 5$ in this paper as recommended by [BGK10].

3.3 Netload Clustering

In data mining, clustering is the general task of dividing a set of objects in the groups within each the objects show more similarity to each other than those in other groups. In order to achieve a better model estimation using KDE methods, the solar generation and daily load profiles with more similar features should be used for training. Therefore in this section, k-means clustering, more specifically its improved version known as k-means^{++}, is used to cluster the data set into several groups. In the following subsections, k-means and k-means^{++} are introduced, and the methods finding the optimal number of clusters are discussed.

3.3.1 *k*-Means Clustering

k-means is an unsupervised learning method which is utilized for clustering the data set including unlabeled data points. Considering the data set $\mathbf{X} \subset \mathbb{R}^{d\times N}$, the object is to find a set of $K \in \mathbb{N}$ centers, $\mathbf{C} = \{C_1, \cdots, C_K\}, \mathbf{C} \subset \mathbb{R}^{d\times K}$, which minimizes the potential function defined as follows:

$$\hat{\phi} = \sum_{X\in\mathbf{X}} \min_{C\in\mathbf{C}} \|X - C\|_2^2. \tag{3.18}$$

Using the obtained center set $\mathbf{C}$, K clusters can be formed around K center points. Each cluster includes a center point and the data points which their distance to the cluster's center point is less than their distance to the other clusters' center points. The procedure of clustering the dataset starts by choosing the initial center pints uniformly at random from $\mathbf{X}$. The algorithm is shown in Algorithm 1 where $\mathbb{G}_i$ is the ith cluster which its cardinality is denoted by $\mathcal{G}_i$. The closest center point to the jth X is denoted by $C_{X_j}^D$, and the distance between them is denoted by $\hat{\phi}_{X_j}$, i.e. $\hat{\phi}_{X_j} = \min\{\hat{\phi}_{(X_j,C_1)}, \cdots, \hat{\phi}_{(X_j,C_K)}\}$, in which $\hat{\phi}_{(X_j,C_i)} = \|X_j - C_i\|_2^2$.

Although $\hat{\phi}$ is monotonically decreasing, there are only K^d possible choices for the clusters, and the iterative process (Algorithm 1) always terminates, k-means may terminate at the points which are not appropriate centers. To address this issue and make the algorithm faster, k-means^{++} is proposed [AV07].

Algorithm 1: k-means clustering.

Initilize: Choose $\mathbf{C}^l \subset \mathbb{R}^{d\times N}$ initial set of center points.
while $\mathbf{C}^{l+1} \neq \mathbf{C}^l$ **do**
  for $i = 1 : K$ **do**
    Set the cluster $\mathbb{G}_i = \left\{\forall X_j \in \mathbf{X} | C^D_{X_j} = C_i\right\}$.
  end
  for $i = 1 : K$ **do**
    $C_i = \frac{1}{\mathcal{G}_i} \sum_{X_j \in \mathbb{G}_i,} X_j$.
  end
end

3.3.2 k-means^{++} Clustering

By weighting the data points using their squared distance from the closest center point, the authors in [AV07] introduce k-means^{++} clustering. Seeding the center points using the weighted data points and augmenting the technique in k-means, it shows faster convergence and less potential functions which means the clusters are optimal. Algorithm 2 shows the augmented steps which significantly improve the clustering results [AV07].

According to the better clustering results reported in the literature for k-means^{++}, it is used in this dissertation for the data clustering before applying KDE methods.

3.3.3 Fining Optimal K

According to the algorithms described in the preceding subsections, the first step of k-means clustering method and its variant is to choose K center points. However, we have not discussed how many center pints should be chosen. Although there is no specific mathematical solution to choose the optimal value of K, there are two popular approaches called *Elbow* criterion and *Silhouette* coefficient which have been shown useful.

In the *Elbow* criterion approach, the potential function (3.18) is calculated for different values of K within each cluster. That is, the total within-cluster sum of square (WCSS)

Algorithm 2: k-Means^{++} clustering.

Initilize: Choose $C_1^l \subset \mathbb{R}^{d\times N}$ uniformly at random.
for $i = 2 : K$ **do**
  Choose $C_i^l = X_j$ with probability $\frac{\min\{\hat{\phi}_{(X_j,C_1)},\cdots,\hat{\phi}_{(X_j,C_{i-1})}\}}{\sum_{X\in\mathbb{X}}\min\{\hat{\phi}_{(X,C_1)},\cdots,\hat{\phi}_{(X,C_{i-1})}\}}$.
end
while $\mathbf{C}^{l+1} \neq \mathbf{C}^l$ **do**
  for $i = 1 : K$ **do**
    Set the cluster $\mathbb{G}_i = \left\{\forall X_j \in \mathbf{X} | C_{X_j}^D = C_i\right\}$.
  end
  for $i = 1 : K$ **do**
    $C_i = \frac{1}{\mathcal{G}_i}\sum_{X_j\in\mathbb{G}_i,} X_j$.
  end
end

value is computed. As the maximum possible number for K is equal to N, increasing K monotonically decreases the potential function value. However, the goal is to choose a small value for K while the potential value has also an acceptable small value. Plotting the potential function for different K values, the optimal choice is the point where the potential function does not change considerably, which is also called the *knee point*.

The *Silhouette* coefficient approach shows how similar the data points in a cluster are to the other points in its cluster comparing to the other clusters. Let us denote the average dissimilarity of each data point ($X_j \in \mathbb{G}_i$) to all the data points is other clusters ($X_{j'} \in \mathbb{C}_{i'}, i' \neq i$) by $\overline{\phi}^b_{X_j}$, i.e.:

$$\overline{\phi}^b_{X_j} = \min_{i\neq i'} \frac{1}{|\mathcal{G}_{i'}|}\sum_{j'\in\mathbb{G}_{i'}} \sqrt{\phi_{(X_j,X_{j'})}}. \tag{3.19}$$

Also, let us denote the average dissimilarity of each data point ($X_j \in \mathbb{G}_i$) to all other points in the same cluster ($X_{j'} \in \mathbb{G}_i, j \neq j'$) by $\overline{\phi}^a_{X_j}$, i.e.:

$$\overline{\phi}^a_{X_j} = \frac{1}{|\mathcal{G}_{i'}| - 1}\sum_{j'\in\mathbb{G}_i} \sqrt{\phi_{(X_j,X_{j'})}}. \tag{3.20}$$

The *Silhouette* coefficient for $X_j \in \mathbb{G}_i$ denoted by Sil_{X_j} is obtained by:

$$Sil_{X_j} = \frac{\overline{\phi}^b_{X_j} - \overline{\phi}^a_{X_j}}{\max\{\overline{\phi}^b_{X_j}, \overline{\phi}^a_{X_j}\}}. \tag{3.21}$$

If the *Silhouette* coefficient is:

- equal to 1, the number of clusters is optimum.
- equal to 0, there is overlapping between the clusters.
- equal to -1, the data point is wrongly assigned to the cluster.

We use the *Elbow* criterion method in the following section to find the optimal number of clusters for netload and solar generation estimation.

3.4 Probabilistic Estimation Results

In this section, the KDE methods (GKDE and DKDE) described in the preceding sections are applied to the probabilistic netload, solar energy, and EV load modeling. For the netload and solar energy, the historical data is first clustered using k-means^{++} method to group the days with similar features. To compare the accuracy of GKDE and DKDE, the mean absolute percentage error (MAPE) and the root-mean-square error (RMSE) are calculated. MAPE is defined as:

$$\text{MAPE} = \frac{100\%}{N} \sum_{t=1}^{N} \left| \frac{\hat{F}_t - F_t}{\hat{F}_t} \right|, \tag{3.22}$$

where $\hat{F}$ is the estimated value obtained by GKDE or DKDE, F is the observed data, and N is the number of estimated values. RMSE is defined as:

$$\text{RMSE} = \sqrt{\frac{1}{N} \sum_{t=1}^{N} \left(\hat{F}_t - F_t\right)^2}. \tag{3.23}$$

3.4.1 Netload Estimation

Considering the daily load profiles, five features can be obtained for each profile which help group the historical data. These five features are: (1) the minimum load demand from

midnight until noon (MinAMP), (2) the minimum load demand from noon until midnight (MinPMP), (3) the maximum load demand from midnight until noon (MaxAMP), (4) the maximum load demand from noon until midnight (MaxPMP), and (5) the total load energy demand (TEC) during the day. The correlation between these features is shown in Fig. 3.1. As the correlation values are small, the features can be used effectively to cluster the daily load profiles.

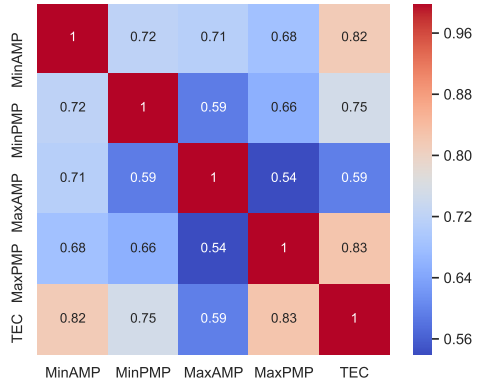

Figure 3.1: Correlation map of the daily load profile features.

Before clustering the daily load profiles, WCSS values are computed for different numbers of clusters which are shown in Fig. 3.2. According to the results, the daily load profiles are divided into 3 groups shown in Fig. 3.3.

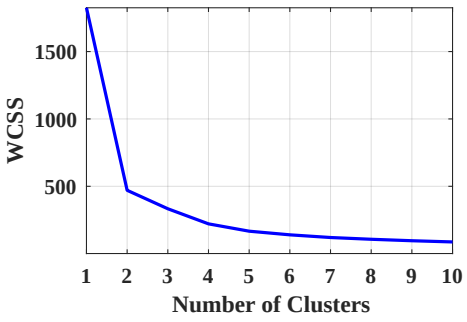

Figure 3.2: WCSS values for various number of daily load profile clusters.

The MAPE and RMSE results for the netload clusters are shown is Table 3.1. Comparing the results, DKDE has a better accuracy owing to its optimal bandwidth selection.

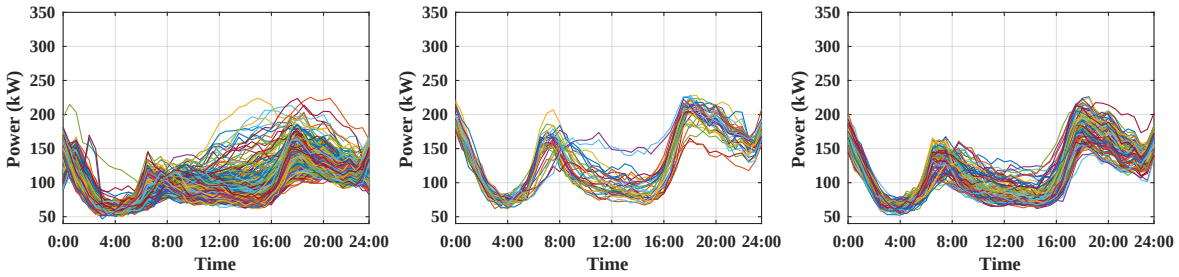

Figure 3.3: Daily load profile clusters, from left to right respectively: cluster#1, cluster#2, and cluster#3.

Table 3.1: MAPE and RMSE results for netload estimation obtained by GKDE and DKDE.

	MAPE			RMSE		
Cluster#	GKDE	DKDE	Improvement (%)	GKDE	DKDE	Improvement (%)
1	17.5	16.4	6.3	0.109	0.105	3.2
2	18.55	16.67	10	0.045	0.041	5.9
3	16.47	15.21	7.6	0.099	0.094	4.6

3.4.2 Solar Generation Estimation

To cluster the daily solar energy generation, four features are considered which are: (1) the duration of solar energy availability (PD), (2) the maximum solar power (MaxP), (3) the time of the maximum solar power (TMaxP), and (4) the total solar energy generation during the day (TotP). The correlation between these features is shown in Fig. 3.4. The correlation values are fairly small meaning that they can provide the promising clustering results.

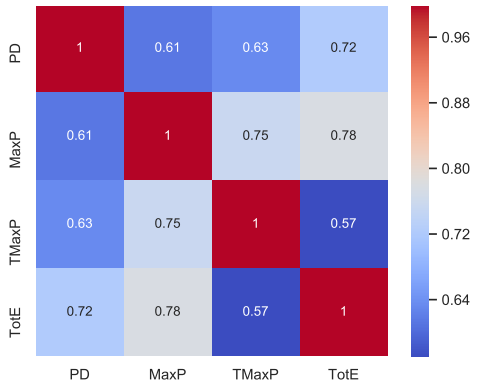

Figure 3.4: Correlation map of the daily solar generation profile features.

WCSS values are computed for different numbers of clusters, and they are shown in Fig. 3.5. According to the results, the daily solar generation profiles are divided into 4 groups shown in Fig. 3.6.

Figure 3.5: WCSS values for various number of daily solar generation clusters.

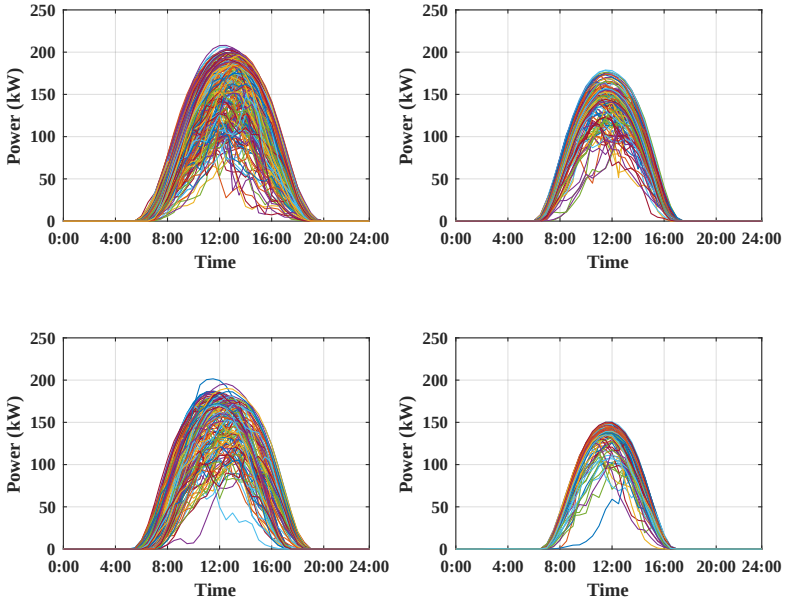

Figure 3.6: Daily solar generation profile clusters.

According to the MAPE and RMSE results shown in Table 3.2, DKDE outperforms GKDE as the adaptive diffusion method finds the optimal bandwidth, while the Silverman's rule of thumb results in an oversmoothed estimation.

Table 3.2: MAPE and RMSE results for solar generation estimation obtained by GKDE and DKDE.

	MAPE			RMSE		
Cluster#	GKDE	DKDE	Improvement (%)	GKDE	DKDE	Improvement (%)
1	22.54	17.37	23	0.096	0.06	37
2	25.70	16.23	37	0.156	0.099	37
3	23.58	14.47	38	0.153	0.112	27
4	23.92	14.41	40	0.152	0.11	27

3.4.3 EV Load Estimation

For the EV load estimation, three random variables should be modeled which are the arrival time, stay duration, and required charging energy. These random variables are estimated for each individual EV owner. The available dataset to apply GKDE and DKDE includes 240 EV owners.

The MAPE and RMSE results for the estimation of the EV load parameters are shown is Table 3.3. As it is expected, DKDE improves the estimation for arrival time, stay duration and charging energy comparing to GKDE.

Table 3.3: MAPE and RMSE results for the estimation of the EV load parameters by GKDE and DKDE.

	MAPE			RMSE		
Estimated Parameter	GKDE	DKDE	Improvement (%)	GKDE	DKDE	Improvement (%)
Arrival Time	24.34	18.99	22	0.089	0.065	27
Stay Duration	98.4	79.4	19.2	0.078	0.039	49
Charging Energy	30.33	11.69	61	0.1146	0.067	41

3.5 Conclusion

In this chapter, two non-parametric probabilistic methods based on kernel density estimation, namely Gaussian KDE and diffusion KDE, have been proposed. Comparing to GKDE, DKDE provides a more accurate estimation on the boundaries owing to its optimal bandwidth selection. The performance of the methods has been evaluated using real netload,

solar energy, and EV load parameters data. For the netload and solar energy generation, the historical data has been first clustered using k-means^{++} clustering to group the load and generation profiles with similar features. Applying GKDE and DKDE, it was shown that DKDE can improve the model estimation accuracy at least 6.3% (MAPE) and 3.2% (RMSE) for netload, and 23% (MAPE) and 27% (RMSE) for solar generation. In addition, both methods applied to EV data to estimate the arrival time, stay duration and charging energy of 240 EV owners. The results showed significant estimation improvement specifically for the charging energy.

CHAPTER 4

Battery Energy Storage for Electric Vehicle Charging Station: Implementation and Emulation

In this chapter, the integration of BESS in an EV charging infrastructure is studied. The purpose of BESS integration here is to reduce the charging cost by shifting the load profile and providing peak shaving. To this end, optimal coordination of BESS charging and discharging with the consideration of EV charging load demand, availability of local energy resources such as solar energy, and the electricity price is of vital importance.

The chapter is presented through two main sections: implementation and emulation.

Implementation: The purpose of the implementation is to show the effectiveness of BESS in shaving the excess power demand in the public ECIs. In addition, the BESS can increase the resiliency of ECI in the case of a failure in the distribution grid which results in blackout or load shedding. In most of the public stations currently available to EV owners, EV charging load control has not been implemented as it needs a secure communication, monitoring system, and efficient controllers. In these facilities, the integration of BESS (with local solar energy resources) gives the ECI the capability to manage the fluctuations and undesirable peak power demands by optimal control of the BESS charging and discharging. The implementation section discusses the details of BESS integration in the Civic Center Public Parking, in the City of Santa Monica, and validates the performance of BESS in shaving the peak load and increasing the resiliency.

Emulation: The purpose of this section is to utilize the probabilistic modeling approach proposed in Chapter 3, i.e. DKDE, for optimal BESS control. In this section, the model of

the aggregated ECI power, which includes the building load, solar power, and EV charging demand, is derived. Afterward, due to the stochasticity of the aggregated ECI power, a Monte Carlo Simulation (MCS) method, more specifically sample average approximation (SAA), is used to solve the stochastic BESS control optimization problem.

The contributions of this chapter are as follows:

1. A mobile battery energy storage (MBESS) setup is developed to provide peak load shaving and emergency power to EV charging stations. The experimental results for the MBESS integration in a public charging station are shown and possible applications are discussed.

2. A stochastic charging/discharging method is developed for BESS integration in the commercial ECIs. The proposed method is based on the non-parametric probability model of the stochastic parameters and MCS method.

4.1 Battery Energy Storage Implementation

MBESS setup includes the multi-module battery energy storage, the bi-directional inverter connecting BESS to the grid and load, the power transformer providing appropriate AC voltage level, as well as the measurement, communication, and monitoring devices. Those components are described in the following, and the collected real data showing the operation of MBESS in different modes are visualized.

4.1.1 Battery Storage Module

In the first phase of our project, a BESS with 2.2 kWh energy capacity including 17 battery cells connected in series was set up, which was able to provide 48 VDC nominal voltage. Each battery cell has a nominal voltage of 3.2 VDC and a nominal capacity of 128 Wh. In order to facilitate the transportation of the battery, the BESS setup with its circuit breaker were installed in a small box Fig. 4.1, called mobile battery module. Through the second phase of the project, the capacity of BESS was scaled up to 8.7 kWh by connecting 3 more

BESS setups in parallel and mounting them on a cart together with the other components as shown in Fig. 4.1.

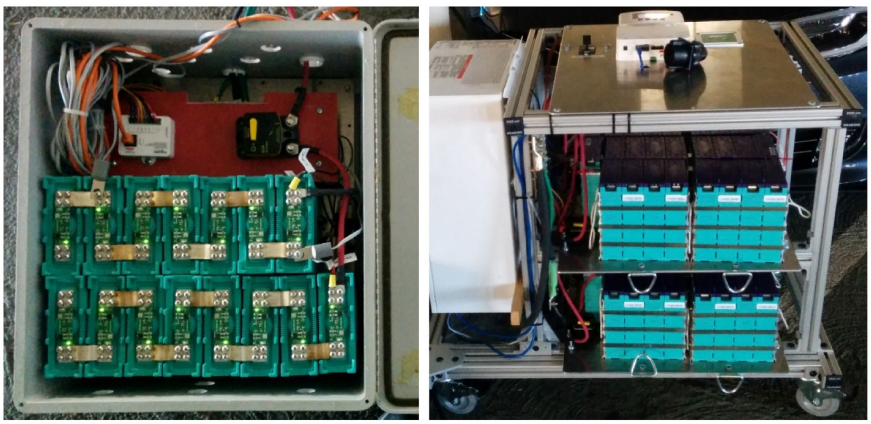

Figure 4.1: Mobile BESS: 2.2 kWh (left), 8.7 kWh (right).

4.1.2 Bi-directional Inverter

BESS and EV charger (as the load) are connected to the main AC distribution grid through a bi-directional inverter Fig. 4.2. The AC supply voltage of the inverter is 240 VAC (phase to phase) and 120 VAC (phase to neutral) with the nominal power rating of 6.8 kW. The DC voltage range is 40-64 VDC (nominal voltage 48 VDC), and the maximum DC current is 140 A. The bi-directional inverter is the interface of BESS with the load as well as the distribution grid, and it communicates with them through the Xanbus protocol [Xana, Xanb].

4.1.3 Power Transformer

The bi-directional inverter used in the setup works only with 240 VAC (phase to phase) as the grid supply. Since the power supply is provided by a commercial 3-phase system, only 208 VAC (phase to phase) voltage is available. Therefore, a 208/240 power transformer is utilized to connect the inverter with the distribution grid. Also, a portable frame, shown in Fig. 4.3 was designed to facilitate its transportation from SMERC lab to the project location.

Figure 4.2: 6.8 kW bi-directional inverter (MBESS charger).

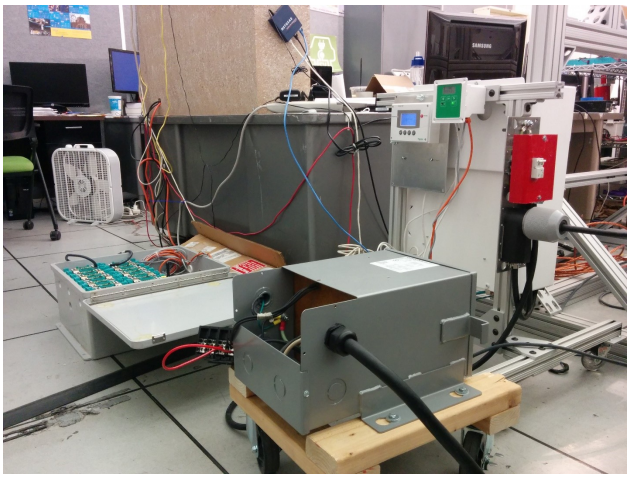

Figure 4.3: 208/240 VAC power transformer.

4.1.4 Measurement and Communication Devices

The BESS voltage and current are measured by Conext Battery Monitor module Fig. 4.4 (on the left) which is able to calculate the state of the charge (SOC), temperature, and voltage imbalance between the paralleled battery cells. A user can communicate with the inverter to monitor its operation and change its internal settings by ComBox module Fig. 4.4 (on the right).

Figure 4.4: Conext and ComBox, measurement and communication devices of MBESS.

4.1.5 Monitoring Interface

The operation of MBESS can be monitored on a computer which is connected to the ComBox module through the Ethernet cable. The interface shows the power flow directions among the grid, battery, and load, as well as their corresponding voltages and currents Fig. 4.5. It also gives the option to store all the measurements by the rate of 1 sample per 5 seconds on an SD card.

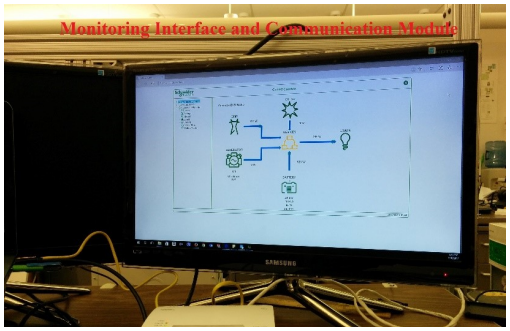

Figure 4.5: MBESS monitoring interface.

4.1.6 Communication Layout

The communication network is a collection of Xanbus-enabled devices which operate individually while interacting with each other through the Xanbus network. In MBESS setup, the components of the Xanbus network are the bi-directional inverter, battery monitoring module, Conext, ComBox, and the system control panel. Those devices are connected together in a series configuration, called daisy chain Fig. 4.6 [Xanb]. Each device is linked with a separate Category 5 (CAT) cable, and two network terminators are required at each

end of the chain to ensure the communication signal quality. The main advantage of this network configuration is its affordability as no network connector is required.

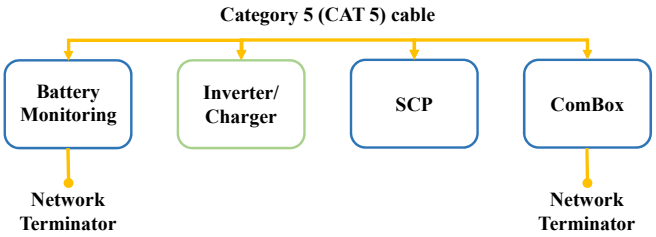

Figure 4.6: Layout of the communication links between the MBESS Xanbus-enable devices.

4.1.7 Electrical Layout

The inverter is the interface of MBESS with the EV charger and the distribution grid. It is able to charge the battery when its voltage is less than a user-defined value, and discharge the battery to supply the load or support the grid if the voltage of the battery is greater than a user-defined threshold. The electrical layout of the inverter, BESS, and the EV charger is shown in Fig. 4.7. As it is seen, the inverter is not connected to the grid directly. The reason is that 240 VAC (phase to phase) voltage is required by the inverter, as discussed (Subsection 4.1.3), while the available 2-phase voltage from the grid is 208 VAC (phase to phase). Therefore, the power transformer is connected between the grid and the inverter and provides the required nominal 2-phase AC voltage.

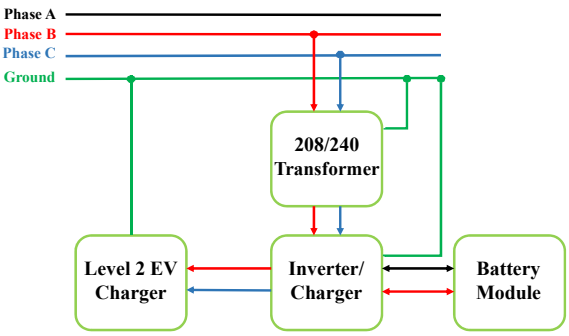

Figure 4.7: Layout of the electrical connection of MBESS with the EV charging system and AC distribution grid.

4.1.8 Operation Modes

Three modes are defining the operation of MBESS based on the voltage of BESS, load current, grid status (if grid supply exists), and the time of the day. Those modes are described in the following.

Mode$_1$- Charging BESS & Supplying Load: In the first mode, the grid charges BESS and supplies the EV charger (load) simultaneously. The power received from the grid is equal to the total power charging the battery storage and supplying the EV charger. For the inverter to start charging the battery storage, there are two conditions which should be met (Fig. 4.8). The first condition relates to the voltage level of the battery, and the second one relates to the time of the day. That is, if the battery voltage (V_{batt}) is less than a threshold (V_{th1}), and the time is between *Chg Block Start* and *Chg Block Stop*, which define the time to stop battery charging and the time to allow charging, respectively, the inverter starts charging BESS.

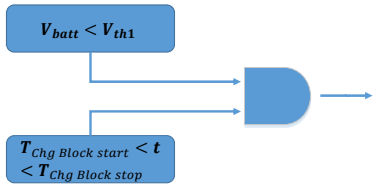

Figure 4.8: Logic diagram for the inverter to start charging BESS- Mode$_1$.

The inverter stops charging the battery if either the charging current ($I_{batt-chg}$) is less than a threshold (I_{th1}) or the charging duration (d_{chg}) becomes larger than a threshold (d_{th}) (Fig. 4.9).

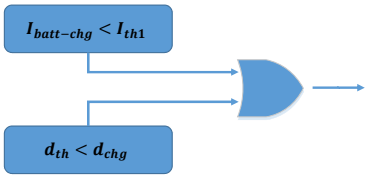

Figure 4.9: Logic diagram for the inverter to stop charging BESS- Mode$_1$.

Mode$_2$- Peak Load Shaving: In the second mode, MBESS provides peak load shaving to reduce electricity cost. It means that the EV charger load is supplied by both the distribution system and BESS, so the energy received from the grid decreases. MBESS starts peak load shaving when the BESS voltage is greater than a user-defined threshold (V_{th2}), the load current (I_L) is greater than a user-defined value (I_{th2}), and the time is within a user-defined period defined by *Load Shave Start* and *Load Shave Stop*. The logic diagram showing the peak load shaving operation mode is displayed in Fig. 4.10.

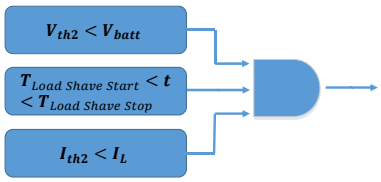

Figure 4.10: Logic diagram for MBESS to provide peak load shaving- Mode$_2$.

Mode$_3$- Islanded Operation: In the third mode, MBESS is disconnected from the AC distribution system (islanded) and supplies the EV charger. To operate in the islanded mode, three conditions should be satisfied simultaneously Fig. 4.11: the BESS voltage should be larger than a threshold (V_{th3}), the grid voltage should be less than a threshold (V_{th4}) meaning that there is no power available from the grid, and the load current (I_L) should be larger than a value (I_{th2}) showing that there is a load to be supplied.

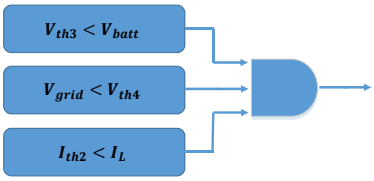

Figure 4.11: Logic diagram for MBSES to supply the load in islanded mode- Mode$_3$.

4.1.9 Experimental Results

The MBESS setup has been tested on the Civic Center parking structure in the City of Santa Monica. The load terminals of the inverter are connected to a level-2 EV charger, and the data is collected for around 1 hour. The measurement samples are recorded every 5 seconds. The results illustrated in Fig. 4.12 show the operation of MBESS in three modes. In the first mode (blue area), there is no load in the system, but the conditions for the inverter to charge BESS are met, therefore BESS is charger by the power from the grid. In the second mode (green area), an EV is plugged in, therefore the power from the grid is charging both BESS and EV simultaneously. In the last mode (grey area), there is no power supply from the grid. However, BESS is capable to supply the EV charger since its voltage (V_{batt}) is more than the defined threshold (V_{th3}). As described earlier, the operation of MBESS in this mode is called islanded mode. The fact that the MBESS setup can provide power to the EV charging station during the outage in the distribution grid verifies increasing the resiliency. Islanded operation mode is specifically desirable when in an emergency situation EV should be charged while there is not power supply from the grid.

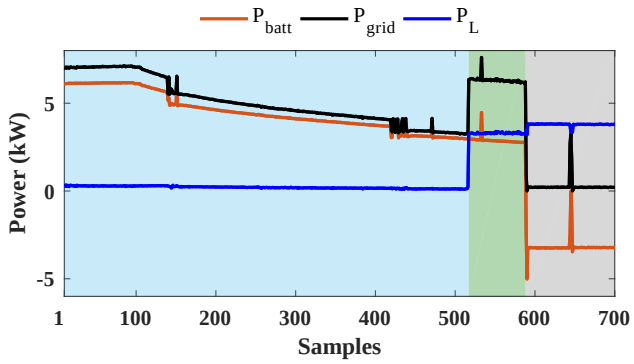

Figure 4.12: Experimental results for the operation of MBESS supplying an EV charging infrastructure..

4.2 Battery Energy Storage Emulation: Stochastic Optimization

In this section, the model of a grid-connected microgrid (μG) consisting of a building (commercial or residential), the uncontrolled EV chargers, PV panels, and BESS is presented. The purpose is to design an optimal BESS charging/discharging method which minimizes the electricity cost of the μG or its total load variations. As the building load, the EV charging demand, and the PV power generation are random variables (RVs), we are dealing with a stochastic optimization problem. To make the problem tractable, SAA which is a distribution-free MCS method is utilized. To generate the scenarios for the stochastic load and generation, DKDE which is introduced in Section 3.2 is used.

4.2.1 Model Description and Problem Formulation

As we consider only the active power of the building load here, instead of the model developed in Section 2.1, we slightly modify the EV model described in Section 2.2 and use it for BESS as follows:

$$c^{bs}(t+1) = \alpha^{bs} c^{bs}(t) + T_d\big(\eta^{bs^+} p^{bs^+}(t) + p^{bs^-}(t)/\eta^{bs^-}\big) \tag{4.1a}$$

$$p^{bs}(t) = p^{bs^+}(t) + p^{bs^-}(t), \tag{4.1b}$$

subjected to the constraints:

$$0 \leqslant p^{bs^+}(t) \leqslant \overline{p}^{bs} \tag{4.2a}$$

$$\underline{p}^{bs} \leqslant p^{bs^-}(t) \leqslant 0 \tag{4.2b}$$

$$0 \leqslant \frac{p^{bs^-}(t)}{\underline{p}^{bs}} + \frac{p^{bs^+}(t)}{\overline{p}^{bs}} \leqslant 1, \tag{4.2c}$$

$$\underline{C}^{bs}(t) \leqslant c^{bs}(t) \leqslant \overline{C}^{bs}(t), \tag{4.2d}$$

in which, the definition of parameters is similar to Sections 2.1 and 2.2.

μG can either receive or inject power from/to the grid, and its exchanged power is limited by the following constraint:

$$\underline{p}^{\mu G} \leqslant p^{\mu G}(t) \leqslant \overline{p}^{\mu G}, \ \forall t \in \mathbb{N}. \tag{4.3}$$

We can write $p^{\mu G}(t)$ as the aggregated power of the PV panels, EV charging, building load, and BESS as follows:

$$p^{\mu G}(t) = p^{bs}(t) + p^{bl}(t, \xi^{bl}) + p^{pv}(t, \xi^{pv}) + p^{aev}(t, \xi^{aev}),\ \forall t \in \mathbb{N}, \tag{4.4}$$

in which, $p^{\mu G} \in \mathbb{R}$ is the total power of μG, p^{bs} is already defined in Section 2.1, and p^{bl}, p^{pv}, and $p^{aev} \in \mathbb{R}$ are the building load demand, PV panel power, and the aggregated EV charging load, respectively. ξ^{bl}, ξ^{pv}, and ξ^{aev} denote, respectively, the uncertainty set of the building load, PV generation, and aggregated EV charging demand. To reduce the computation burden of the scenario generation, we define an aggregated RV as follows:

$$p^{bpe}(t, \xi) = p^{bl}(t, \xi^{bl}) + p^{pv}(t, \xi^{pv}) + p^{aev}(t, \xi^{aev}),\ \forall t \in \mathbb{N}, \tag{4.5}$$

therefore (4.4) can be rewritten as:

$$p^{\mu G}(t) = p^{bs}(t) + p^{bpe}(t, \xi),\ \forall t \in \mathbb{N}. \tag{4.6}$$

The optimal BESS charging/discharging control (OBESC) with the objective function $\mathbf{F}^{\mu\mathbf{G}}$ is written as:

$$\begin{aligned} V_{\mu G} := \min_{\mathbf{p}^{\mu G}} \mathbb{E}[\mathbf{F}^{\mu G}(\mathbf{p}^{\mu G}, \mathbf{p}^{bpe})] \\ \text{s.t. } (4.1) - (4.6). \end{aligned} \tag{4.7}$$

in which, $\mathbb{E}[.]$ is the expected value.

4.2.2 Sample Average Approximation

As there is an RV in OBESC problem, deterministic methods can not be used directly. However, using SAA which is an MCS technique makes our stochastic optimization problem tractable. To this end, DKDE is used first to find a non-parametric distribution estimation for the RV, $\mathbf{p}^{bpe}$. Afterward, a large number of samples, called scenarios, are generated for each of which the optimization problem (4.7) is solved using deterministic methods. If an appropriate number of scenarios is generated, their average approaches to the expectation value [SDR09]. It should be noted that the average of the generated scenarios converges

to the expectation if the optimization variable is continuous and the random variables are independent and identically distributed (i.i.d). According to the model developed for μG, the optimization variable in (4.7) is continuous. Also, we have only one random variable ($p^{bpe}(t,\xi)$), and use DKDE to estimate its p.d.f instead of considering $p^{bl}(t,\xi^{bl})$, $p^{pv}(t,\xi^{pv})$, and $p^{aev}(t,\xi^{aev})$ separately. therefore SAA converges to the expectation value for our problem.

Algorithm 3 shows the application of SAA for OBESC. N_{it} denotes the number of iterations that the procedure is repeated, and N_{sc} denotes the number of scenarios generated at each iteration. $\mathbf{F}_{k,l}^{\mu G}$ shows the calculated optimal value at the lth scenario of the kth iteration, and $\mathbf{F}_{k}^{\mu G}$ denotes their average for the kth iteration. $\mathbf{F}_{opt}^{\mu G}$ is the expected optimal value for OBESC.

Algorithm 3: SAA procedure for OBESC.

Initialization: Set the values for $\mathbf{C}^{bs}(t=0)$, $\mathbf{C}^{bs}(t=N)$, N_{it}, N_{sc}
for $k = 1 : N_{it}$ **do**
  for $l = 1 : N_{sc}$ **do**
    Generate $p_{k,l}^{bpe}$ using DKDE.
    Solve (4.7).
    $\mathbf{F}_{k,l}^{\mu G} = F^{opt}$.
  end
  $\mathbf{F}_{k}^{\mu G} = \frac{1}{N_{sc}} \sum_{l=1}^{N_{sc}} \mathbf{F}_{k,l}^{\mu G}$.
end
$\mathbf{F}_{opt}^{\mu G} = \mathbb{E}[\mathbf{F}_{k}^{\mu G}]$

4.2.3 Numerical Simulation

In this subsection, OBESC is applied to a grid-connected μG shown in Fig. 4.13. The data sets for the solar energy and building load demand are collected from [Aus], and the aggregated EV charging profile is collected in the UCLA campus parking lots by SMERC.

The simulation parameters and the corresponding values are shown in Table 4.1.

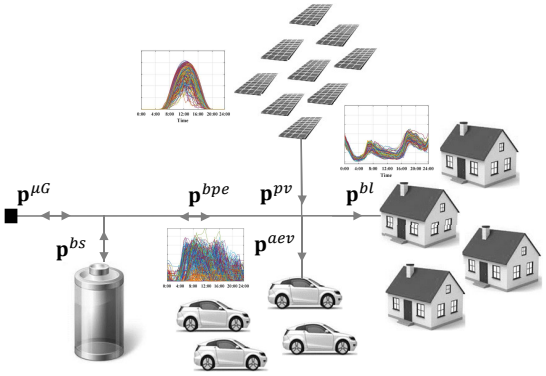

Figure 4.13: Grid-connected μG with BESS, PV panels and uncontrolled EV charging system.

Table 4.1: μG, BESS, and SAA simulation parameters.

Parameter	**Value**	**Parameter**	**Value**
$\overline{\mathbf{C}}^{bs}$	40 [kWh]	$\underline{\mathbf{C}}^{bs}$	4 [kWh]
$\overline{\mathbf{p}}^{bs}$	20 [kW]	$\underline{\mathbf{p}}^{bs}$	-20 [kW]
$\overline{\mathbf{p}}^{\mu G}$	30 [kW]	$\underline{\mathbf{p}}^{\mu G}$	-30 [kW]
$(\alpha^{bs}, \eta^{bs^+}, \eta^{bs^-})$	$(0.99, 0.95, 0.95)$	N	48
N_{it}	50	N_{sc}	$\{50, 100, 300, 500\}$

Two objective functions are defined to assess the effect of BESS on the μG operation. The first objective aims at cost reduction (CR), and the second one is to provide load variance minimization (LVM). CR function is defined by:

$$\mathbf{F}_{cr}^{\mu G}(\mathbf{p}^{\mu G}) := \mathbf{\Pi}^T.\mathbf{p}^{\mu G} \tag{4.8}$$

where $\mathbf{\Pi} \in \mathbb{R}^N$ is the wholesale electricity price from CAISO [CAI]. LVM function is defined as:

$$\mathbf{F}_{lvm}^{\mu G}(\mathbf{p}^{\mu G}) := \left\| \overline{\mathbf{\Omega}}^{\mu G} - \mathbf{p}^{\mu G} \right\|_2, \tag{4.9}$$

in which, $\overline{\mathbf{\Omega}}^{\mu G}$ is the average power of μG, and it is defined as:

$$\mathbf{\Omega}^{\mu G} := \frac{1}{N} \sum_{t=1}^{N} p^{\mu G}(t). \tag{4.10}$$

The aggregated load data (p^{bpe}) is clustered using the k-means^{++} clustering method. Then, DKDE is applied to model the optimization problem RV. For each cluster, OBESC problem is solved by Algorithm 3, and for different number of scenarios, the expected value of the objective function (Mean), its standard deviation (STD), and the computation time (CT) are calculated. For cluster#1, the results are shown in Table 4.2. As it is expected, increasing the number of scenarios increases CT but decreases STD. Also, CT in LVM problem is more than CR, as it takes a longer time to find the solution for a quadratic objective function comparing to a liner function.

Table 4.2: Expected value, STD, and CT for various number of scenarios- cluster#1.

N_{sc}	Mean_{CR}	STD_{CR}	ST_{CR} (sec)	Mean_{LVM}	STD_{LVM}	CT_{LVM} (sec)
50	23.08	0.243	850	22.90	0.639	1098
100	23.08	0.179	1704	22.96	0.475	2197
300	23.08	0.105	5092	22.93	0.299	6634
500	23.08	0.094	8481	22.93	0.217	10825

The μG and BESS powers for both CR and LVM optimization functions are shown in Fig. 4.14 and Fig. 4.15, respectively. Considering the BESS power in Fig. 4.14, charging and discharging depend on the energy price. That is, when the price is high, BESS supplies the load to decrease the peak power demand from the grid, while the grid charges BESS and supplies the load when the electricity price is low. Also comparing μG power in LVM with CR, BESS integration makes more capacity available for supplying additional load in LVM mode, while the μG power is close to the constraint defined in (4.3) in CR mode.

The Mean, STD, and CT results obtained for cluster#2 in both CR and LVM modes are shown in Table 4.3.

Table 4.3: Expected value, STD and CT for various number of scenarios- cluster#2.

N_{sc}	Mean_{CR}	STD_{CR}	ST_{CR} (sec)	Mean_{LVM}	STD_{LVM}	CT_{LVM} (sec)
50	18.79	0.246	836	11.13	0.573	1109
100	18.77	0.174	1682	11.19	0.378	2193
300	18.73	0.106	5089	11.19	0.202	6448
500	18.75	0.089	8448	11.20	0.179	10873

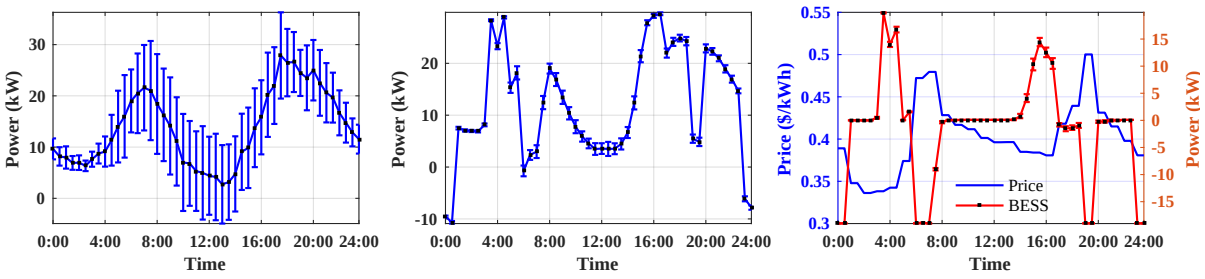

Figure 4.14: μG power without (left) and with (middle) BESS, electricity price and BESS power profile (right) for CR problem- cluster#1.

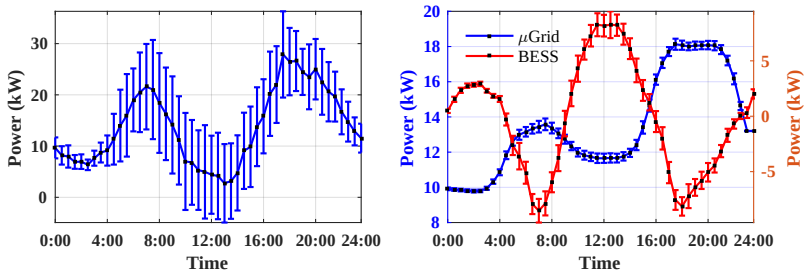

Figure 4.15: μG power without BESS (left), μG power with BESS and charging/discharging profile of BESS (right) for LVM problem- cluster#1.

The μG power without and with BESS as well as the charging/discharging profile of BESS for both CR and LVM modes which are obtained for cluster#2 are shown in Fig. 4.16 and Fig. 4.17, respectively. Comparing to cluster#1, the expected value for both optimization functions is smaller as the total load profile of μG has smaller peak loads and fluctuations.

The Mean, STD, and CT results obtained for cluster#3 in both CR and LVM modes are shown in Table 4.4.

Table 4.4: Expected value, STD and CT for various number of scenarios- cluster#3.

N_{sc}	Mean_{CR}	STD_{CR}	ST_{CR} (sec)	Mean_{LVM}	STD_{LVM}	CT_{LVM} (sec)
50	13.11	0.214	860	12.32	0.659	1073
100	13.12	0.133	1702	12.30	0.469	2171
300	13.12	0.079	4950	12.31	0.268	6431
500	13.13	0.058	8376	12.31	0.201	10633

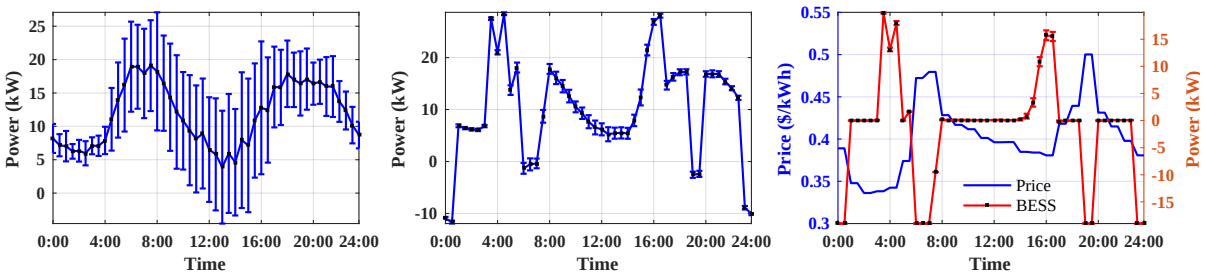

Figure 4.16: μG power without (left) and with (middle) BESS, electricity price and BESS power profile (right) for CR problem- cluster#2.

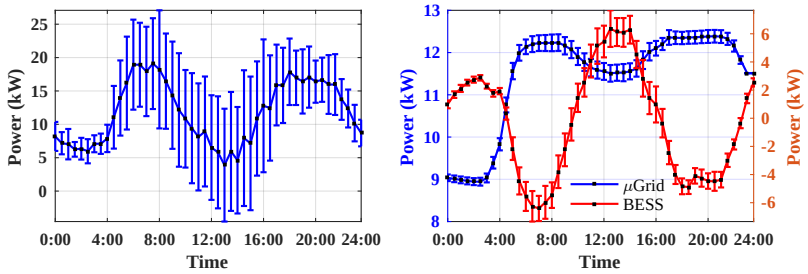

Figure 4.17: μG power without BESS (left), μG power with BESS and charging/discharging profile of BESS (right) for LVM problem- cluster#2.

The μG power without and with BESS as well as the charging/discharging profile of BESS for both CR and LVM modes which are obtained for cluster#3 are shown in Fig. 4.18 and Fig. 4.19, respectively.

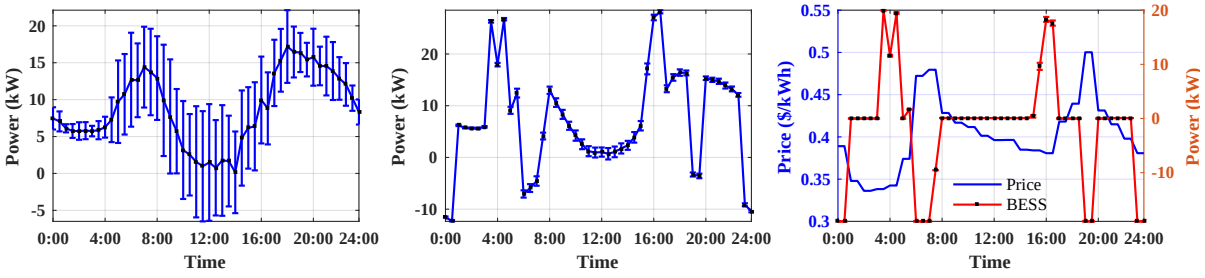

Figure 4.18: μG power without (left) and with (middle) BESS, electricity price and BESS power profile (right) for CR problem- cluster#3.

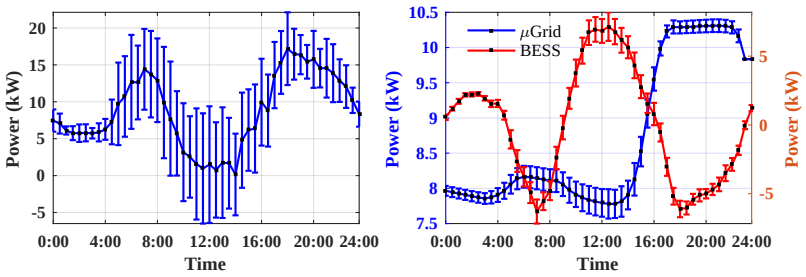

Figure 4.19: μG power without BESS (left), μG power with BESS and charging/discharging profile of BESS (right) for LVM problem- cluster#3.

The Mean, STD, and CT results obtained for cluster#4 in both CR and LVM modes are shown in Table 4.5.

Table 4.5: Expected value, STD and CT for various number of scenarios- cluster#4.

N_{sc}	Mean_{CR}	STD_{CR}	ST_{CR} (sec)	Mean_{LVM}	STD_{LVM}	CT_{LVM} (sec)
50	29.46	0.320	894	26.81	0.742	1123
100	29.48	0.186	1697	26.86	0.593	2189
300	29.46	0.105	5076	26.79	0.282	6476
500	29.48	0.088	8335	26.82	0.245	10881

The μG power without and with BESS as well as the charging/discharging profile of BESS for both CR and LVM modes which are obtained for cluster#3 are shown in Fig. 4.20 and Fig. 4.21, respectively.

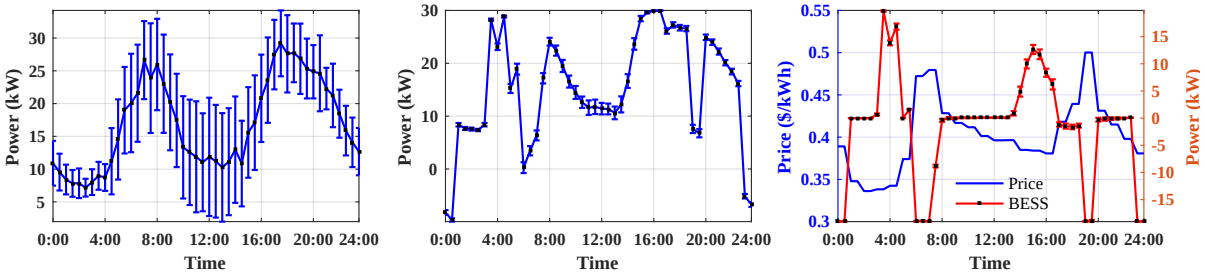

Figure 4.20: μG power without (left) and with (middle) BESS, electricity price and BESS power profile (right) for CR problem- cluster#4.

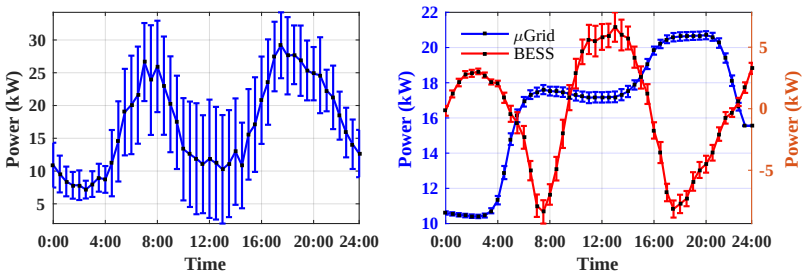

Figure 4.21: μG power without BESS (left), μG power with BESS and charging/discharging profile of BESS (right) for LVM problem- cluster#3.

In all clusters, the results reveal that BESS integration in μG can effectively reduce electricity cost and minimize the load variance. In the latter case, load variance minimization results in more available capacity on the μG feeder which can be utilized for supplying additional load.

4.3 Conclusion

In this chapter, the prototyped MBESS has been presented, and its integration in a real EV charging system has been shown. The experimental results reveal that BESS is capable of providing load leveling, charging cost reduction, and emergency power services to ECI. Based on our experience, it is worthwhile to mention that currently one of the main obstacles in implementing and testing BESS is that the setup components are not vendor-free, and they all should be ordered from the similar vendors. This issue can make the system maintenance costly. In addition, the cost of BESS installation is significant, an in some cases it can be more than the cost of the system itself.

In addition to prototyping BESS, the integration of BESS in a microgrid consisting of a building, EV charging system, and PV panels has been modeled by the numerical simulations, and a stochastic method for its optimal operation has been developed. The purpose of the BESS integration is to provide two services: electricity cost reduction and load variance minimization. Due to the stochasticity of the building load, EV charging demand, and

solar power, a stochastic optimization problem has been formulated. To make the problem tractable, SAA which is an MCS method has been applied. The numerical simulation results show the efficacy of BESS in accommodating EV charging demand by preventing the total power of the microgrid from exceeding the feeder capacity constraint. BESS can also reduce the electricity cost by optimal charging and discharging. Depending on the EV charging system operator, the optimal control of BESS can either reduce the electricity bill or utilize the feeder capacity efficiently so that additional loads (e.g. EV chargers) can be added to the microgrid.

CHAPTER 5

EV Charging Scheduling with Feeder Capacity Constraints: Fully Distributed Hierarchical ADMM

In this chapter, a hierarchical distributed framework for optimal coordination of EVs' charging demand with the consideration of feeder capacity constraints is proposed. The proposed framework consists of three layers of entities including CA, the feeder agents or EVAs, and EVs, in which each individual entity has its own objective function. By exploiting the mathematical properties of the EVCS problem, the interaction between the agents is formulated as a hierarchical *sharing problem* which is solved efficiently by ADMM in a distributed fashion. The developed hierarchical ADMM is embedded in RH feedback control to make the optimization results robust against the uncertainties in the system. RH provides the agents with Plug and Play (PnP) capability as well, i.e. they may change their optimization objective function at any RH iterations. The performance of the proposed framework in satisfying distribution feeder capacity constraint and LVM is validated by the numerical simulations.

5.1 Problem Formulation

We consider an ECI with a hierarchical trilayer structure shown Fig. 5.1 including CA, several EVAs, and the corresponding EV chargers. Defining an agent for each feeder provides the chance to include the feeder capacity constraints in the scheduling problem and to improve the flexibility of the infrastructure by considering an objective function for each EVA. The objective of the EV charging scheduling is not only to alleviate the negative effects of uncontrolled EV charging load on the system, but also to deploy EVs for regulation services such as load leveling. Accordingly, in the proposed general framework each of the ECI agents,

namely CA, EVAs, and EVs, has its own objective function. The purpose of the agents is to optimize their local objectives while the local and coupled constraints, introduced in the following, are satisfied.

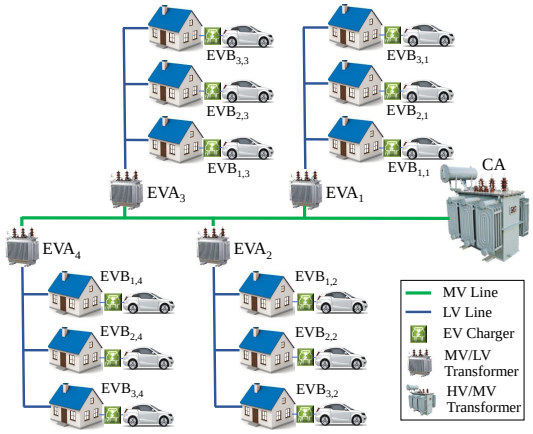

Figure 5.1: Multi-agent trilayer EV charging infrastructure.

Considering that the charging infrastructure has $\mathcal{N}^v \in \mathbb{N}$ EVs, $\mathbb{N}^a$ denotes the set of EVAs, $\mathbb{N}_j^v$ denotes the set of EVs supplied by the jth EVA, and their cardinalities are shown by $\mathcal{N}^a$ and $\mathcal{N}_j^v$, respectively. $EV_{i,j}$ shows the ith EV supplied by the jth EVA.

It is assumed that each $EV_{i,j}$ is located in either a commercial or a residential building. Hereafter, $EVB_{i,j}$ is used to show $EV_{i,j}$ and its corresponding building. Assuming that each EVB is equipped with a solar panel and considering the EV load model (2.4)-(2.5), the total load demand of $EVB_{i,j}$ is obtained by:

$$p_{i,j}^{evb}(t) = p_{i,j}^{l}(t) + p_{i,j}^{pv}(t) + p_{i,j}^{ev}(t) = p_{i,j}^{uc}(t) + p_{i,j}^{ev}(t), \tag{5.1}$$

where $p_{i,j}^{evb}$, $p_{i,j}^{l}$, $p_{i,j}^{pv}$, $p_{i,j}^{uc} \in \mathbb{R}$. $p_{i,j}^{evb}$ is the total load demand, $p_{i,j}^{l}$ is the total building load excluding the EV charging load, $p_{i,j}^{pv}$ is the solar panel power output, and $p_{i,j}^{uc}$ is the total netload demand (load plus solar power).

The set of feasible trajectories of $EVB_{i,j}$ is defined as:

$$\mathbb{P}_{i,j}^{evb} = \left\{ \mathbf{p}_{i,j}^{ev} \in \mathbb{R}^N \mid (2.4) - (2.5) \text{ and } (5.1),\ \forall t \in [\![t', t'+N-1]\!] \right\}. \tag{5.2}$$

It is the responsibility of each EVA to prevent its aggregated EV power demand from exceeding the available feeder capacity. This is shown by:

$$p_j^a(t) \leqslant \overline{P}_j^a(t) \tag{5.3a}$$

$$p_j^a(t) = \sum_{i \in \mathbb{N}_j^v} p_{i,j}^{ev}(t) \tag{5.3b}$$

$$\overline{P}_j^a(t) = \overline{P}_j^{a_c} - \sum_{i \in \mathbb{N}_j^v} p_{i,j}^{evb}(t), \tag{5.3c}$$

where $p_j^a,\ \overline{P}_j^a,\ \overline{P}_j^{a_c} \in \mathbb{R}$. p_j^a is the aggregated EV power demand of the jth EVA, $\overline{P}_j^a$ is its maximum capacity available for EV power demand, and $\overline{P}_j^{a_c}$ is the maximum capacity of the feeder supplying the jth EVA. According to (5.3b), the maximum capacity available for EV charging load is time-varying as it depends on the aggregated netload demand, while the maximum feeder capacity is a constant value depending on the technical specification of the feeder.

CA controls the total EV power demand of the distribution grid so that it does not exceed the maximum capacity available for EV charging, which is determined by DMS. This constraint is shown by:

$$p^{ca}(t) \leqslant \overline{P}^{ca}(t) \tag{5.4a}$$

$$p^{ca}(t) = \sum_{j \in \mathbb{N}^a} p_j^a(t) \tag{5.4b}$$

$$\overline{P}^{ca}(t) = \overline{P}^{ca_c} - \sum_{j \in \mathbb{N}^a} p_j^a(t), \tag{5.4c}$$

where $p^{ca},\ \overline{P}^{ca},\ \overline{P}^{ca_c} \in \mathbb{R}$. p^{ca} is the aggregated EVAs' power demand, $\overline{P}^{ca}$ is the grid's maximum capacity available for EVAs' load demand, and $\overline{P}^{ca_c}$ is the maximum available capacity to supply the loads. Similar to EVAs' constraints, the maximum capacity available for EVAs is time-varying as it depends on the aggregated EVAs' demand, while t$\overline{P}^{ca_c}$ is a constant value depending on the technical specifications of the grid.

The objective function of EVCS is threefold which is written as follows:

$$\begin{aligned} V := \min_{\mathbf{p}^{ca}, \mathbf{p}^a, \mathbf{p}^{ev}} \ & \mathbf{F}^{ca}(\mathbf{p}^{ca}) + \mathbf{F}^a(\mathbf{p}^a) + \mathbf{F}^{ev}(\mathbf{p}^{ev}) \\ \text{s.t. } & (5.2) - (5.4),\ \forall i \in \mathbb{N}_j^v,\ \forall j \in \mathbb{N}^a, \end{aligned} \tag{5.5}$$

where $\mathbf{F}^{ca}$, $\mathbf{F}^{a}$, and $\mathbf{F}^{ev}$ are the convex objective functions of the ECI's agents which are coupled by the constraints (5.3) and (5.4). The constraints on the EVs and their corresponding EVB shown by (5.2) are local constraints.

We show that the optimization problem in (5.5) is the *sharing problem* which can be solved in a distributed fashion. The objective function can be written as:

$$\begin{aligned} V &:= \min_{\mathbf{p}^{ca},\mathbf{p}^{a},\mathbf{p}^{ev}} \mathbf{F}^{ca}(\mathbf{p}^{ca}) + \sum_{j\in\mathbb{N}^a} \mathbf{F}^{a}_{j}(\mathbf{p}^{a}_{j}) + \sum_{j\in\mathbb{N}^a}\sum_{i\in\mathbb{N}^v_j} \mathbf{F}^{ev}_{i,j}(\mathbf{p}^{ev}_{i,j}) \\ &= \min_{\mathbf{p}^{ca},\mathbf{p}^{a},\mathbf{p}^{ev}} \mathbf{F}^{ca}(\mathbf{p}^{ca}) + \sum_{j\in\mathbb{N}^a} \big(\mathbf{F}^{a}_{j}(\mathbf{p}^{a}_{j}) + \sum_{i\in\mathbb{N}^v_j} \mathbf{F}^{ev}_{i,j}(\mathbf{p}^{ev}_{i,j})\big), \end{aligned} \tag{5.6}$$

in which the first expression is the CA's objective function, and the second expression includes the objective function of each EVA and its corresponding EVBs. We define the functions:

$$\mathbf{F}'_{j}(\mathbf{p}^{ev}_{i,j}, \mathbf{p}^{a}_{j}) = \sum_{i\in\mathbb{N}^v_j} \mathbf{F}^{ev}_{i,j}(\mathbf{p}^{ev}_{i,j}) + \mathbf{F}^{a}_{j}(\mathbf{p}^{a}_{j}) \tag{5.7a}$$

$$\mathbf{F}'(\mathbf{p}^{ev}, \mathbf{p}^{a}) = \sum_{j\in\mathbb{N}^a} \mathbf{F}'_{j}(\mathbf{p}^{ev}_{i,j}, \mathbf{p}^{a}_{j}), \tag{5.7b}$$

in order to rewrite (5.6) in the form which can be solved in a distributed manner by ADMM as follows:

$$\begin{aligned} V &:= \min_{\mathbf{p}^{ca},\mathbf{p}^{a},\mathbf{p}^{ev}} \mathbf{F}^{ca}(\mathbf{p}^{ca}) + \mathbf{F}'(\mathbf{p}^{ev}, \mathbf{p}^{a}) \\ &\text{s.t. } \mathbf{p}^{ca}_{j} - \mathbf{p}^{a}_{j} = 0,\ j \in [\![1, \mathcal{N}^a]\!], \end{aligned} \tag{5.8}$$

where only the coupled constraint between the CA and EVAs is shown. Note that $\mathbf{p}^{ca}$ and $\mathbf{p}^{a}$ have the same dimension, which is shown by the coupled constraint. This results in the objective function in the form of the *sharing problem* which is further discussed in the following section.

5.2 Hierarchical Alternative Direction Method of Multipliers

In this section, ADMM algorithm is briefly introduced to solve the convex optimization problem, formulated in the preceding section. It is also shown how the EVCS problem is a special case of the block separable problems referred to as the *sharing problem* [BPE11, Chapter 7.3].

5.2.1 ADMM

The problem in (5.8) is solved by ADMM, which is a variant of the augmented Lagrangian approach and uses the partial updates of the dual variables in each iteration. For a given time horizon $N \in \mathbb{N}$, the augmented Lagrangian of (5.8) $\mathcal{L} : \mathbb{R}^{\mathcal{N}^v N} \times \mathbb{R}^{\mathcal{N}^a N} \times \mathbb{R}^{\mathcal{N}^a N} \times \mathbb{R}^{\mathcal{N}^a N}$ is given by:

$$\mathcal{L}_\rho(\mathbf{p}^{ca}, \mathbf{p}^a, \mathbf{p}^{ev}, \lambda) = \mathbf{F}^{ca}(\mathbf{p}^{ca}) + \mathbf{F}'(\mathbf{p}^{ev}, \mathbf{p}^a) + \lambda^T(\mathbf{p}^{ca} - \mathbf{p}^a) + \frac{\rho}{2} \left\| \mathbf{p}^{ca} - \mathbf{p}^a \right\|_2^2, \tag{5.9}$$

with the Lagrangian multipliers $\lambda = (\lambda_1^T, \ldots, \lambda_{\mathcal{N}^a}^T)^T$, which are also called dual variables, and $\rho \in \mathbb{R}_{>0}$ is the penalty factor.

Theorem 5.2.1. [BPE11, Chapter 3.2] Let the extended-real-valued functions $\mathbf{F}^{ca}$ and $\mathbf{F}'$ be closed, convex and proper. Also, suppose that a saddle point $(\mathbf{p}^{ca^\star}, \mathbf{p}^{a^\star}, \mathbf{z}^{ev^\star}, \lambda^\star)$ of the Lagrangian $\mathcal{L}_0$ exists, i.e.:

$$\mathcal{L}_0(\mathbf{p}^{ca^\star}, \mathbf{p}^{a^\star}, \mathbf{z}^{ev^\star}, \lambda) \leqslant \mathcal{L}_0(\mathbf{p}^{ca^\star}, \mathbf{p}^{a^\star}, \mathbf{z}^{ev^\star}, \lambda^\star) \leqslant \mathcal{L}_0(\mathbf{p}^{ca}, \mathbf{p}^a, \mathbf{p}^{ev}, \lambda^\star),$$

holds for all λ and all $(\mathbf{p}^{ca}, \mathbf{p}^a, \mathbf{p}^{ev})$. Then, the following iterative primal and dual updates:

$$(\mathbf{p}_j^a, \mathbf{p}_j^{ev})^{k+1} := \underset{\mathbf{p}_j^a, \mathbf{p}_j^{ev}}{\operatorname{argmin}} \mathcal{L}_\rho(\mathbf{p}^{ca^k}, \mathbf{p}^a, \mathbf{p}^{ev}, \lambda^k), \ \forall j \in \mathbb{N}_a \tag{5.10a}$$

$$\mathbf{p}^{ca^{k+1}} := \underset{\mathbf{p}^{ca}}{\operatorname{argmin}} \mathcal{L}_\rho(\mathbf{p}^{ca}, \mathbf{p}^{a^{k+1}}, \mathbf{p}^{ev^{k+1}}, \lambda^k) \tag{5.10b}$$

$$\lambda^{k+1} := \underset{\lambda}{\operatorname{argmin}} \mathcal{L}_\rho(\mathbf{p}^{ca^{k+1}}, \mathbf{p}^{a^{k+1}}, \mathbf{p}^{ev^{k+1}}, \lambda), \tag{5.10c}$$

satisfy the following properties for any feasible initial values $\mathbf{p}^{ca^0}$, $\mathbf{p}^{a^0}$, $\mathbf{p}^{ev^0}$, λ^0 and fixed penalty term ρ [BFG18].

- $(\mathbf{p}^{ca^k} - \mathbf{p}^{a^k})_{k \in \mathbb{N}}$ converges to zero which ensures the feasibility of the optimization problem (5.8).
- for $k \to \infty$, $(\mathbf{p}^{ca^k}, \mathbf{p}^{a^k}, \mathbf{p}^{ev^k})_{k \in \mathbb{N}}$ converges to $(\mathbf{p}^{ca^\star}, \mathbf{p}^{a^\star}, \mathbf{p}^{ev^\star})$ which gives the optimal value of (5.8), i.e. $V^\star$.
- for $k \to \infty$, the dual variable λ^k converges to the optimal dual point $\lambda^\star$.

The first update, (5.10a), can be computed in a distributed manner and in parallel by each EVA due to the separability of the cost function and the penalty term. Expanding (5.10a), we have:

$$(\mathbf{p}_j^a, \mathbf{p}_j^{ev})^{k+1} := \underset{\mathbf{p}_j^a, \mathbf{p}_j^{ev}}{\operatorname{argmin}} \mathbf{F}'_j(\mathbf{p}_j^a, \mathbf{p}_j^{ev}) + \lambda_j^T(\mathbf{p}_j^a - \mathbf{p}_j^{ca^k}) + \frac{\rho}{2}\left\|\mathbf{p}_j^a - \mathbf{p}_j^{ca^k}\right\|_2^2,\ \forall j \in \mathbb{N}_a. \tag{5.11}$$

The second update, (5.10b), is written as:

$$\mathbf{p}^{ca^{k+1}} := \underset{\mathbf{p}^{ca}}{\operatorname{argmin}} \mathbf{F}^{ca}(\mathbf{p}^{ca}) + \lambda^T(\mathbf{p}^{a^{k+1}} - \mathbf{p}^{ca}) + \frac{\rho}{2}\left\|\mathbf{p}^{a^{k+1}} - \mathbf{p}^{ca}\right\|_2^2. \tag{5.12}$$

Since $\mathcal{L}_\rho$ is not differentiable at λ, the third update, (5.10c), is solved using the gradient method for each element of the vector λ, i.e.:

$$\lambda_j^{k+1} = \lambda_j^k + \rho(\mathbf{p}_j^{a^{k+1}} - \mathbf{p}_j^{ca^{k+1}}),\ \forall j \in \mathbb{N}_a. \tag{5.13}$$

5.2.2 Scaled Form

ADMM can be written in a different form by combining the linear and quadratic penalty terms and scaling the dual variable. Defining $r = \mathbf{p}^a - \mathbf{p}^{ca}$, we have [BPE11, Chapter 3.1.1]:

$$\lambda^T r + \frac{\rho}{2}\|r\|_2^2 = \frac{\rho}{2}\left\|r + \frac{1}{\rho}\lambda\right\|_2^2 - \frac{1}{2\rho}\|\lambda\|_2^2 = \frac{\rho}{2}\|r + \nu\|_2^2 - \frac{1}{2}\|\nu\|_2^2, \tag{5.14}$$

where $\nu = \frac{1}{\rho}\lambda$. Therefore, ADMM updates can be expressed in the scaled form as:

$$(\mathbf{p}_j^a, \mathbf{p}_j^{ev})^{k+1} := \underset{\mathbf{p}_j^a, \mathbf{p}_j^{ev}}{\operatorname{argmin}} \mathbf{F}'_j(\mathbf{p}_j^a, \mathbf{p}_j^{ev}) + \frac{\rho}{2}\left\|\mathbf{p}_j^a + \nu_j^k - \mathbf{p}_j^{ca^k}\right\|_2^2,\ \forall j \in \mathbb{N}_a \tag{5.15}$$

$$\mathbf{p}^{ca^{k+1}} := \underset{\mathbf{p}^{ca}}{\operatorname{argmin}} \mathbf{F}^{ca}(\mathbf{p}^{ca}) + \frac{\rho}{2}\sum_{j\in\mathbb{N}^a}\left\|\mathbf{p}_j^{a^{k+1}} + \nu_j^k - \mathbf{p}_j^{ca}\right\|_2^2 \tag{5.16}$$

$$\nu_j^{k+1} = \nu_j^k + \mathbf{p}_j^{a^{k+1}} - \mathbf{p}_j^{ca^{k+1}},\ \forall j \in \mathbb{N}_a. \tag{5.17}$$

The first and the third update steps of ADMM, i.e. (5.15) and (5.17), respectively, are solved by EVAs in parallel, while the second update (5.16) is solved by CA.

As it is seen, CA has to solve an optimization problem with $\mathcal{N}^a \times N$ variables meaning that the complexity of the optimization problem solved by CA increases with the number of EVAs. However, it will be possible to make the number of variables in CA's problem independent of the number of EVAs, if the optimization problem can be written in the form of the *sharing problem*, which is shown in the following.

5.2.3 Sharing Problem

According to (5.4), the function $\mathbf{F}^{ca}$ takes the sum of individual EVAs' decision variables as input. By introducing $\overline{\mathbf{p}}^{ca} = \frac{1}{\mathcal{N}^a} \sum_{j \in \mathbb{N}^a} \mathbf{p}_j^{ca}(t)$ and $\overline{\mathbf{p}}^{a} = \frac{1}{\mathcal{N}^a} \sum_{j \in \mathbb{N}^a} \mathbf{p}_j^{a}(t)$, the scaled form of ADMM, (5.15)-(5.17), is written in the following form which is called the *sharing* ADMM.

$$(\mathbf{p}_j^a, \mathbf{p}_j^{ev})^{k+1} := \underset{\mathbf{p}_j^a, \mathbf{p}_j^{ev}}{\operatorname{argmin}} \mathbf{F}'_j(\mathbf{p}_j^a, \mathbf{p}_j^{ev}) + \frac{\rho}{2} \left\| \mathbf{p}_j^a - \mathbf{p}_j^{a^k} + \overline{\mathbf{p}}^{a^k} - \overline{\mathbf{p}}^{ca^k} + \overline{\nu}^k \right\|_2^2, \ \forall j \in \mathbb{N}_a \tag{5.18}$$

$$\overline{\mathbf{p}}^{ca^{k+1}} := \underset{\mathbf{p}^{ca}}{\operatorname{argmin}} \mathbf{F}^{ca}(\mathcal{N}^a \overline{\mathbf{p}}^{ca}) + \frac{\mathcal{N}^a.\rho}{2} \left\| \overline{\mathbf{p}}^{a^{k+1}} - \overline{\mathbf{p}}^{ca} + \overline{\nu}^k \right\|_2^2 \tag{5.19}$$

$$\overline{\nu}^{k+1} = \overline{\nu}^k + \overline{\mathbf{p}}^{a^{k+1}} - \overline{\mathbf{p}}^{ca^{k+1}}. \tag{5.20}$$

Lemma 5.2.2. [BFG18] For given a and $b_j \in \mathbb{R}^N$ $(j \in \mathbb{N}^a)$, we have $c_j^\star = b_j + a - \overline{b}$, with $\overline{b} = \frac{1}{\mathcal{N}^a} \sum_{j \in \mathbb{N}^a} b_j$, as the optimal value:

$$c_j^\star := \underset{c_j \in \mathbb{R}^N}{\operatorname{argmin}} \sum_{j \in \mathbb{N}^a} \|c_j - b_j\| \quad \text{s.t.} \quad \frac{1}{\mathcal{N}^a} \sum_{j \in \mathbb{N}^a} c_j = a.$$

Proof. For $b_j = 0$ $(j \in \mathbb{N}^a)$, the triangle inequality implies that:

$$\|\mathcal{N}^a.a\| = \min_{c_j : \frac{1}{\mathcal{N}^a} \sum\limits_{j \in \mathbb{N}^a} c_j = a} \left\| \sum_{j \in \mathbb{N}^a} c_j \right\| \leqslant \min_{c_j : \frac{1}{\mathcal{N}^a} \sum\limits_{j \in \mathbb{N}^a} c_j = a} \sum_{j \in \mathbb{N}^a} \|c_j\|,$$

where the equality holds for $c_j = a$ $(j \in \mathbb{N}^a)$. Using the coordinate transformation $\tilde{c}_j = c_j - b_j$, the equality constraint results in

$$\frac{1}{\mathcal{N}^a} \sum_{j \in \mathbb{N}^a} \tilde{c}_j = \frac{1}{\mathcal{N}^a} \sum_{j \in \mathbb{N}^a} c_j - \frac{1}{\mathcal{N}^a} \sum_{j \in \mathbb{N}^a} b_j = a - \overline{b},$$

which verifies the assertion. □

Now, we use the lemma to prove the *sharing* ADMM. More details are provided in [BPE11, Chapter 7.3].

Proof. Applying Lemma 5.2.2 to (5.16), we obtain:

$$\mathbf{p}_j^{ca^{k+1}} = \mathbf{p}_j^{a^{k+1}} + \nu_j^k + \overline{\mathbf{p}}^{ca^{k+1}} - \overline{\mathbf{p}}^{a^{k+1}} - \overline{\nu}^k, \tag{5.21}$$

for $j \in \mathbb{N}^a$. Therefore, (5.16) is rewritten as:

$$\overline{\mathbf{p}}^{ca^{k+1}} := \underset{\overline{\mathbf{p}}^{ca}}{\operatorname{argmin}} \mathbf{F}^{ca}(\mathcal{N}^a \overline{\mathbf{p}}^{ca}) + \frac{\rho}{2} \sum_{j \in \mathbb{N}^a} \left\| \overline{\mathbf{p}}^{a^{k+1}} + \overline{\nu}^k - \overline{\mathbf{p}}^{ca} \right\|_2^2,$$

which yields (5.19). Substituting (5.21) for (5.17) gives:

$$\nu_j^{k+1} = \overline{\nu}^k + \overline{\mathbf{p}}^{a^{k+1}} - \overline{\mathbf{p}}^{ca^{k+1}},$$

which means that the dual updates for all EVAs are equal, i.e. $\nu_j^{k+1} = \nu_{j'}^{k+1}$ for all $j \neq j' \in \mathbb{N}^a$. Therefore, the dual update of ADMM is independent of the number of EVAs and is written as (5.20). Finally, replacing the results in (5.15), we can obtain (5.18). □

To decrease the communication overhead between CA and EVAs, we define $\mathcal{V}^k = \overline{\nu}^k + \overline{\mathbf{p}}^{a^k} - \overline{\mathbf{p}}^{ca^k}$. Thus, at each ADMM iteration after the third update (5.20), CA broadcasts $\mathcal{V}$ to EVAs.

5.2.4 Fully Distributed Hierarchical ADMM

Hereafter, the iterative ADMM procedure between CA and the EVAs is called *ADMM₁*. Considering the first update of *ADMM₁* (5.18), each EVA has to solve an optimization problem of $(\mathcal{N}_j^v + 1) \times N$ unknown variables. This limits the scalability of the charging scheduling algorithm. Also, as each EV has to communicate its information, such as arrival time, departure time, and required energy with the corresponding EVA, EV owners' privacy may not be preserved. Therefore, we further explore the first update of *ADMM₁* in order to propose a fully distributed charging scheduling algorithm where each EV schedules its own charging profile through communication with its EVA.

Considering (5.6) and (5.7a), the first update of *ADMM₁* (5.18) for the jth EVA can be written as follows:

$$(\mathbf{p}_j^a, \mathbf{p}_{i,j}^{ev})^{k+1} := \underset{\mathbf{p}_j^a, \mathbf{p}_{i,j}^{ev}\ \forall i \in \mathbb{N}_j^v}{\operatorname{argmin}} \mathbf{F}_j^a(\mathbf{p}_j^a) + \sum_{i \in \mathbb{N}_j^v} \mathbf{F}_{i,j}^{ev}(\mathbf{p}_{i,j}^{ev}) + \frac{\rho}{2} \left\| \mathbf{p}_j^a - \mathbf{p}_j^{a^k} + \overline{\mathbf{p}}^{a^k} - \overline{\mathbf{p}}^{ca^k} + \overline{\nu}^k \right\|_2^2.$$

Considering (5.3b), which shows the coupled constraint between each EVA and its EVs, the second and third parts of the above expression are the functions of $\sum_{i \in \mathbb{N}_j^v} \mathbf{p}_{i,j}^{ev}$, and it can be

written as follows:

$$(\mathbf{p}_j^a, \mathbf{p}_{i,j}^{ev})^{k+1} := \underset{\mathbf{p}_j^a, \mathbf{p}_{i,j}^{ev} \ \forall i \in \mathbb{N}_j^v}{\operatorname{argmin}} \mathbf{F}"_j(\sum_{i \in \mathbb{N}_j^v} \mathbf{p}_{i,j}^{ev}) + \sum_{i \in \mathbb{N}_j^v} \mathbf{F}_{i,j}^{ev}(\mathbf{p}_{i,j}^{ev}).$$

According to Lemma 5.2.2, the above optimization problem is the *sharing problem*, and it can be solved by a similar iterative procedure (5.18)-(5.20), however between each EVA and EVs which it supplies. Hereafter, the *sharing* ADMM which is executed between each EVA and its EVs is called *ADMM₂*. Therefore, *ADMM₂* for the jth EVA, namely *ADMM*$_{2,j}$, is written as follows:

$$\begin{gathered} \mathbf{p}_{i,j}^{ev^{l+1}} := \underset{\mathbf{p}_{i,j}^{ev}}{\operatorname{argmin}} \mathbf{F}_{i,j}^{ev}(\mathbf{p}_{i,j}^{ev}) + \frac{\gamma}{2} \left\| \mathbf{p}_{i,j}^{ev} - \mathbf{p}_{i,j}^{ev^l} + \overline{\mathbf{p}}_j^{ev^l} - \overline{\mathbf{p}}_j^{a^l} + \theta_j^l \right\|_2^2 \\ \text{s.t. } (5.2) \end{gathered} \tag{5.22}$$

$$\begin{gathered} \overline{\mathbf{p}}_j^{a^{l+1}} := \underset{\overline{\mathbf{p}}_j^a}{\operatorname{argmin}} \mathbf{F}^a(\mathcal{N}_j^v \overline{\mathbf{p}}_j^a) + \frac{\rho}{2} \left\| \mathcal{N}_j^v \overline{\mathbf{p}}_j^a - \mathbf{p}_j^{a^k} + \mathcal{V}^k \right\|_2^2 + \frac{\mathcal{N}_j^v . \gamma}{2} \left\| \overline{\mathbf{p}}_j^a - \theta_j^l - \overline{\mathbf{p}}_j^{ev^{l+1}} \right\|_2^2) \\ \text{s.t. } (5.3) \end{gathered} \tag{5.23}$$

$$\theta_j^{l+1} = \theta_j^l + \overline{\mathbf{p}}_j^{ev^{l+1}} - \overline{\mathbf{p}}_j^{a^{l+1}}, \tag{5.24}$$

where $\overline{\mathbf{p}}_j^{ev} \in \mathbb{R}^N$, $\overline{\mathbf{p}}_j^{ev} = \frac{1}{\mathcal{N}_j^v} \sum_{i \in \mathbb{N}_j^v} \mathbf{p}_{i,j}^{ev}$ and $\gamma \in \mathbb{R}_{>0}$. Similar to *ADMM₁*, to decrease the communication overhead, we define $\Theta_j^l = \theta_j^l + \overline{\mathbf{p}}_j^{ev^l} - \overline{\mathbf{p}}_j^{a^l}$. Thus, at each *ADMM₂* iteration after the third update (5.24), the jth EVA broadcasts Θ_j to its EVs. Note that in (5.23), we replace $\overline{\nu}^k + \overline{\mathbf{p}}^{a^k} - \overline{\mathbf{p}}^{ca^k}$ with $\mathcal{V}^k$.

The whole procedure of the proposed fully distributed optimal EVCS including the two-layer hierarchical ADMM is shown in Algorithm 4, where line 5 to line 18 show *ADMM₂* which is solved in parallel by EVAs and their corresponding EVs. For more details about the stopping criteria, we refer to [BPE11, Chapter 3.3]

5.2.5 Receding Horizon Hierarchical ADMM

In this subsection, we apply RH to the hierarchical ADMM , celled RH-ADMM, to generate the optimal feedback control sequences for the EV chargers. Utilizing RH results in a more

Algorithm 4: Hierarchical ADMM.

Initialization: Set initial values for $\mathbf{p}^{ca^0}$, $\mathbf{p}^{a^0}$, $\mathbf{p}^{ev^0}$, γ^0, and θ^0.
$k \leftarrow 0$.
$l \leftarrow 0$.
while $Err_1 < Th_1$ **do**
  for $j = 1 : \mathcal{N}^a$ **do**
    while $Err_2 < Th_2$ **do**
      for $i = 1 : \mathcal{N}_j^v$ **do**
        calculate $\mathbf{p}_{i,j}^{ev^{l+1}}$ by (5.22).
      end
      update $\overline{\mathbf{p}}_j^{ev^{l+1}} = \frac{1}{\mathcal{N}_j^v} \sum_{i=1}^{\mathcal{N}_j^v} \mathbf{p}_{i,j}^{ev^{l+1}}$.
      Calculate $\overline{\mathbf{p}}_j^{a^{l+1}}$ by (5.23).
      Update θ_j^{l+1} by (5.24).
      Update & broadcast Θ_j^{l+1} to $\forall i \in \mathbb{N}_j^v$.
      Update Err_2.
      $l \leftarrow l + 1$.
    end
    Send $\mathbf{p}_j^{a^{k+1}} = \mathcal{N}_j^v . \overline{\mathbf{p}}_j^{a^{l+1}}$ to CA.
  end
  update $\overline{\mathbf{p}}^{a^{k+1}} = \frac{1}{\mathcal{N}^a} \sum_{j=1}^{\mathcal{N}^a} \mathbf{p}_j^{a^{k+1}}$.
  Calculate $\overline{\mathbf{p}}^{ca^{k+1}}$ by (5.19).
  Update $\overline{\nu}$ by (5.20).
  Update & broadcast $\mathcal{V}$ to $\forall j \in \mathbb{N}^a$.
  Update Err_1.
  $k \leftarrow k + 1$.
end

robust optimal EVCS, as it iteratively updates the control sequences according to the most recent EV load demand requests and other measurement variables of the system. This also helps reduce system modeling errors [RM09].

The proposed RH-ADMM executes the following steps consecutively. First, according to the predicted EV charging requests and other required data at the time instant t over the time horizon $N \in \mathbb{N}$, Algorithm 4 finds $\mathbf{p}^{ev^\star}(\cdot)$. Then, only the first element of $\mathbf{p}_{i,j}^{ev^\star}(\cdot)$ is implemented by $EV_{i,j}$. Afterward, t is incremented, and the same procedure is repeated. The RH-ADMM is shown in Algorithm 5. In addition to the advantages mentioned above, there is one more advantage for applying RH to the proposed hierarchical framework. It gives the flexibility to ECI agents to change their objective functions, as long as it is convex, at each RH iteration. It is worthy to mention that in this case, as each optimization function is solved locally, the agents do not need to notify each other about changing the objective function. This feature is also known as PnP [BFG18].

Algorithm 5: Hierarchical RH-ADMM.

1 **while** $t \leqslant N$ **do**
2 **Initialization** Update the arrival/departure time, initial state of energy of EVs, other required data.
3 Run Hierarchical ADMM, Algorithm 4, to calculate $\mathbf{p}^{ev^\star}(\cdot)$, $\mathbf{c}^{ev^\star}(\cdot)$, and $\mathbf{p}^{evb^\star}(\cdot)$.
4 Apply the first element of the optimal value $\mathbf{p}_{i,j}^{ev^\star}(\cdot), \forall i \in \mathbb{N}_j^v$ & $\forall j \in \mathbb{N}^a$.
5 Increment the time index t.
6 **end**

5.3 Numerical Simulations and Discussion

In this section, first, the optimization objective functions are defined, and different performance metrics are introduced. Then, in order to evaluate the performance of the proposed hierarchical RH-ADMM, the numerical simulations are executed, and the results are discussed. Through this section, the optimization problems are solved by CVX [GB14] using a

PC with Intel® Core™ i7 − 4770 3.40 GHz CPU, 4 cores and 8 GB RAM.

5.3.1 Case Study Setup

For the numerical simulations, we assume that the purpose of CA is to minimize the peak load in the distribution grid, which is equivalent to LVM [SHM11], while EVs aim at minimizing their charging cost. Therefore, CA needs to have access to the netload demand prediction of the feeders over the EV charging scheduling horizon, and each EVB should have knowledge about the arrival time, departure time, and required energy of its own EV. We assume that CA receives the netload demand prediction from DMS, and EVBs have a *priori* knowledge about their EVs' charging data or predict it using the method proposed in Chapter 3.

To formulate CA's objective function, we define $\Omega_j(t)$ of the jth EVA by:

$$\Omega_j(t) := \sum_{i=1}^{\mathcal{N}_j^v} p_{i,j}^{uc}(t). \tag{5.25}$$

Also, $\overline{\Omega}(t)$ over the time horizon $N \in \mathbb{N}$ is defined by:

$$\overline{\Omega}(t) := \frac{1}{N} \sum_{t=t'}^{t'+N-1} \sum_{j=1}^{\mathcal{N}^a} \Omega_j(t). \tag{5.26}$$

Hence, the CA's objective function is written as:

$$\begin{aligned} \mathbf{F}^{ca}(\mathbf{p}^{ca}) := \min_{\mathbf{p}^{ca}} \big(\overline{\mathbf{\Omega}} - \sum_{j=1}^{\mathcal{N}^a} (\mathbf{\Omega}_j + \mathbf{p}_j^a)\big)^2 \\ \text{s.t. (5.4).} \end{aligned} \tag{5.27}$$

For EVAs, it is assumed that their purpose is only to keep the total charging demand of the feeder less than the capacity constraint (5.3). Therefore, the objective function of the jth EVA is the indicator function defined as follows:

$$\mathbf{F}_j^a(\mathbf{p}_j^a) := \min_{\mathbf{p}_j^a} \begin{cases} 0, & \text{if } \mathbf{p}_j^a \leqslant \overline{\mathbf{P}}_j^a \\ \infty, & \text{otherwise.} \end{cases} \tag{5.28}$$

The objective function of $EVB_{i,j}$ is the inner product of Π and the charging profile,

which is written as follows:

$$\begin{aligned} \mathbf{F}^{ev}_{i,j}(\mathbf{p}^{ev}_{i,j}) &:= \min_{\mathbf{p}^{ev}_{i,j}} \boldsymbol{\Pi}^T.\mathbf{p}^{ev}_{i,j} \\ &\text{s.t. (5.2)}, \end{aligned} \tag{5.29}$$

where $\boldsymbol{\Pi} \in \mathbb{R}^N$ is the wholesale electricity price available from CAISO [CAI].

Other objective functions which can be defined for EVs are CO_2 emission minimization and peak shaving [DPM18]. In the former, the EV is charged over the time periods when CO_2 emission at the system level is low, which can be achieved by weighting the charging profile by the emission vector, and the result is a convex objective function. In the latter, EV is charged such that the least-square error of the building load demand, i.e. (5.1), over the optimization horizon decreases, which is a quadratic convex function.

According to (5.27)-(5.29), the objective function of EVCS (5.5) is written as follows:

$$\begin{aligned} V &:= \min_{\mathbf{p}^{ca},\mathbf{p}^{a},\mathbf{p}^{ev}} \sum_{j\in\mathbb{N}^a}\sum_{i\in\mathbb{N}^v_j}(\boldsymbol{\Pi}^T.\mathbf{u}_{i,j}) + \Big(\overline{\boldsymbol{\Omega}} - \sum_{j=1}^{\mathcal{J}}\big(\boldsymbol{\Omega}_j + \mathbf{w}_j\big)\Big)^2 \\ &\text{s.t. (5.2)} - \text{(5.4)}, \forall i \in \mathbb{N}^v_j \ \& \ \forall j \in \mathbb{N}^a. \end{aligned} \tag{5.30}$$

5.3.2 Performance Metrics

According to the CA's objective function, three metrics are defined to assess the performance of the proposed hierarchical RH-ADMM. The first performance metric is the peak-to-peak (PTP) variation of the power demand, which is the difference between the maximum and minimum total power demand of the distribution grid over the time horizon $N \in \mathbb{N}$, and it is obtained by:

$$\text{PTP} = \max_{t\in[\![1,N]\!]} \varepsilon(t) - \min_{t\in[\![1,N]\!]} \varepsilon(t), \tag{5.31}$$

where $\varepsilon(t) = \sum_{j\in\mathbb{N}^a}\sum_{i\in\mathbb{N}^v_j} p^{evb}_{i,j}(t), \varepsilon(t) \in \mathbb{R}$.

The second performance metric is the peak-to-average (PTA) [DPM18], which is given by:

$$\text{PTA} = \frac{\max_{t\in[\![1,N]\!]}\varepsilon(t)}{E(t)}, \tag{5.32}$$

where $E(t) = \frac{1}{N} \sum_{t\in[\![1,N]\!]} \sum_{j\in\mathbb{N}^a} \sum_{i\in\mathbb{N}_j^v} p_{i,j}^{uc}(t),\ E(t) \in \mathbb{R}$ is the average of the total netload demand of the distribution grid over the time horizon $N \in \mathbb{N}$.

The last performance metric is the root-mean-square (RMS) deviation from the average which is given by:

$$\text{RMS} = \sqrt{\frac{1}{N} \sum_{t=1}^{N} \big(E(t) - \varepsilon(t)\big)^2}. \tag{5.33}$$

5.3.3 Simulation Results

The proposed framework is applied to an ECI including 5 EVAs and 300 EVBs, where the real netload demand dataset is available on [Aus], and it is assumed that the departure and arrival times of the EVs are normally distributed over $[\texttt{5:00} - \texttt{9:00}]$ and $[\texttt{15:00} - \texttt{20:00}]$, respectively. In the following, the simulation results comparing coordinated EV charging (CC) and uncoordinated EV charging (uCC), with and without RH, as well as the feeders' loading condition with and without capacity constraints are illustrated. In uCC, EVs start charging with the maximum power rating as soon as they are plugged. In addition, PnP feature is shown for the case in which an EV owner changes the charging mode from CR to the battery degradation cost reduction (BDR). There, it is also discussed how the total load demand profile is affected when the EV owners prefer to charge their EV in BDR mode, instead of CR mode.

RH and Feeder Constraints: the effectiveness of the proposed framework in feeder constraint satisfaction is shown, and its robustness to the netload demand uncertainty is evaluated. To this end, CC is executed for the netload demand with (PreError) and without (noPreError) prediction error. Then, CC is scheduled for three cases: using RH and feeder constraints (RH-CC-PreError), without RH but with feeder constraints (nRH-CC-PreError), and with RH but without feeder constraints (Unconstrained CC). As it is shown in Fig. 6.2, CC flattens the load profile in all simulated cases. The figure also verifies that RH makes the proposed framework robust against the netload prediction error, as the load profile obtained by nRH-CC-PreError considerably deviates from the expected total load profile specifically at the end of the scheduling time horizon ($[\texttt{20:00} - \texttt{24:00}]$).

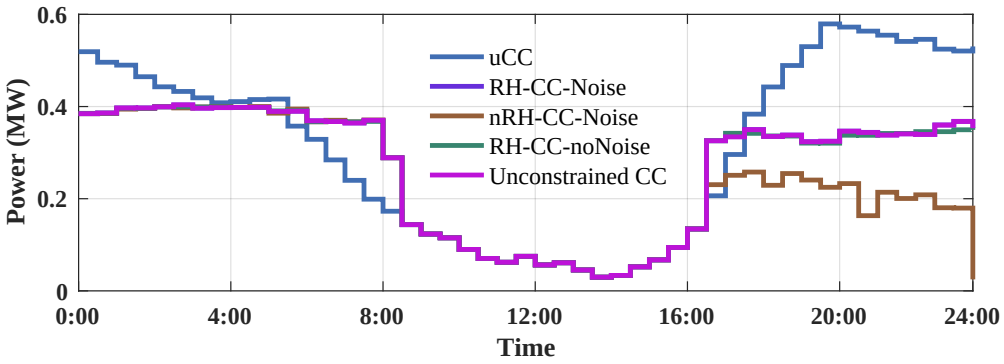

Figure 5.2: Total load profile for uCC, RH-CC with and without prediction error, nRH-CC, and unconstrained CC.

Fig. 5.3 shows the aggregated daily charging costs for EVAs using uCC and CC. It obviously justifies that the annual charging cost saving using the RH-ADMM can be substantial.

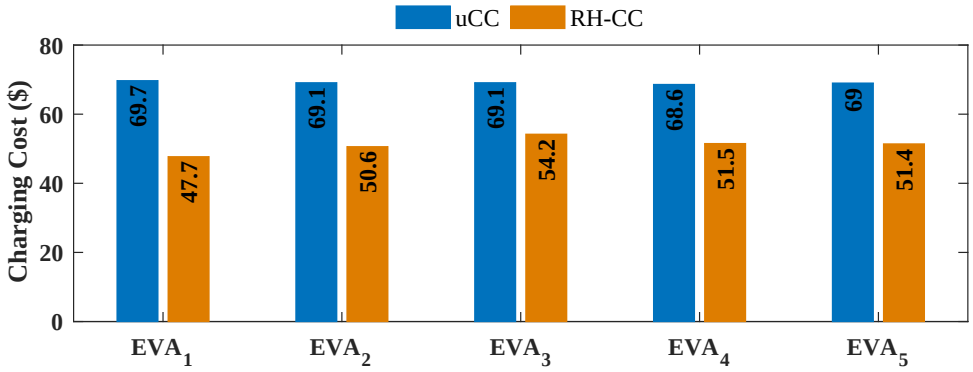

Figure 5.3: Comparing the charging cost of uCC with the proposed CC.

Considering that the maximum loading capacity is 82 kW for EVA_1 and 78 kW for the other EVAs, if the feeder constraints are not included in the EVCS problem, all the feeders experience overloading condition (Fig. 5.4). However, the consideration of the feeder limitations as the charging scheduling optimization constraints avoids feeders' overloading as shown in Fig. 5.5.

EV Penetration Level: the proposed charging algorithm is simulated for different EV penetration levels in the distribution grid, namely 25%, 50% and 75%. In all three scenarios,

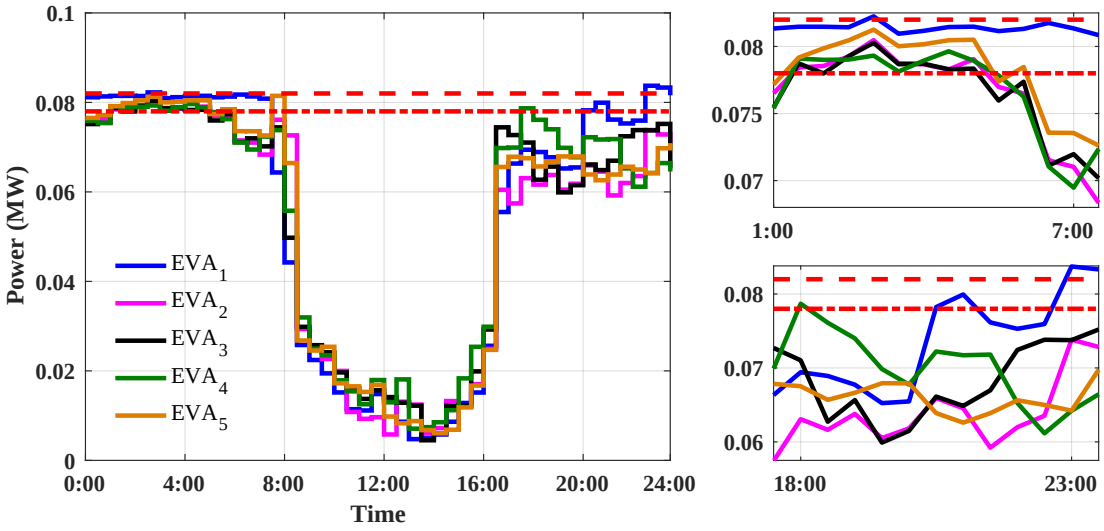

Figure 5.4: Feeder overloading condition in unconstrained CC.

EVs charge only in CR mode. In Fig. 5.6, the illustrated results compare the total load demand profile with (CC-RH-CR) and without (uCC) EV load scheduling for different EV penetrations, and they validate that the proposed RH-ADMM effectively shaves the peak load and smooths the total load profile.

Moreover, to show the performance of RH-ADMM, the algorithm is run for 1 RH iteration with 2 and 4 cores, and the computation time and memory usage is measured for various EV penetration levels for which the results are tabulated in Table 5.1. The results show that both the computation time and memory usage increase with EV penetration growth. However, it is worthwhile to note that the proposed framework is designed for a multi-agent ECI, and it is not supposed to run on a server similar to [RGJ17].

Table 5.1: Computation Performance of RH-ADMM for Various EV Penetrations.

	Core#	25%	50%	75%	100%
Computation Time (sec.)	2	537.2	568.4	591.6	614.3
	4	409.7	423.3	434.5	446.8
Memory Usage (MB)	2	36.11	36.40	36.68	36.96
	4	36.11	36.40	36.68	36.96

PnP and BDR: as it was mentioned earlier, one advantage of RH is PnP in terms of

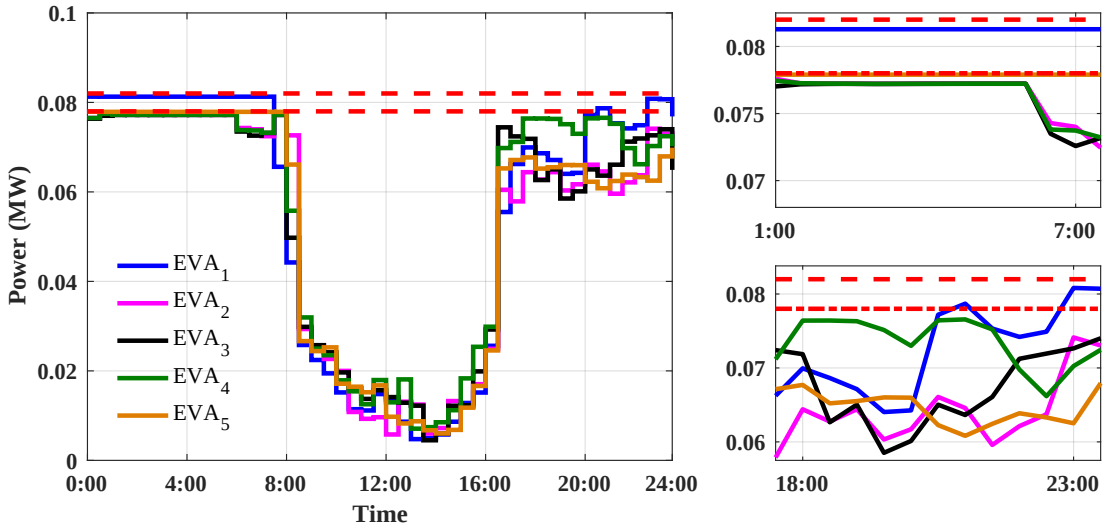

Figure 5.5: Feeder constraints' satisfaction using RH-ADMM.

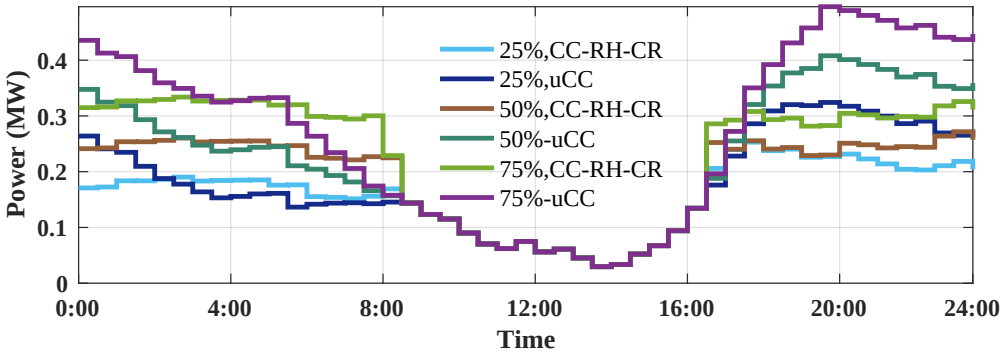

Figure 5.6: Total load profile for various EV penetrations charging in CR mode.

agents' objective functions. That is, each agent may change its objective function at any RH iterations. This is illustrated in Fig. 5.7 where the charging profile of EV, which is plugged in at `19:30` and unplugged at `5:00`, respectively, is displayed. Notice that EV does not start charging until `22:00` because of the high electricity price. The EV charger works in CR mode until `24:00` at which it switches to BDR mode. The BDR optimization function is defined by [MSF13]:

$$\mathbf{F}_{i,j}^{ev}(\mathbf{p}_{i,j}^{ev}) := \min_{\mathbf{p}_{i,j}^{ev}} \delta \left\|\mathbf{p}_{i,j}^{ev}\right\|_2^2, \tag{5.34}$$

where $\delta \in \mathbb{R}$ is the simplified battery degradation cost. $\left\|\mathbf{p}_{i,j}^{ev}\right\|_2^2$ penalizes the fluctuation of the charging power, therefore it will result in a constant charging profile if no other

constraints affect it. The figure shows the charging powers and the energy profiles with and without PnP.

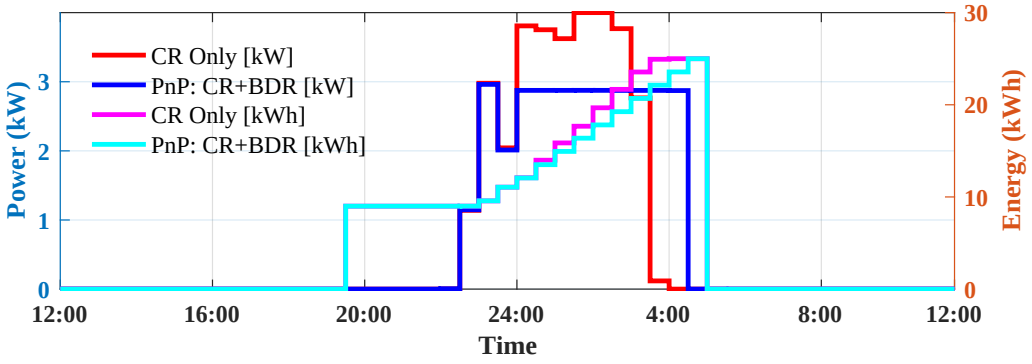

Figure 5.7: PnP using RH-ADMM.

It is shown in Fig. 5.8 that the total load profile is affected if a considerable percentage of the EV owners are interested to charge their EVs only in BDR mode. By increasing the number of EVs charging in BDR mode, less RMS and PTP improvements are obtained. Considering a weighting factor for EVBs' objective function, the performance metrics are improved or degraded by decreasing or increasing the weighting factor, while EVBs' local objective functions show the opposite behavior.

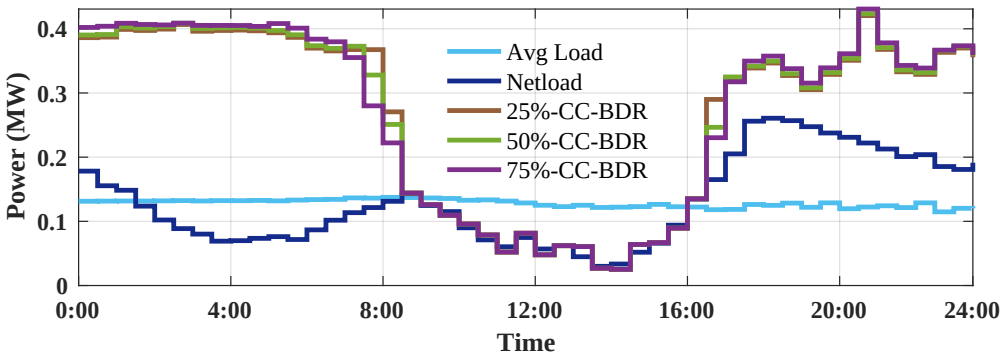

Figure 5.8: Total load profile for various numbers of EVs charging in BDR mode.

To better illustrate the effectiveness of the proposed EVCS, the values obtained for the performance metrics in Fig. 5.6 and Fig. 5.8 are summarized in Table 6.1. As it is clear, all three performance metrics are significantly improved by the proposed hierarchical EVCS

Table 5.2: Performance Metrics Improvement Using RH-ADMM.

Charging Type	EV Penetration%	PTP%	PTA%	RMS%
CR	25	24	22	32
	50	33	31	33
	75	34	32	29
	100	36	34	28
Charging Type	EV% in BDR	PTP%	PTA%	RMS%
CR+BDR	25	35	37	26
	50	34	34	25
	75	33	32	24

framework.

5.4 Conclusion

In this chapter, a multi-agent framework for optimal EV charging scheduling has been proposed. In the proposed method, CA only communicates with EVAs, and each EVA communicates with the EVs which it supplies. The EV charging optimization problem has been formulated as a two-layer hierarchical *sharing problem* which is solved efficiently by ADMM. The first sharing problem is between CA and EVAs, and the second one is between each EVA and its EVs. The features of the proposed framework are that the feeder capacity constraints are considered in the optimization problem, and each agent has its own objective function solved locally. Furthermore, to make the EV charging optimal solution robust against the uncertainties and to provide PnP for the ECI agents, the proposed hierarchical ADMM has been embedded in the receding horizon control. The simulation results for an EV charging infrastructure including 5 EVAs and 300 EVs using real data verify the effectiveness of the proposed hierarchical RH-ADMM in feeder capacity constraint satisfaction, load variance minimization, and charging cost reduction.

CHAPTER 6

Hierarchical Distributed Framework for EV Charging Scheduling Using Exchange Problem

In this chapter, a distributed trilayer multi-agent framework is proposed for optimal EVCS. The framework reduces the negative effects of the electric vehicle charging demand on the electrical grids. To solve the scheduling problem, a novel hierarchical distributed EVCS (HDEVCS) is developed as the *exchange problem*, where the agents are clustered based on their coupling constraints. According to the separability of the agents' objectives and the clusters' coupled constraints, HDEVCS is solved efficiently in a distributed manner by ADMM. The ECI structure considered in this chapter is similar to Fig. 5.1 which consists of CA, EVAs, and EV chargers; each agent has its own local objective function and constraints, while its performance is influenced by the other agents due to the coupled constraints. Comparing to the exiting trilayer methods, HDEVCS reduces the convergence time and the iteration numbers since its structure allows the agents to update their primal optimization variable simultaneously. The performance of HDEVCS is evaluated by the numerical simulations of two small and large scale case studies consisting of 306 and 9051 agents, respectively. The results verify the scalability and efficiency of the developed method, as it reduces the convergence time and iteration numbers by 60% compared to the state-of-the-art methods, flattens the aggregated load profile of the distribution grid, and decreases the charging cost for the EV owners without violating the grid feeders' capacity constraints.

6.1 Problem Formulation

The trilayer ECI includes CA, EVA, and EVB agents. The objective of EVCS is to generate a sequence of feasible EV charging profiles which minimize (maximize) a desirable loss (revenue) function while the operational constraints are satisfied. The objective of the trilayer EVCS is threefold which is written as:

$$\begin{aligned} V &:= \min_{\mathbf{p}^{ca},\mathbf{p}^{a},\mathbf{p}^{ev}} \mathbf{F}^{ca}(\mathbf{p}^{ca}) + \sum_{j\in\mathbb{N}_a} \left(\mathbf{F}^{a}_{j}(\mathbf{p}^{a}_{j}) + \sum_{i\in\mathbb{N}^{v}_{j}} \mathbf{F}^{ev}_{i,j}(\mathbf{p}^{ev}_{i,j})\right) \\ &= \min_{\mathbf{p}^{ca},\mathbf{p}^{a},\mathbf{p}^{ev}} \mathbf{F}^{ca}(\mathbf{p}^{ca}) + \mathbf{F}^{a}(\mathbf{p}^{a}) + \mathbf{F}^{ev}(\mathbf{p}^{ev}) \\ &\qquad \text{s.t. } (5.2)-(5.4),\ \forall i \in \mathbb{N}^{v}_{j},\ \forall j \in \mathbb{N}^{a}, \end{aligned} \tag{6.1}$$

where $\mathbf{F}^{ca}$, $\mathbf{F}^{a}$, and $\mathbf{F}^{ev}$ are the convex objective functions of CA, EVAs, and EVs, respectively. The constraint set of EVBs (5.2) as well as (5.3a) and (5.4a) are the local constraints, while (5.3b) and (5.4b) are the coupled constraints of the scheduling problem (6.1).

We define an auxiliary variable for each EVA_j as $\mathbf{p}^{au}_{j} = -\mathbf{p}^{a}_{j}$ in order to rewrite (6.1) in the *exchange problem* form which can be solved efficiently by ADMM. Considering (5.3b) and (5.4b), we have:

$$\mathbf{p}^{ca} + \sum_{j\in\mathbb{N}^{a}} \mathbf{p}^{a}_{j} + \sum_{j\in\mathbb{N}^{a}} \mathbf{p}^{au}_{j} + \sum_{j\in\mathbb{N}^{a}} \sum_{i\in\mathbb{N}^{v}_{j}} \mathbf{p}^{ve}_{i,j} = \mathbf{0}, \tag{6.2}$$

where $\mathbf{0} \in \mathbb{R}^{N}$ is the zero vector. This equality constraint helps us write (6.1) as a hierarchical *exchange problem*. In that way, we do not write the local constraints and only show the coupled constraint (6.2).

$$\begin{aligned} V &:= \min_{\mathbf{p}^{ca},\mathbf{p}^{a},\mathbf{p}^{ev}} \mathbf{F}^{ca}(\mathbf{p}^{ca}) + \mathbf{F}^{a}(\mathbf{p}^{a}) + \mathbf{F}^{au}(\mathbf{p}^{au}) + \mathbf{F}^{ev}(\mathbf{p}^{ev}) \\ &\qquad \text{s.t. } (6.2), \end{aligned} \tag{6.3}$$

in which $\mathbf{F}^{au}$ denotes the indicator function depending on the EVAs' auxiliary variable ($\mathbf{p}^{au}$), and it is defined as follows for the jth EVA:

$$\mathbf{F}^{au}_{j}(\mathbf{p}^{au}_{j}) = \begin{cases} 0, & \text{if } \mathbf{p}^{au}_{j} = -\mathbf{p}^{a}_{j} \\ \infty, & \text{otherwise.} \end{cases} \tag{6.4}$$

In the following subsection, it is shown that the optimization problem in (6.3) is the hierarchical *exchange problem* which can be solved in a distributed manner by ADMM. It is called HDEVCS as the proposed framework results in the network through which CA communicates only with EVAs, and EVAs communicate with their own EVs. That is, there is no direct communication between CA (the highest-level agent) and EVs (the lowest-level agent), so the proposed EVCS has a hierarchical structure. Nevertheless, all the agents solve their optimization problem locally and simultaneously which decreases the convergence time and communication overhead.

6.2 Hierarchical Distributed EVCS

In this section, the EVCS problem is manipulated mathematically to derive the hierarchical and clustered *exchange problem*. Then, ADMM is applied to solve it in a fully distributed manner.

6.2.1 Exchange Problem and HDEVCS

To derive HDEVCS framework, the following aggregated objective function and optimization variable are introduced.

$$\mathbf{F} = (\mathbf{F}^{ca}, \mathbf{F}^{au}, \mathbf{F}^{a}, \mathbf{F}^{ev})$$

$$\mathbf{p} = (\mathbf{p}^{ca}, \mathbf{p}^{au}, \mathbf{p}^{a}, \mathbf{p}^{ev}),$$

where $\mathbf{F}, \mathbf{p} \in \mathbb{R}^{\mathcal{N}^f \times N}$, $\mathcal{N}^f = (\mathcal{N}^v + 2 \times \mathcal{N}^a + 1) \in \mathbb{N}$. Therefore, we can rewrite (6.3) as:

$$\begin{aligned} V := \min & \sum_{n=1}^{\mathcal{N}^f} \mathbf{F}_n(\mathbf{p}_n) + \mathbf{G}(\mathbf{z}) \\ \text{s.t. } & \mathbf{p}_n = \mathbf{z}_n, \ \forall n \in [\![1, \mathcal{N}^f]\!], \end{aligned} \tag{6.6}$$

where $\mathbf{z} \in \mathbb{R}^{\mathcal{N}^f \times N}$, and $\mathbf{G}(\mathbf{z})$ is the indicator function defined by:

$$\mathbf{G}(\mathbf{z}) = \begin{cases} 0, & \text{if } \sum_{n=1}^{\mathcal{N}^f} \mathbf{z}_n = \mathbf{0} \\ \infty, & \text{otherwise.} \end{cases} \tag{6.7}$$

The augmented Lagrangian of (6.6) is written as:

$$\mathcal{L}_\rho(\mathbf{p}, \mathbf{z}, \lambda) = \mathbf{F}(\mathbf{p}) + \mathbf{G}(\mathbf{z}) + \lambda^T(\mathbf{p} - \mathbf{z}) + \frac{\rho}{2} \|\mathbf{p} - \mathbf{z}\|_2^2, \tag{6.8}$$

in which ρ is the penalty factor, and λ is the Lagrangian variable, also known as the dual variable. The Lagrangian (6.8) can be solved by ADMM using the partial updates of the dual variables in each iteration. The iterative primal and dual updates of ADMM are:

$$\mathbf{p}^{k+1} := \underset{\mathbf{p}}{\operatorname{argmin}}\, \mathcal{L}_\rho(\mathbf{p}, \mathbf{z}^k, \lambda^k) \tag{6.9a}$$

$$\mathbf{z}^{k+1} := \underset{\mathbf{z}}{\operatorname{argmin}}\, \mathcal{L}_\rho(\mathbf{p}^{k+1}, \mathbf{z}, \lambda^k) \tag{6.9b}$$

$$\lambda^{k+1} := \underset{\lambda}{\operatorname{argmax}}\, \mathcal{L}_\rho(\mathbf{p}^{k+1}, \mathbf{z}^{k+1}, \lambda), \tag{6.9c}$$

in which k is the iteration index. Hereafter, the scaled form of ADMM (5.14) is used where $\Lambda = \lambda/\rho$. The first step of ADMM (6.9a) is expanded as:

$$\mathbf{p}^{k+1} = \sum_{n=1}^{\mathcal{N}^f} \left(\mathbf{F}_n(\mathbf{p}_n) + \frac{\rho}{2} \left\| \mathbf{p}_n - \mathbf{z}_n^k + \Lambda_n^k \right\| \right), \tag{6.10}$$

which is separable and can be solved in parallel by each agent of ECI, i.e. CA, EVAs and EVs. Further details will be provided after simplifying the ADMM steps using the *exchange problem*.

According to (6.6), each $\mathbf{z}_n$ is equivalent to $\mathbf{p}_n$. Using the defined auxiliary variable $\mathbf{p}^{au}$ and also (5.3b) and (5.4b), the charging infrastructure can be partitioned into $\mathcal{N}^c = (\mathcal{N}^a + 1)$ clusters denoted by **CL**s. For each cluster, the coupled equality constraint which is the summation of the involved agents' primal variables is defined. That equality constraint is equal to zero, and it is known as the *equilibrium constraint*. The clusters and the corresponding *equilibrium constraints* of HDEVCS are defined as follows:

- $\mathbf{CL}_j$, $\forall j \in [\![1, (\mathcal{N}^c - 1)]\!]$, includes EVA_j and $EVB_{i,j}$, $\forall i \in \mathbb{N}_j^v$, and its *equilibrium constraint* is $\sum_{i=1}^{\mathcal{N}_j^v} \mathbf{p}_{i,j}^{ev} + \mathbf{p}_j^{au} = \mathbf{0}$.
- $\mathbf{CL}_{\mathcal{N}_c}$ includes CA and all EVAs, and its *equilibrium constraint* is $\sum_{j=1}^{\mathcal{N}^a} \mathbf{p}_j^a + \mathbf{p}^{ca} = \mathbf{0}$.

- According to the equality constraints of the defined clusters, we have:

$$\sum_{n\in\mathbf{CL}_j}\mathbf{z}_n=\mathbf{0},\ \forall j\in[\![1,\mathcal{N}^c]\!]. \tag{6.11}$$

The above three statements mean that the charging infrastructure includes $\mathcal{N}_c$ clusters where the interaction among the agents within each cluster can be written as the *exchange problem*. To show that, we write the Lagrangian for $\mathbf{z}$ (6.9b) in a partitioned form as:

$$\mathcal{L}(\mathbf{z},\upsilon)=\sum_{j=1}^{\mathcal{N}_c}\sum_{n\in\mathbf{CL}_j}\left(\frac{\rho}{2}\left\|\mathbf{p}_n^{k+1}-\mathbf{z}_n+\Lambda_n^k\right\|_2^2+\upsilon_j\mathbf{z}_n\right), \tag{6.12}$$

where υ_j is the Lagrangian multiplier corresponding to the coupled equality constraint of the jth **CL**. Using the KKT conditions for each cluster and adding up the gradients of Lagrangian in terms of $\mathbf{z}_n,\ n\in\mathbb{N}_j^c$, we have:

$$\nabla_{\mathbf{z}_n}\mathcal{L}(\mathbf{z}_n,\upsilon_j)=0\Rightarrow\mathbf{z}_n=\mathbf{p}_n^{k+1}+\Lambda_n^k-\frac{1}{\rho}\upsilon_j \tag{6.13}$$

$$\nabla_{\upsilon_j}\mathcal{L}(\mathbf{z}_n,\upsilon_j)=0\Rightarrow\sum_{n\in\mathbb{N}_j^c}\mathbf{z}_n=\mathbf{0} \tag{6.14}$$

$$(6.13),(6.14)\Rightarrow\sum_{n\in\mathbb{N}_j^c}\left(\mathbf{p}_n^{k+1}+\Lambda_n^k\right)-\frac{\mathcal{N}_j^c.\upsilon_j}{\rho}=\mathbf{0},$$

where $\mathbb{N}_j^c$ is the set of the agents in the jth **CL**, and $\mathcal{N}_j^c$ denotes its cardinality. Finally, the dual variable of the jth **CL** is obtained by:

$$\upsilon_j=\rho\big(\overline{\mathbf{p}}_j^{k+1}+\overline{\Lambda}_j^k\big), \tag{6.15}$$

in which $\overline{\mathbf{p}}_j=\frac{1}{\mathcal{N}_j^c}\sum\limits_{n\in\mathbb{N}_j^c}\mathbf{p}_n$, and $\overline{\Lambda}_j=\frac{1}{\mathcal{N}_j^c}\sum\limits_{n\in\mathbb{N}_j^c}\Lambda_n$. Using (6.13) and (6.15), a closed-form to update $\mathbf{z}_n,\ n\in\mathbb{N}_j^c$ is obtained as:

$$\mathbf{z}_n^{k+1}=\mathbf{p}_n^{k+1}-\overline{\mathbf{p}}_j^{k+1}+\mathbf{\Lambda}_n^k-\overline{\Lambda}_j^k. \tag{6.16}$$

Using the gradient method, Λ_n is updated by:

$$\Lambda_n^{k+1}=\Lambda_n^k+\mathbf{p}_n^{k+1}-\mathbf{z}_n^{k+1}. \tag{6.17}$$

Substituting (6.16) for (6.17) gives:

$$\Lambda_n^{k+1} = \overline{\mathbf{p}}_j^{k+1} + \overline{\Lambda}_j^k, \tag{6.18}$$

meaning that the dual updates for all the agents in $\mathbf{CL}_j$ shown by $\overline{\Lambda}_j$ are equal and independent of the number of agents. Therefore, $\mathbf{z}_n^{k+1}$ is obtained by:

$$\mathbf{z}_n^{k+1} = \mathbf{p}_n^{k+1} - \overline{\mathbf{p}}_j^{k+1}. \tag{6.19}$$

In (6.10), substituting (6.19) for $\mathbf{z}_n$ eliminates the second primal-update step of ADMM (6.9b), so there is not any sequential primal update in HDEVCS owing to reformulating EVCS as the *exchange problem*. Now, it can be shown that the primal variables ($\mathbf{p}_n$) are updated in parallel by CA, EVAs, and EVs at each iteration of HDEVCS using ADMM.

– primal variable update for $EV_{i,j}$, $\forall i \in \mathbb{N}_j^c$:

$$\begin{aligned} \mathbf{p}_{i,j}^{ev^{k+1}} = \underset{\mathbf{p}_{i,j}^{ev}}{\operatorname{argmin}} \big(& \mathbf{F}_{i,j}^{ev}(\mathbf{p}_{i,j}^{ev}) + \frac{\rho}{2} \left\| \mathbf{p}_{i,j}^{ev} - \mathbf{p}_{i,j}^{ev^k} + \overline{\mathbf{p}}_j^k + \overline{\Lambda}_j^k \right\|_2^2 \big) \\ & \text{s.t. (5.2).} \end{aligned} \tag{6.20}$$

– primal variable update for $EVA_{j'}$, $j' \in \mathbb{N}_j^c$:

$$\begin{aligned} \mathbf{p}_{j'}^{a^{k+1}} = \underset{\mathbf{p}_{j'}^{a}, \mathbf{p}_{j'}^{au}}{\operatorname{argmin}} \big(& \mathbf{F}_{j'}^{a}(\mathbf{p}_{j'}^{a}) + \frac{\rho}{2} \left\| -\mathbf{p}_j^a + \mathbf{p}_{j'}^{a^k} + \overline{\mathbf{p}}_{j'}^k + \overline{\Lambda}_{j'}^k \right\|_2^2 \\ & + \frac{\rho}{2} \left\| \mathbf{p}_{j'}^{a} - \mathbf{p}_{j'}^{a^k} + \overline{\mathbf{p}}_{\mathcal{N}^c}^k + \overline{\Lambda}_{\mathcal{N}^c}^k \right\|_2^2 \big) \\ & \text{s.t. (5.3),} \end{aligned} \tag{6.21}$$

in which $-\mathbf{p}_{j'}^a$ substitutes for $\mathbf{p}_{j'}^{au}$ in the second right-hand-side expression, meaning that the jth EVA deals with only one primal variable.

– primal variable update for CA:

$$\begin{aligned} \mathbf{p}^{ca^{k+1}} = \underset{\mathbf{p}^{ca}}{\operatorname{argmin}} \big(& \mathbf{F}^{ca}(\mathbf{p}^{ca}) + \frac{\rho}{2} \left\| \mathbf{p}^{ca} - \mathbf{p}^{ca^k} + \overline{\mathbf{p}}_{\mathcal{N}^c}^k + \overline{\Lambda}_{\mathcal{N}^c}^k \right\|_2^2 \big) \\ & \text{s.t. (5.4).} \end{aligned} \tag{6.22}$$

After updating the primal variables by all the agents in parallel (6.20)-(6.22), EVs send out their updated variable to their EVAs, and EVAs transmit their updated variable to

CA. The average power ($\overline{\mathbf{p}}_j$) and the dual variable ($\overline{\Lambda}_j$) for each $\mathbf{CL}_j$ are updated by EVAs and CA. To lower the communication overhead, $\overline{\Omega}_j$ is broadcast to the other agents in $\mathbf{CL}_j$ which is defined as $\overline{\Omega}_j = \overline{\mathbf{p}}_j + \overline{\Lambda}_j$. The whole procedure of the proposed HDEVCS is shown in Algorithm 6, where r and s are the primal and dual residuals, respectively, and Th_p and Th_d are their corresponding feasibility tolerance. For more details about primal and dual residuals and stopping criteria, we refer to [BPE11, Chapter 3.3].

The communication network links between the agents as well as the broadcast variables within each $\mathbf{CL}_j$ are shown in Fig. 6.1. Note that the index of each cluster, i.e. $\mathbf{CL}_j$, is shown next to the agent which updates the average power ($\overline{\mathbf{p}}_j$) and the dual variable ($\overline{\mathbf{\Lambda}}_j$).

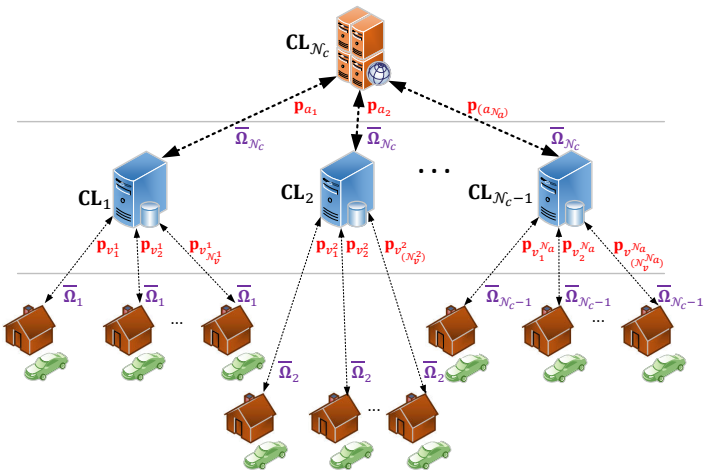

Figure 6.1: HDEVCS's communication network and broadcast signals.

6.2.2 Receding Horizon HDEVCS: RH-HDEVCS

Similar to RH-ADMM developed in 5.2.5, the receding horizon feedback control is applied to HDEVCS to generate the optimal control sequences for the EV chargers. Utilizing RH gives the flexibility to the EV owners, EVAs, and CA to change their objective functions, as long as it is convex and feasible, at any RH iteration. In that case, as each agent's optimization function is solved locally, they do not need to notify other agents about changing the objective function. RH-HDEVCS shown in Algorithm 7 executes the following steps consecutively. First, according to the requested EV charging and total netload demand of the system at

Algorithm 6: HDEVCS

Initialization: Set initial values for $\mathbf{p}^{ca^0}$, $\mathbf{p}^{a^0}$, $\mathbf{p}^{ev^0}$, and Λ^0.
$k \leftarrow 0$.
$l \leftarrow 0$.
while $Err_p > Th_p$ or $Err_d > Th_d$ **do**
  for all CA, EVAs, and EVs **do in parallel**
    Update $\mathbf{p}_{i,j}^{ev^{k+1}}$ $\forall EVB_{i,j},\ i \in \mathbb{N}_j^v,\ j \in \mathbb{N}^a$, by (6.20).
    Update $\mathbf{p}_{j'}^{a^{k+1}}$ $\forall EVA'_j,\ j' \in \mathbb{N}^a$ by (6.21).
    Update $\mathbf{p}^{ca^{k+1}}$ by (6.22).
  end for
  for $j = 1 : \mathcal{N}^c$ **do in parallel**
    if $j \in [\![1, \mathcal{N}^c - 1]\!]$ **then**
      EVA_j receives $\mathbf{p}_{i,j}^{ev^{k+1}}, \forall EVB_{i,j} \in \mathbf{CL}_j$.
      Update $\overline{\mathbf{p}}_j^{k+1} = \frac{1}{\mathcal{N}_j^c} \sum_{n \in \mathbb{N}_j^c} \mathbf{p}_n^{k+1}$.
      Update $\overline{\Lambda}_j^{k+1} = \overline{\mathbf{p}}_j^{k+1} + \overline{\Lambda}_j^k$.
      Broadcast $\overline{\Omega}_j^{k+1}$ to $\forall EVB_{i,j} \in \mathbf{CL}_j$.
      Update $\mathbf{r}_j^{k+1}$,$\mathbf{s}_j^{au^{k+1}}$ and $\mathbf{s}_{i,j}^{ev^{k+1}}$, $\forall i \in \mathbb{N}_j^c$.
    else
      CA receives $\mathbf{p}_j^{a^{k+1}}, \forall j \in \mathbb{N}^a$.
      Update $\overline{\mathbf{p}}_{\mathcal{N}^c}^{k+1} = \frac{1}{(\mathcal{N}^a+1)}(\sum_{j \in \mathbb{N}^a} \mathbf{p}_j^{a^{k+1}} + \mathbf{p}^{ca^{k+1}})$.
      Update $\overline{\Lambda}_{\mathcal{N}^c}^{k+1} = \overline{\mathbf{p}}_{\mathcal{N}^c}^{k+1} + \overline{\Lambda}_{\mathcal{N}^c}^k$.
      Broadcast $\overline{\Omega}_{\mathcal{N}^c}^{k+1}$ to all EVAs.
      Update $\mathbf{r}_j^{k+1}$, $\mathbf{s}^{ca^{k+1}}$ and , $\mathbf{s}_j^{a^{k+1}}$, $\forall j \in \mathbf{CL}_{\mathcal{N}^c}$.
    end if
  end for
end while

time instant t over the time horizon $N \in \mathbb{N}$, Algorithm 6 finds the optimal values of the primal variables indicated by $\mathbf{p}^\star(\cdot)$. Then, only the first element of $\mathbf{p}^\star(\cdot)$ is implemented by each agent. Lastly, t is incremented, and the same procedure is repeated.

Algorithm 7: RH-HDEVCS

1: **while** $t \leqslant N$ **do**
2: Update EVs' arrival/departure time, initial state of energy, and charging energy demand, and EVAs' and CA's available capacities.
3: Run HDEVCS, Algorithm 6, to calculate $\mathbf{p}^\star(\cdot)$.
4: Apply the first element of the optimal value of $\mathbf{p}^\star(\cdot)$ for each agent.
5: Increment the time index t.
6: **end while**

6.3 Numerical Simulations and Discussion

In this section, the performance of HDEVCS is evaluated for two case studies, a small-scale system and a large-scale system, which are called $System_1$ and $System_2$, respectively. To show the effectiveness of the proposed EVCS, its performance is compared with uCC (defined in Section 5.3.3) and semi-coordinated charging (sCC) methods, in which the EVs charge with a constant power rating while they are plugged in.

Through all the simulations, the maximum power rating for EV chargers is 4 kW. The real netload dataset of EVBs is collected from [Aus] provided for 300 residential customers, and the wholesale electricity price is available from the California Independent System Operator-CAISO [CAI]. All the simulations are executed by MATLAB on a PC with Intel® Core™ $i7-4770$ 3.40 GHz CPU, 4 cores and 8 GB RAM, and the convex optimization problems are solved by CVX [GB14]. To assess the performance of HDEVCS for LVM, the metrics defined in Subsection 5.3.2 are used.

6.3.1 *System$_1$*: Small-Scale Case Study

System$_1$ consists of 5 EVAs each of which is supplying 60 EVs. The simulations are executed for two scenarios with different set of objective functions for EVAs and EVs. Based on the National Household Travel Survey (NHTS) 2017 ([SMN17]), the required charging energy, arrival time, and departure time of the EVs are generated as follows: the initial and designated EVs' battery energies are normally distributed over $[8, 10]$ kWh and $[22, 25]$ kWh, respectively; EVs' arrival and departure times are normally distributed in $[\texttt{16:30}, \texttt{20:30}]$ and $[\texttt{6:00}, \texttt{9:30}]$, respectively.

Scenario 1: In the first scenario, the purpose of CA is to minimize the peak load demand in the system which is equivalent to LVM ([SHM11]), EVAs keep their aggregated EV charging power less than the maximum available capacity, and EVs aim at reducing their charging cost. Defining the aggregated netload demand of the jth EVA, $j \in \mathbb{N}^a$ by:

$$p_j^{a_n}(t) := \sum_{i \in \mathbb{N}_j^v} p_{i,j}^{uc}(t), \tag{6.23}$$

LVM is obtained by minimizing:

$$\begin{aligned} \mathbf{F}^{ca}(\mathbf{p}^{ca}) &:= \big(\mathbf{E} - \mathbf{p}^{ca} - \sum_{j \in \mathbb{N}^a} \mathbf{p}_j^{a_n}\big)^2 \\ &\text{s.t. (5.4)}, \end{aligned} \tag{6.24}$$

in which $\mathbf{E}$ is defined in Subsection 5.3.2. As we assume that EVAs' purpose is only to keep their aggregated EV charging demand less than the feeder capacity constraint (5.3a), $\mathbf{F}_j^a$ is defined by:

$$\begin{aligned} \mathbf{F}_j^a(\mathbf{p}_j^a) &:= \mathbf{I}_j^a(\mathbf{p}_j^a) \\ &\text{s.t. (5.3)}, \ \forall j \in \mathbb{N}^a, \end{aligned} \tag{6.25}$$

where $\mathbf{I}_j^a$ is the indicator function which is defined as:

$$\mathbf{I}_j^a(\mathbf{p}_j^a) = \begin{cases} 0, & \text{if (5.3) is satisfied} \\ \infty, & \text{otherwise.} \end{cases} \tag{6.26}$$

$EV_{i,j}^{ev}$'s objective function is defined by:

$$\begin{aligned} \mathbf{F}_{i,j}^{ev}(\mathbf{p}_{i,j}^{ev}) &:= \mathbf{\Pi}^T.\mathbf{p}_{i,j}^{ev} \\ \text{s.t. } (5.2),\ \forall i \in \mathbb{N}_j^v,\ \forall j \in \mathbb{N}^a. \end{aligned} \tag{6.27}$$

The simulation results of HDEVCS compared with uCC and sCC are illustrated in Fig. 6.2. LVM+CR-1 and LVM+CR-2 show the aggregated load profile (the aggregated EV charging demand plus netload) when the weighting factor for (6.27) is 1 and 10, respectively. By decreasing the weighting factor, the load profile becomes smoother at the cost of a more expensive charging for the EV owners.

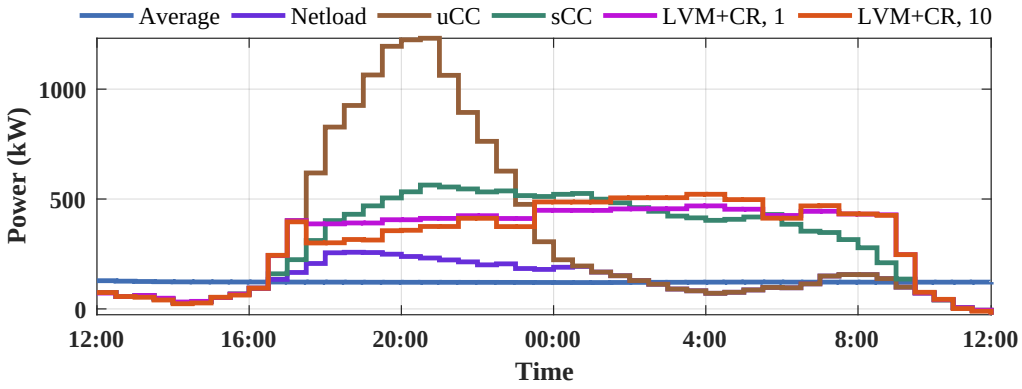

Figure 6.2: Aggregated load profile for uCC, sCC and HDEVCS for two different CR weighting factors, 1 and 10.

In Fig. 6.3, it is shown that EVCS is effective in limiting the aggregated load demand to the capacity of the EVAs' feeders. While sCC does not have any control on the aggregated EV load (Fig. 6.3: left), HDEVCS will not let the capacity constraints (105 kW) be violated (Fig. 6.3: right) even if the EV agents choose a high weighting factor to greedily reduce their charging cost. These results highlight the importance of optimal coordination of EV charging in supplying more load demand without expansion of the grid capacity.

Scenario 2: In the second scenario, it is assumed that CA's purpose is still LVM (6.24), while EVAs aim at reducing the aggregated charging cost, and EVs plan for reducing their

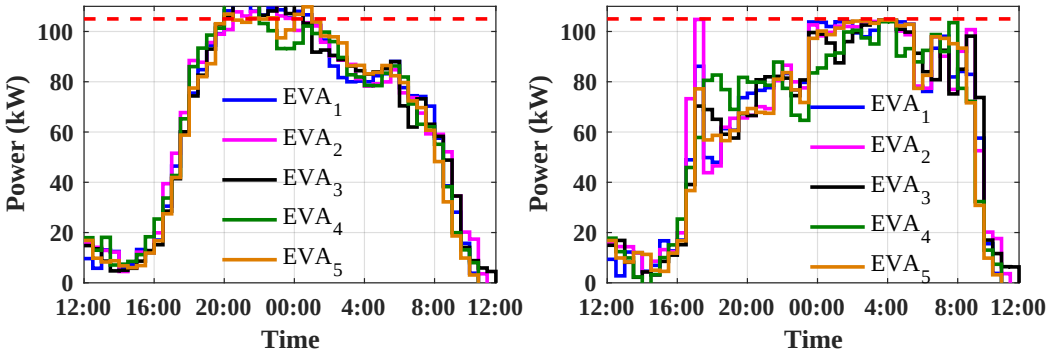

Figure 6.3: EVAs' feeder constraint violation by sCC (left) and feeder constraint satisfaction by HDEVCS (right) for LVM+CR-2 mode.

battery degradation cost. Thus, we have:

$$\begin{aligned} &\mathbf{F}_j^a(\mathbf{p}_j^a) := \mathbf{\Pi}^T.\mathbf{p}_j^a \\ &\text{s.t. } (5.3),\ \forall j \in \mathbb{N}^a. \end{aligned} \tag{6.28}$$

To define EVs' optimization function, the battery degradation model is borrowed from [MZL15] which is presented as:

$$\begin{aligned} &\mathbf{F}_{i,j}^{ev}(\mathbf{p}_{i,j}^{ev}) := \gamma_{i,j}^{ev_1}\mathbf{p}_{i,j}^{ev^2} + \gamma_{i,j}^{ev_2}\mathbf{p}_{i,j}^{ev} + \gamma_{i,j}^{ev_3} \\ &\text{s.t. } (5.2),\ \forall i \in \mathbb{N}_j^{ev},\ \forall j \in \mathbb{N}^a, \end{aligned} \tag{6.29}$$

where $\gamma_{i,j}^{ev_1}$, $\gamma_{i,j}^{ev_2}$, and $\gamma_{i,j}^{ev_3}$ are the constant coefficients depending on the number, nominal voltage value and price of the energy units of the battery cells.

The aggregated load profiles obtained by HDEVCS are compared with uCC and sCC in Fig. 6.4. Similar to the first scenario, the simulations are carried out for two different weighting factors of EVs' objective function, i.e. 1 and 10, which are shown by LVM+CR+BDR-1 and LVM+CR+BDR-2, respectively. In both modes, the weighting factor of CR which is EVAs' objective function is equal to 10.

As it is illustrated, the aggregated load profile in both modes is flattened by HDEVCS while the capacity constraints of EVAs' are not exceeded (Fig. 6.5).

To compare the performance of HDEVCS in the first and second scenarios, the aggregated CR and BDR for EVAs is shown in Fig. 6.6 and Fig. 6.7, respectively. Since the

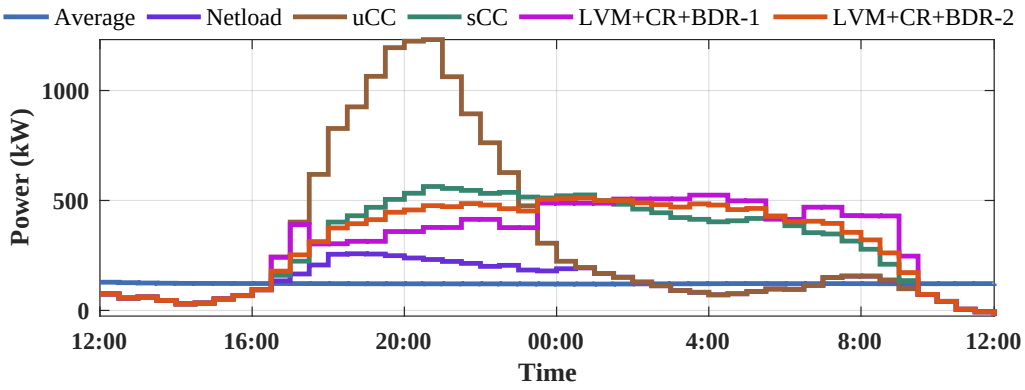

Figure 6.4: Aggregated load profile for uCC, sCC and HDEVCS for two different BDR weighting factors, 1 and 10.

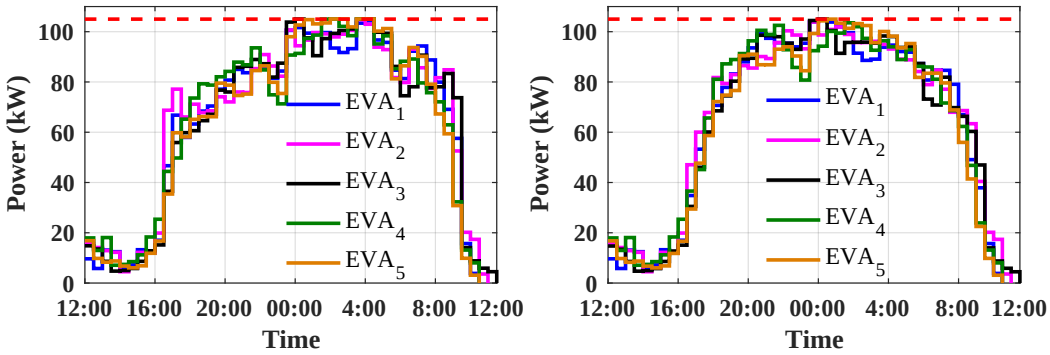

Figure 6.5: EVAs' feeder constraint satisfaction in LVM+CR+BDR-1 (left) and LVM+CR+BDR-2 (right) modes by HDEVCS.

weighting factor of CR objective function in LVM+CR-2 is larger than the weighting factor in LVM+CR-1, the least aggregated CR for all EVAs is achieved by LVM+CR-2 (Fig. 6.6). As EVs start charging with the maximum power rating in uCC mode, their charging cost is more than all other modes. Considering Fig. 6.7, the least battery degradation cost is achieved by uCC, sCC, LVM+CR+BDR-1, and LVM+CR+BDR-1. The reason is that the charging power profile in uCC and sCC is constant which according to (6.29) minimizes the battery degradation cost. In LVM+CR+BDR-1 and LVM+CR+BDR-2 modes, BDR cost is the objective function of EVs, therefore EVCS reduces BDR as well. However, battery degradation cost is larger in LVM+CR-1 and LVM+CR-2 as EVs try to reduce their charg-

ing cost only, and battery degradation reduction is not considered in the EVCS optimization function.

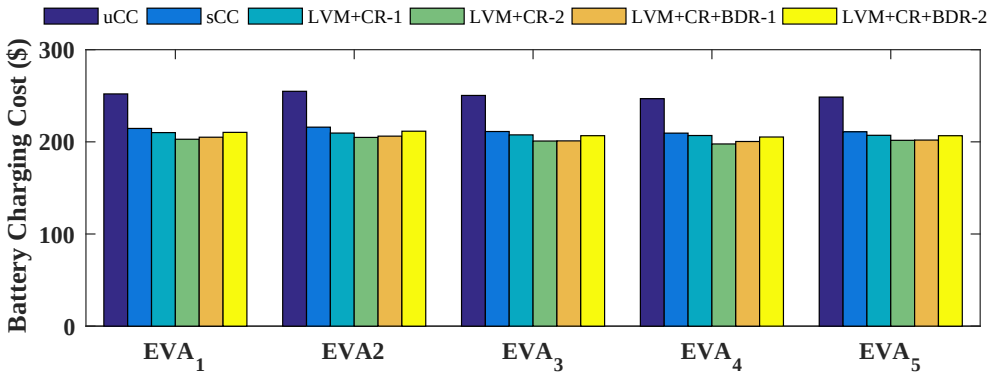

Figure 6.6: Aggregated EV charging cost of EVAs for different charging modes.

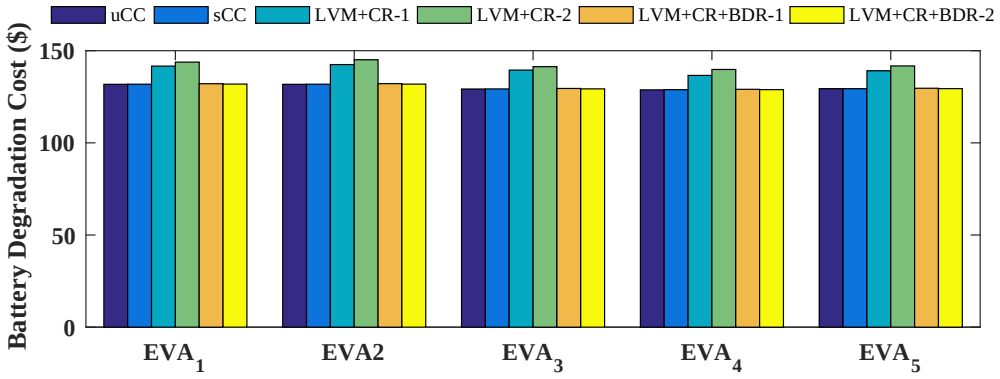

Figure 6.7: Aggregated EV battery degradation cost of EVAs for different charging modes.

To further clarify the comparison of different simulated scenarios and the charging modes, the results are summarized in Table 6.1 where the best result obtained for each metric is shown in bold. As it is expected, LVM+CR-1 gives the lowest accumulated PTP, PTA, and RMS since the weighting factors of LVM and CR are equal, while the least aggregated charging cost is obtained by increasing the weight of CR in LVM+CR-2. As it was discussed earlier, the lowest accumulated BDR is achieved by uCC, sCC, LVM+CR+BDR-1, and LVM+CR+BDR-1. The last column of the table shows the normalized accumulated objective values obtained by each charging mode. The weighting factors of the normalized values are equal to 1. Given that, LVM-CR-1 charging mode results in the best accumulated

performance, and uCC charging mode leads to the worst performance.

Table 6.1: LVM, CR, and BDR Improvement Using HDEVCS.

EVCS Mode	PTP(kW)	PTA	RMS(kW)	ACC[1]($)	BDC[2]($)	NAP[3]
uCC	1257	0.21	419.0	1253	**651**	4.91
sCC	589	0.10	272.5	1062	652	3.34
LVM+CR-1	**494**	**0.08**	**258.2**	1041	699	**3.20**
LVM+CR-2	548	0.09	263.0	**1008**	712	3.28
LVM+CR+BDR-1	549	0.09	263.6	1015	652	3.21
LVM+CR+BDR-2	533	0.09	264.2	1040	**651**	3.22

[1] aggregated charging cost.

[2] aggregated battery degradation cost.

[3] normalized accumulated performance.

PnP: As mentioned before, the advantage of RH-HDEVCS is PnP in terms of the agents' objective function. That is, each agent may change its objective function in any RH iteration. This is illustrated in Fig. 6.8 where an EV is plugged in at `21:00` when its battery energy is 10 kWh, and it is unplugged at `6:30` when it is fully charged. The EV is charged in CR mode until `23:30` when the EV owner switches the charging mode to sCC, i.e. charging with constant power. The desired energy stored in the battery at departure time is 24 kWh.

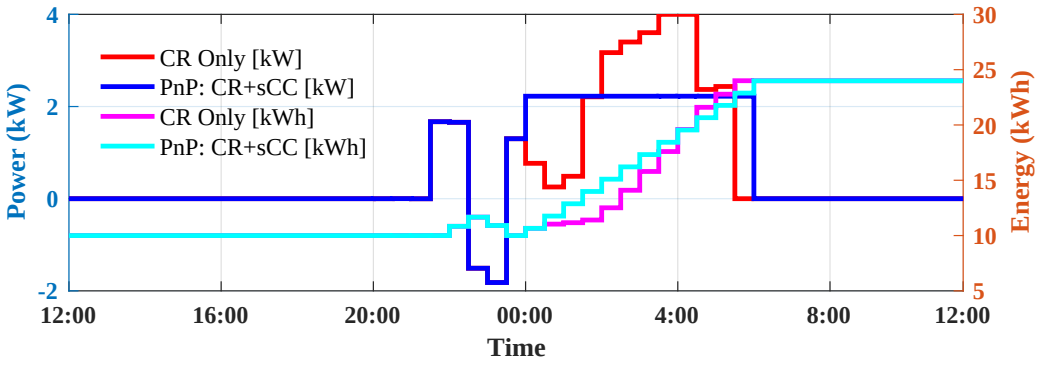

Figure 6.8: PnP using RH-HDEVCS: the EV agent switches from CR mode to sCC mode at `23:30`.

6.3.2 *System*$_2$: Large-Scale Case Study

System$_2$ consists of 50 EVAs each of which is supplying 180 EVs. The simulations are executed for two main scenarios with similar objective functions but different constraints. The objective function in both scenarios includes LVM and CR. However, the feeder capacity constraints are considered only in the first scenario (C/LVM+CR), while there is no feeder constraint in the second scenario (UnC/LVM+CR). In C/LVM+CR, the maximum loading capacity is 180 kW for the feeders supplying EVA_6 and EVA_{11} and 175 kW for the other feeders. The required charging energy, arrival time, and departure time of the EVs are generated as follows: the initial and designated EVs' battery energies are normally distributed over $[8, 10]$ kWh and $[22, 25]$ kWh, respectively; for 50% of EVs, the arrival and departure times are normally distributed in $[\texttt{16:30}, \texttt{20:30}]$ and $[\texttt{6:00}, \texttt{9:30}]$, respectively; for the rest of EVs, the arrival and departure times are normally distributed in $[\texttt{6:00}, \texttt{9:30}]$ and $[\texttt{16:30}, \texttt{20:30}]$, respectively.

The aggregated load profiles obtained by sCC, C/LVM+CR, and UnC/LVM+CR are shown in Fig. 6.9. The load profiles of C/LVM+CR and UnC/LVM+CR coincide, and they perfectly fill in the valley (in $[\texttt{9:00}, \texttt{15:00}]$) and shave the peak loads (at `0:00`, `7:00` and `18:30`) which are seen in sCC load profile.

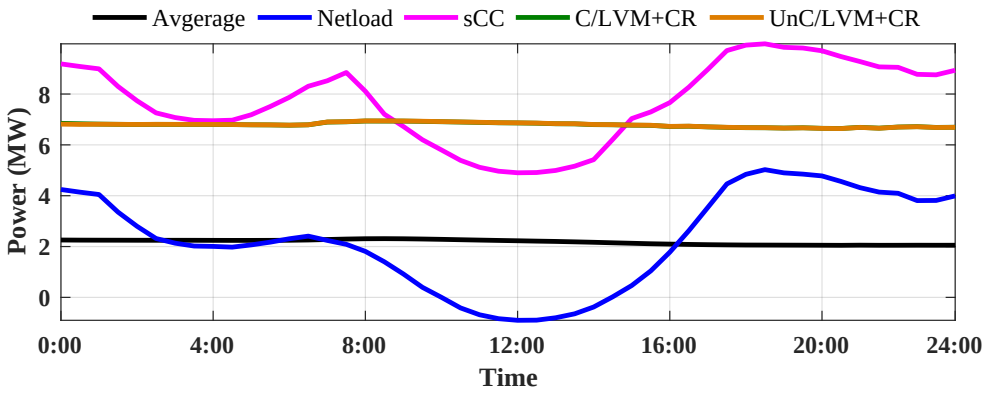

Figure 6.9: Aggregated load profile for sCC, C/LVM+CR, and UnC/LVM+CR.

Although the load profiles of C/LVM+CR and UnC/LVM+CR are similar, their EVAs' feeder load profiles are different. Comparing Fig. 6.10 with Fig. 6.11, several EVA feeders are

overloaded in UnC/LVM+CR scenario while all the EVA feeder loads meet the constraints in C/LVM+CR. This means that EVCS with feeder capacity constraints can accommodate a large population of EVs without any grid feeder expansion requirement. The other difference between C/LVM+CR and UnC/LVM+CR is recognized by comparing the EVAs' aggregated charging costs in Fig. 6.12 and Fig. 6.13. Although the difference is not considerable, UnC/LVM+CR has less charging cost owing to the fact that EVs have more flexibility to shift their charging demand to the time periods with lower electricity price since there is no constraint on the EVAs' feeders.

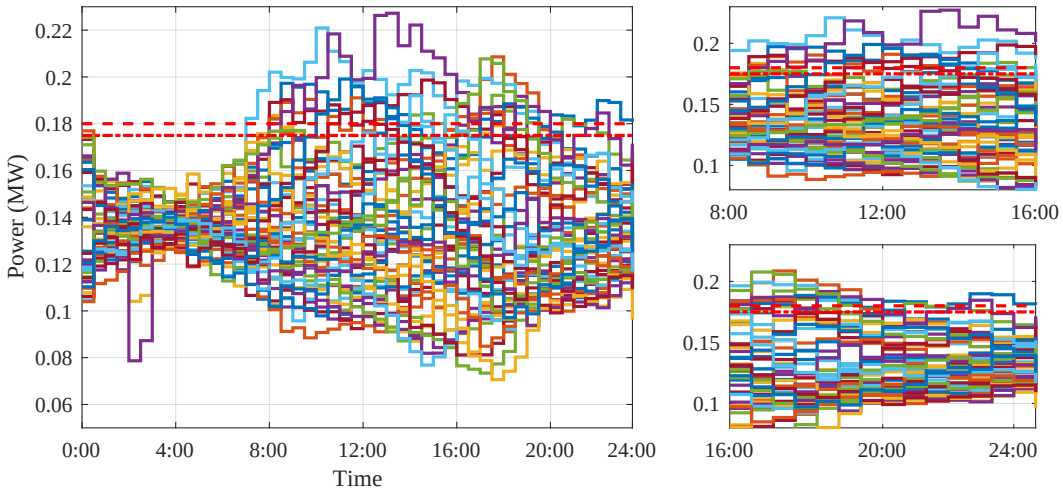

Figure 6.10: EVAs' feeder constraint violation in UnC/LVM+CR.

6.3.3 Comparison with Hierarchical ADMM

As it is already discussed, HDEVCS reduces the communication overhead and the convergence time compared to the methods in which the agents update their primal variable sequentially in two different steps. In this subsection, HDEVCS is compared with the hierarchical ADMM proposed in Chapter 5. The hierarchical ADMM consists of two layers of the *sharing problem*. The first layer is executed between CA and EVAs, and the second layer between each EVA and its EVs. Therefore, the ECI agents do not update their primal variable at the same time. To show the advantage of the proposed HDEVCS designed based on the *exchange problem*, we run LVM+CR-1 charging mode for both $System_1$ and $System_2$

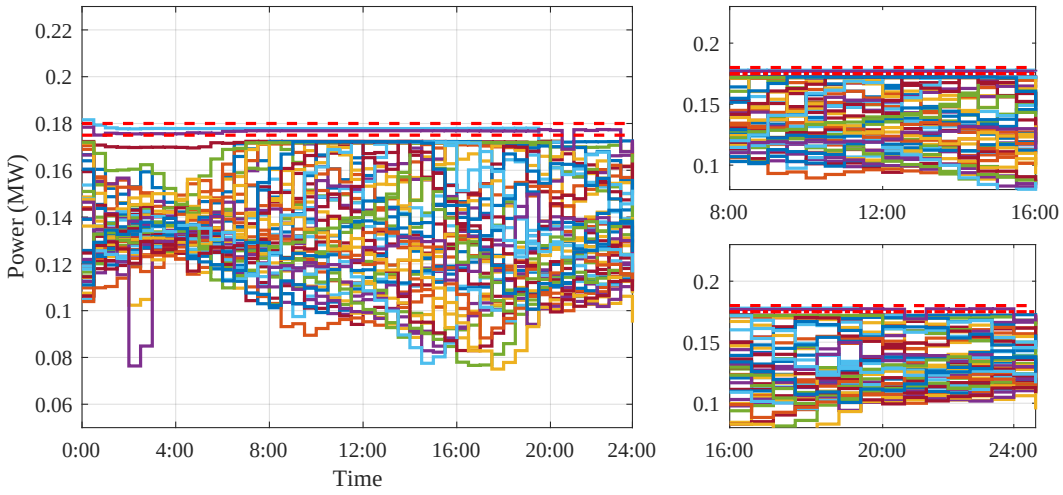

Figure 6.11: EVAs' feeder constraint satisfaction in C/LVM+CR.

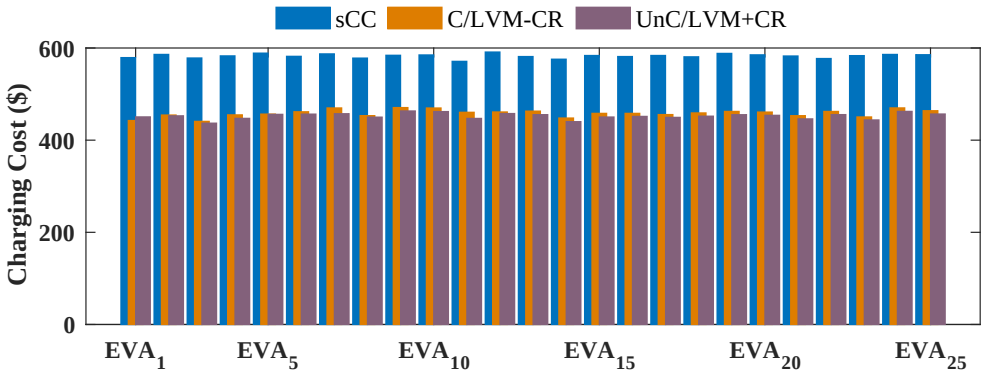

Figure 6.12: Aggregated charging cost of EVA_1-EVA_{25} by different charging modes.

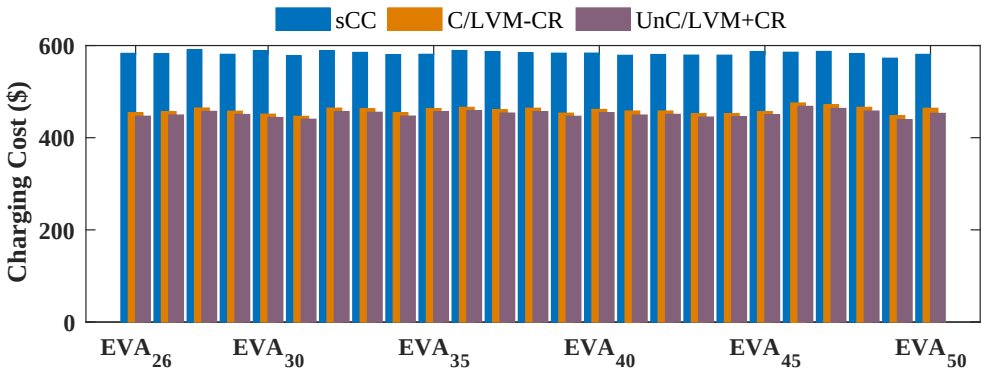

Figure 6.13: Aggregated charging cost of EVA_{26}-EVA_{50} by different charging modes.

Table 6.2: Comparison between HDEVCS and the hierarchical ADMM (Chapter 5).

Method	Case Study	Convergence Time (s)	Iterations
HDEVCS	$System_1$	178.72	64
	$System_2$	3331.5	1193
Hierarchical ADMM	$System_1$	446.8	161
	$System_2$	8204.1	2938

by the hierarchical ADMM. The convergence time and the number of iterations are shown in Table 6.2. For both methods, the penalty factors are similar ($\rho = 1$).

As it is shown, HDEVCS improves convergence time by 60% compared to the hierarchical ADMM. The convergence time, however, for $System_2$ will be still considerable (≈ 50 min) if HDEVCS is embedded in RH as the netload dataset is collected every 30 min, meaning that RH-HDEVCS should converge in less than 30 min. However, it is worthy to mention that the computation times in Table 6.2 are obtained by a CPU with 4 cores, while RH-HDEVCS is proposed to be implemented in a multi-agent framework. Also, chances are the convergence time further improves using adaptive penalty term [XFG16, XLL17].

6.4 Conclusion

In this chapter, a trilayer multi-agent framework for the optimal EV charging coordination was proposed to reduce the load variance and charging cost without violating the feeders' capacity constraints. By exploiting the configuration of the charging network and the mathematical properties of the EVCS problem, a novel hierarchical distributed method has been developed based on the *exchange problem* for the optimal charging coordination problem which is solved by ADMM. Owing to the properties of the derived hierarchical *exchange problem*, the second primal-update step of ADMM is eliminated, therefore all the agents update their primal variable in parallel, which results in the reduction of convergence time and iteration numbers. In addition, embedding the proposed method in the receding horizon feedback control gives flexibility to the agents to change their objective function in any

receding horizon iteration. To evaluate the performance of HDEVCS, it has been applied to two case studies, a small-scale and a large-scale system. The results have revealed that HDEVCS can reduce the peak load demand as well as EV charging and battery degradation costs significantly, while the grid feeders' capacity constraints are not violated. This means that the grid can accommodate a large population of EVs without investment in the grid capacity expansion.

CHAPTER 7

Distributed EV Charging Scheduling in Distribution Networks

As it is discussed in Subsection 1.3.3, EVMS can be considered as an integrated load management module in DMS. In this case, the model of the distribution grid (introduced in Section 2.4) is considered in optimal load scheduling. If only DSO handles the EVCS problem, the size of the optimization problem including the grid model and EV charging variables will be significantly large. Therefore in this chapter, a distributed method is proposed to make the charging coordination problem scalable and alleviate its computation burden for DSO. In the proposed method, DSO solves the voltage regulation problem with the consideration of the power flow model in the grid, while EVAs solve their local problem including EV charging cost reduction and the corresponding constraints. To ensure that the aggregated active and reactive loads of EVAs meet the DSO's requirement, EVCS is formulated as the *consensus problem* which is solved efficiently in an iterative procedure between DSO and EVAs by ADMM. To show the effectiveness of the proposed distributed *consensus* EVCS (DCEVCS), it is applied to the IEEE-13 bus system, and the results are discussed for different scenarios.

7.1 Model Description

A residential distribution grid including a set of EVAs through which EVBs are supplied is assumed. $\mathbb{N}^a$ denotes the set of grid EVAs, which its cardinality is shown by $\mathcal{N}^a$. In addition, the set of EVBs which are supplied through the jth EVA and its cardinality are shown by $\mathbb{N}_j^v$ and $\mathcal{N}_j^v$, respectively. $EVB_{i,j}$ denotes the ith EVB supplied by the jth EVA. The electricity consumption model of the EVB, which is equipped with a solar panel and an

EV charger is displayed in Fig. 7.1.

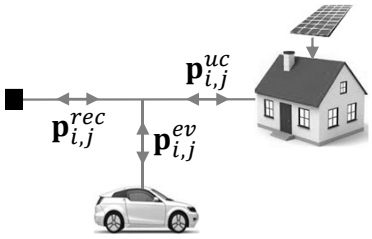

Figure 7.1: Building model with EV charger and solar panel.

Accordingly, the load model of $EVB_{i,j}$ is written as:

$$p_{i,j}^{evb}(t) = p_{i,j}^{uc}(t) + p_{i,j}^{ev}(t), \tag{7.1}$$

where $p_{i,j}^{evb}(t) \in \mathbb{R}$. The set of feasible trajectories of $EVB_{i,j}$ is defined as:

$$\mathbb{P}_{i,j}^{evb} = \mathbb{P}_{i,j}^{ev}, \tag{7.2}$$

in which $\mathbb{P}_{i,j}^{ev}$ is already defined in Section 2.2.

According to the model defined for EVBs, the aggregated active and reactive powers of the jth EVA are obtained by:

$$P_j^a(t) = p_j^{bs}(t) + p_j^{auc}(t) + \sum_{i \in \mathbb{N}_j^r} (p_{i,j}^{ev}(t)) \tag{7.3a}$$

$$Q_j^a(t) = q_j^{bs}(t) + q_j^{auc}(t), \tag{7.3b}$$

in which $p_j^{auc}(t) = \sum_{i \in \mathbb{N}_j^v} p_{i,j}^{uc}(t)$ and $q_j^{auc}(t) = \sum_{i \in \mathbb{N}_j^v} q_{i,j}^{uc}(t)$ are, respectively, the aggregated uncontrollable active and reactive powers. $p_j^{bs}(t)$ and $q_j^{bs}(t) \in \mathbb{R}$ are already defined in Section 2.1. If the jth EVA does not have BES, $p_j^{bs}(t)$ and $q_j^{bs}(t)$ will be neglected in (7.3). In that case, the jth EVA does not contribute to the reactive power, and the *consensus* variable, which will be discussed in the following sections, includes only the active power. In addition, we introduce:

$$p_j^{ac}(t) = \sum_{i \in \mathbb{N}_j^v} p_{i,j}^{ev}(t), \ j \in \mathbb{N}^a, \tag{7.4}$$

as the aggregated controllable load of the jth EVA.

7.2 Problem Formulation

The distribution grid includes DSO and EVAs agents, where the goal of DSO is to regulate the nodal voltages while meeting the power flow constraints, and EVAs target LVM on their supplying feeder as well as electricity cost reduction for their customers. Accordingly, the objective function of EVCS is threefold which is written as follows:

$$V_{evcs} := \min_{\mathbf{V},\mathbf{I},\mathbf{P},\mathbf{Q}} \sum_{j\in\mathbb{N}_b/1} \|\mathbf{v}_j - \mathbf{v}_{ref}\|_2^2 + \sum_{j\in\mathbb{N}^a} \Big(\big(\overline{\mathbf{\Omega}}_j^p - \mathbf{p}_j^{bs} - \mathbf{p}_j^{ac}\big)^2 + \big(\overline{\mathbf{\Omega}}_j^q - \mathbf{q}_j^{bs}\big)^2 + \sum_{i\in\mathbb{N}_j^v} \mathbf{\Pi}^T.\mathbf{p}_{i,j}^{ev} \Big)$$
$$\text{s.t. } \mathbb{P}_{i,j}^{evb},\ \mathbb{P}_j^{bs},\ \text{and (7.3)}\ \forall i \in \mathbb{N}_j^v,\ j \in \mathbb{N}^a,\ (2.15) - (2.16), \tag{7.5}$$

where the first RHS expression is the voltage regulation function, the second and third expressions minimize the active and reactive power variances, respectively, and the last expression minimizes the customers' charging cost. $\overline{\mathbf{\Omega}}_j^p$ and $\overline{\mathbf{\Omega}}_j^q$ are, respectively, the average active and reactive powers of the jth EVA which can be calculated similar to (5.26). The grid power flow model $(2.15) - (2.16)$ is considered as the DSO's local constraint, and the rest are the EVAs' local constraints.

The optimal load coordination (7.5) is a non-convex problem due to the equality constraint (2.15d). For a large-scale distribution grid with significant number of EVAs and EVs, solving (7.5) centrally is not computationally efficient for DSO. Therefore in the following section, a multi-agent method is proposed by the *consensus* ADMM to solve (7.5) using the distributed optimization.

7.3 Scalable EV Load Coordination

In this section, ADMM is used to solve the optimization problem (7.5) in a distributed manner such that DSO and EVAs communicate iteratively. However, (2.15d) should be relaxed as it is a non-convex constraint, otherwise ADMM is not applicable. According to [GLT15], (2.15d) can be relaxed to a convex second-order cone as:

$$V_j(t) I_{jj'}(t) \geq P_{jj'}^2(t) + Q_{jj'}^2(t), \tag{7.6}$$

where j and $j' \in \mathbb{N}_b$. The sufficient conditions to make the relaxation tight are [Low14a, Low14b]: (i) the grid should be radial; (ii) bus voltages should be very close to the nominal value; and (iii) the active and reactive powers injected to the buses should not be too large. As it was discussed earlier, most of the distribution grids are radial (1st condition); the voltage regulation keeps the nodal voltages close to the nominal value (2nd condition); also, as we do not have large distributed energy resources here, there is not a considerable power injection in the grid nodes (3rd condition).

Replacing (2.15d) by (7.6) in (7.5), the EVCS optimization problem will be the *consensus problem* [BPE11, Chapter 7.1], if it is written as follows:

$$V_{rlc} := \min_{\mathbf{P},\mathbf{Q}} \sum_{j\in\mathbb{N}_b/1} \|\mathbf{v}_j - \mathbf{v}_{ref}\|_2^2 + \sum_{j\in\mathbb{N}^a} \Big(\big(\overline{\mathbf{\Omega}}_j^p - \mathbf{p}_j^{bs} - \mathbf{p}_j^{ac}\big)^2 + \big(\overline{\mathbf{\Omega}}_j^q - \mathbf{q}_j^{bs}\big)^2 + \sum_{i\in\mathbb{N}_j^v} \mathbf{\Pi}^T.\mathbf{p}_{i,j}^{ev} \Big)$$
$$\text{s.t.} \begin{cases} \mathbf{P}_j = \mathbf{P}_j^a \\ \mathbf{Q}_j = \mathbf{Q}_j^a \end{cases} \quad \forall j \in \mathbb{N}^a, \tag{7.7}$$

where only the *consensus* constraint matching the DSO's desired active and reactive powers with EVAs' is shown. Now, we can rewrite 7.5 in the form of a distributed structure using ADMM, called DCEVCS, to be solved iteratively between DSO and EVAs as follows:

$$(\mathbf{P}_j^{a^{k+1}}, \mathbf{Q}_j^{a^{k+1}}) := \underset{\mathbf{P}_j^a, \mathbf{Q}_j^a}{\operatorname{argmin}} \Big(\big(\overline{\mathbf{\Omega}}_j^p - \mathbf{p}_j^{bs} - \mathbf{p}_j^{ac}\big)^2 + \big(\overline{\mathbf{\Omega}}_j^q - \mathbf{q}_j^{bs}\big)^2 + \sum_{i\in\mathbb{N}_j^v} \mathbf{\Pi}^T.\mathbf{p}_{i,j}^{ev}$$
$$+\tfrac{\rho}{2} \left\|\mathbf{P}_j^a - \mathbf{P}_j^k + \mathbf{v}_j^k\right\|_2^2 + \tfrac{\rho}{2} \left\|\mathbf{Q}_j^a - \mathbf{Q}_j^k + \mathbf{u}_j^k\right\|_2^2 \Big)$$
$$\text{s.t. } \mathbb{P}_{i,j}^{evb},\ \mathbb{P}_j^{bs},\ \text{and (7.3)},\ \forall i \in \mathbb{N}_j^v,\ j \in \mathbb{N}^a \tag{7.8}$$

$$(\mathbf{P}_j^{k+1}, \mathbf{Q}_j^{k+1}) := \underset{\mathbf{P},\mathbf{Q},\mathbf{V},\mathbf{I}}{\operatorname{argmin}} \Big(\sum_{j\in\mathbb{N}_b/1} \|\mathbf{v}_j - \mathbf{v}_{ref}\|_2^2$$
$$+\tfrac{\rho}{2} \sum_{j\in\mathbb{N}^a} \left\|\mathbf{P}_j^{a^{k+1}} - \mathbf{P}_j + \mathbf{v}_j^k\right\|_2^2 + \tfrac{\rho}{2} \sum_{j\in\mathbb{N}^a} \left\|\mathbf{Q}_j^{a^{k+1}} - \mathbf{Q}_j + \mathbf{u}_j^k\right\|_2^2 \Big)$$
$$\text{s.t. (2.15a)} - \text{(2.15c)},\ \text{(2.16) and (7.6)} \tag{7.9}$$

$$\begin{cases} \mathbf{v}_j^{k+1} = \mathbf{v}_j^k + \mathbf{P}_j^{a^{k+1}} - \mathbf{P}_j^{k+1} \\ \mathbf{u}_j^{k+1} = \mathbf{u}_j^k + \mathbf{Q}_j^{a^{k+1}} - \mathbf{Q}_j^{k+1} \end{cases} \quad \forall j \in \mathbb{N}^a, \tag{7.10}$$

where k is the ADMM iteration index, ρ is the penalty factor, and $\mathbf{v}_j$ and $\mathbf{u}_j$ are the dual variables relating to the *consensus* constraints on active and reactive powers of the jth EVA, respectively. At each iteration k, EVAs solve (7.8) in parallel and send the pair of $(\mathbf{P}_j^{a^{k+1}}, \mathbf{Q}_j^{a^{k+1}})$ to DSO. Then, DSO solves (7.9) to regulate the voltage and satisfy the power flow constraints. Afterward, it updates the dual variables (7.10) and sends the pairs of $(\mathbf{P}_j^{k+1}, \mathbf{Q}_j^{k+1})$ and $(\mathbf{v}_j^{k+1}, \mathbf{u}_j^{k+1})$ to EVAs. This procedure, which is called DCEVCS and shown in Algorithm 8, is repeated until the stopping criteria are satisfied [BPE11, Chapter 7.1]. In Algorithm 8, Err includes the primal and residual errors, and Th is the acceptable error threshold.

Algorithm 8: DCEVCS.

Initialization: Set initial values for $\mathbf{P}^0$, $\mathbf{P}^{a^0}$, $\mathbf{Q}^0$, $\mathbf{Q}^{a^0}$, $\mathbf{p}^{bs^0}$, $\mathbf{q}^{bs^0}$, $\mathbf{p}^{ev^0}$, $\mathbf{v}^0$, and $\mathbf{u}^0$.
$k \leftarrow 0$.
while $Err < Th$ **do**
    for $j = 1 : \mathcal{N}^a$ **do**
        Calculate $(\mathbf{P}_j^a, \mathbf{Q}_j^a)$ by (7.8).
        Send $(\mathbf{P}_j^a, \mathbf{Q}_j^a)$ to DSO.
    end
    Calculate $(\mathbf{P}_j, \mathbf{Q}_j)$, $\forall j \in \mathbb{N}^a$ by (7.9).
    Update $(\mathbf{v}_j, \mathbf{u}_j)$, $\forall j \in \mathbb{N}^a$ by (7.10).
    Broadcast $(\mathbf{P}_j, \mathbf{Q}_j)$ and $(\mathbf{v}_j, \mathbf{u}_j)$ to EVAs.
    Update Err.
    $k \leftarrow k + 1$.
end

7.4 Numerical Simulations and Discussion

In this section, the developed DCEVCS is applied to the modified IEEE-13 bus system shown in Fig. 7.2, which is represented as a single-phase balanced distribution grid with six EVAs.

The aggregators are located at bus# 634, 646, 675, 680, 652 and 611, which are supplying 104, 112, 88, 110, 96, and 108 EVBs, respectively.

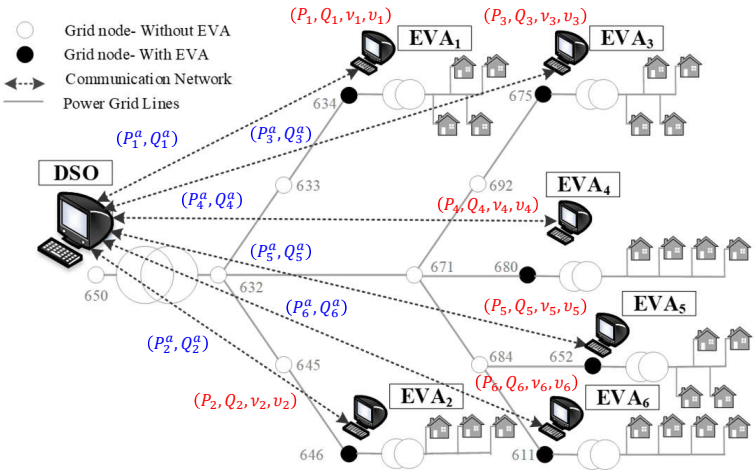

Figure 7.2: IEEE-13 bus system with the proposed DCEVCS communication network and the exchanged data between DSO and EVAs.

Although EV charging in sCC mode results in unacceptable voltage drop and feeder overloading (Fig. 7.3), we will show through different scenarios that DCEVCS mitigates these issues effectively. The netload dataset of EVBs is collected from [Aus], and the day-ahead wholesale electricity price is available from the California Independent System Operator-CAISO [CAI]. The simulation parameters are summarized in Table 7.1. The simulated scenarios are executed by MATLAB on a PC with Intel® Core™ i7 – 4770 3.40 GHz CPU, 4 cores and 8 GB RAM, and the convex optimization problems are solved by CVX [GB14].

Table 7.1: EV, BESS and DCEVCS simulation parameters.

Parameter	Value	Parameter	Value	Parameter	Value
$\overline{\mathbf{p}}^{ev}$, $\underline{\mathbf{p}}^{ev}$	4, −4 [kW]	$C(t_0)^{ev}$	$\{8, 9, 10\}$ [kWh]	$C(t_f)^{ev}$	$\{23, 24, 25\}$ [kWh]
$\underline{\mathbf{C}}_{bs}$	11 [kWh]	$\overline{\mathbf{C}}_{bs}$	100 [kWh]	$\overline{\mathbf{s}}_{bs}$	100 [kVA]
(α, η^+, η^-)	$(0.99, 0.95, 095)$	$(\overline{\mathbf{v}}, \underline{\mathbf{v}})$	$(0.96, 1.02)$ [p.u.]	$\mathbf{v}_{ref}$	1.0 [p.u.]
N	48	(ρ_p, ρ_q)	$(0.1, 0.1)$	–	–

To verify the effectiveness of DCEVCS in mitigating the negative effects of the EV charging load on the distribution grid, four scenarios defined as follows are simulated.

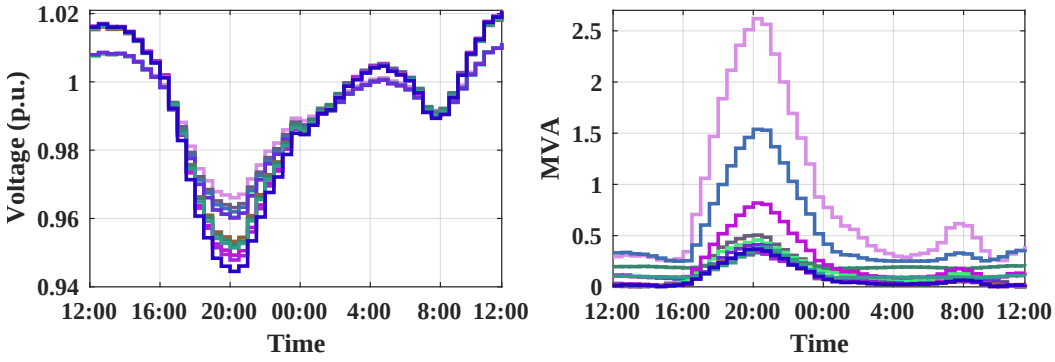

Figure 7.3: Significant voltage drop (left) and feeder overloading (right) in the grid due to EV charging in sCC mode

.

Scenario$_1$: EV charging load is controlled using DCEVCS, but EV chargers do not have V2G capability.

Scenario$_2$: EV charging load is controlled using DCEVCS, and EV chargers have V2G capability.

Scenario$_3$: EV charging load is not controlled, but EVAs have BESS to mitigate EV charging load's effects on the feeder loading condition.

Scenario$_4$: EV charging load is controlled using DCEVCS without V2G capability, and EVAs have BESS.

As it was shown, one of the major effects of EV charging load is on the nodal voltage profiles. DCEVCS can keep the nodal voltages within the acceptable range through controlling either EV charging load or BESS as shown in Fig. 7.4. As it is expected, the deployment of both EV charging and BESS control, i.e. Scenario$_4$, results in better nodal voltages. Scenario$_2$ is slightly better than Scenario$_1$ owing to the EV participation in V2G. However, the difference is not considerable as the price of selling energy to the grid by the EV owners is equal to the price of buying energy, and EV owners can only benefit from V2G if they sell energy. That is, if EV owners do not benefit due to the spinning reserve capacity which they provide for the grid [KT05], participation in V2G is not attractive. The total

percentage of the voltage deviations from the reference value (1 p.u.) are, respectively, 0.98, 0.94, 0.34, and 0.56 for Scenario_1 to Scenario_4. Showing the minimum and maximum voltage in Scenario_x by $(\mathbf{v}_{min}, \mathbf{v}_{max})_x$, the results are $(0.975, 1.021)_1$, $(0.979, 1.021)_2$, $(0.977, 1.014)_3$, and $(0.981, 1.01)_4$. The reason for a smoother voltage profile in Scenario_3 comparing with Scenario_1 and Scenario_2 is that the charging cost reduction is excluded from the optimization problem (7.5), therefore there is more flexibility to shift the EV charging load.

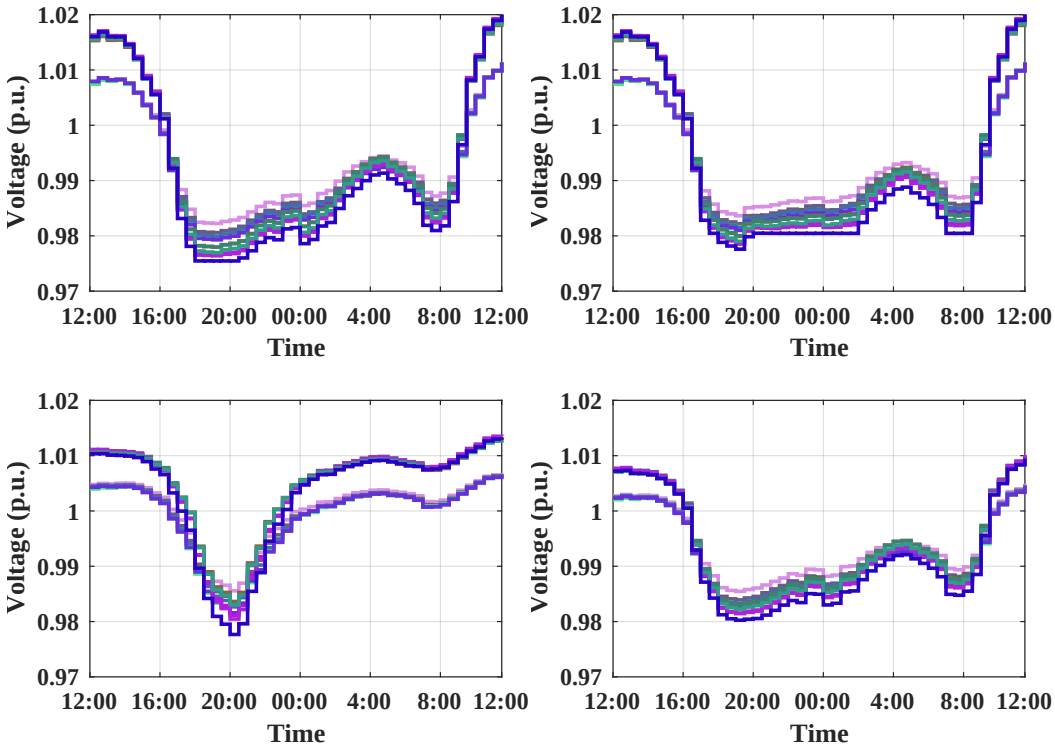

Figure 7.4: Voltage profiles of the grid buses for Scenario_1 (top-left), Scenario_2 (top-right), Scenario_3 (bottom-left), and Scenario_4 (bottom-right)

.

According to the objective function of DCEVCS, EVAs are interested in minimizing the load variance on their feeders. Considering the results shown in Fig. 7.5, the loading stress on the grid lines in Scenario_3 is significant. Specifically, the main feeder of the distribution grid where the HV/MV transformer is installed has the peak load of 2.2396 MVA, while the peak load of the HV/MV transformer is 1.152, 1.159, and 1.1622 in Scenario_1, Scenario_2, and Scenario_4, respectively. These results verify the necessity of EVCS for the accommodation of

transportation *Electrification* in the power grids. Without EV charging control, the power grid feeders will be overloaded even if BESS is deployed in the grid, which necessitates the grid capacity expansion.

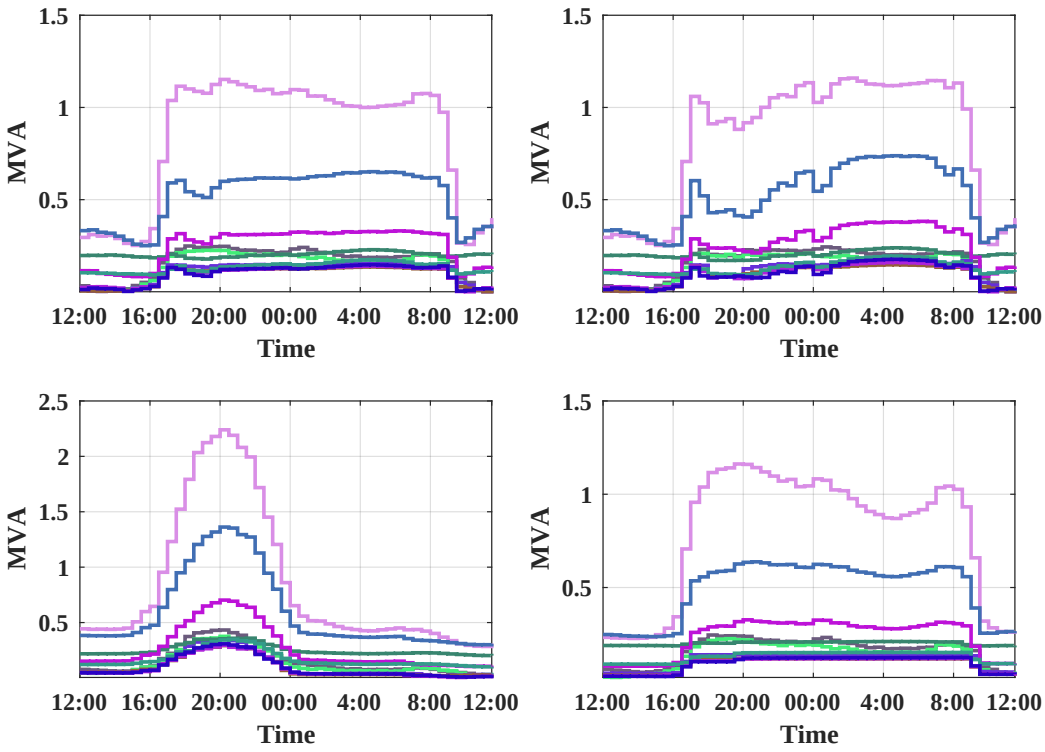

Figure 7.5: Loading profile of the grid lines for Scenario_1 (top-left), Scenario_2 (top-right), Scenario_3 (bottom-left), and Scenario_4 (bottom-right).

To make it more clear how DCEVCS minimizes the load variance on the feeders supplying EVAs, the results obtained for PTP, PTA, and RMS defined in (5.31), (5.32), and (5.33), respectively, are shown in Fig. 7.6 to Fig. 7.8. Scenario_4 achieves better results owing to the flexibility provided by EV charging and BESS control, and Scenario_3 shows the worse results as EVs do not participate in EVCS.

Considering Fig. 7.9 where the active (solid line) and reactive (dashed line) powers of BESS in Scenario_3 and Scenario_4 are shown, it reveals that the reactive power of BESS plays a key role in the voltage regulation. According to the EV charging model in Section 2.2, reactive power compensation is not provided by EVs. Therefore, the voltage profiles

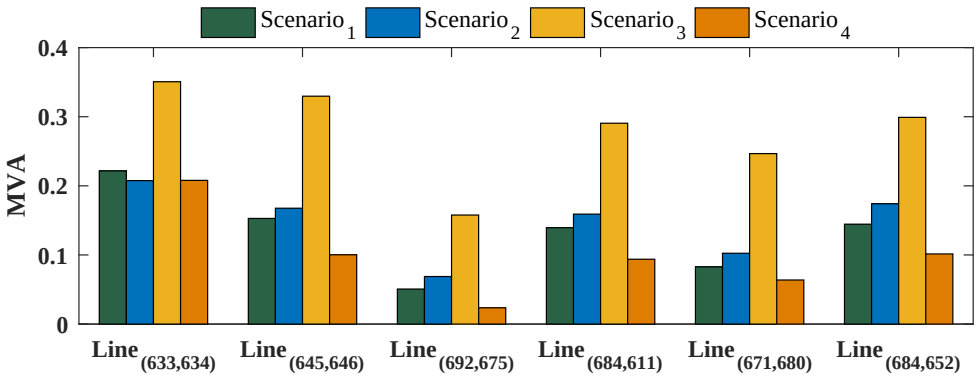

Figure 7.6: PTP of the EVAs' power profile obtained from the defined scenarios.

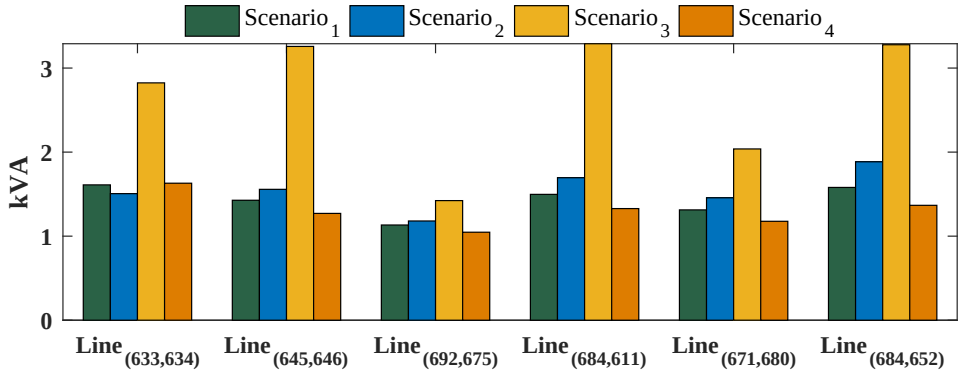

Figure 7.7: PTA of the EVAs' power profile obtained from the defined scenarios.

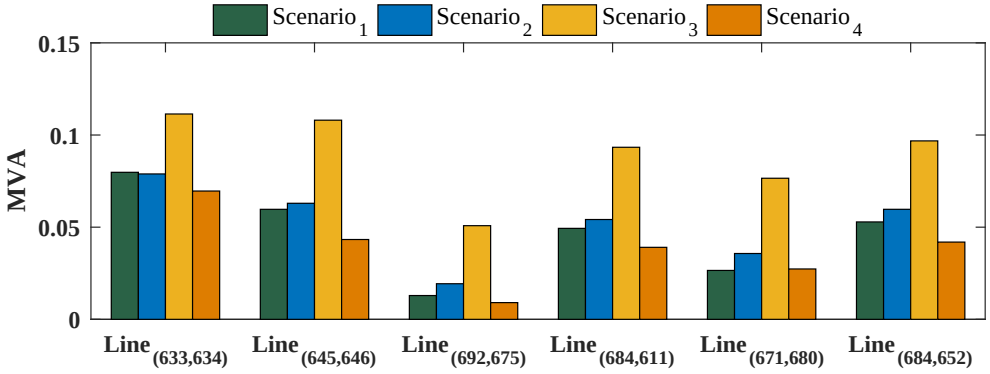

Figure 7.8: RMS of the EVAs' power profile obtained from the defined scenarios.

obtained in Scenario_3 and Scenario_4 are better than the others.

The main incentive for the EV owners to participate in DCEVCS is the charging cost reduction. Scenario_3 is excluded from CR results as the optimization function provides

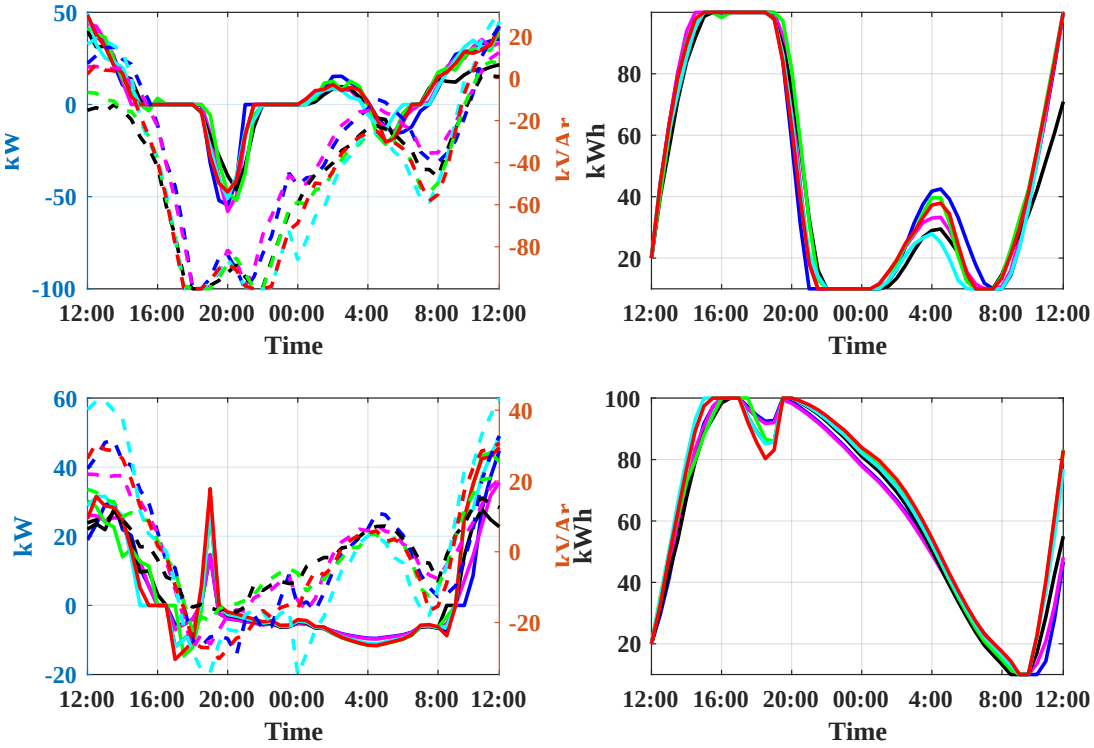

Figure 7.9: Active and reactive powers (left) and energy (right) of BESS for Scenario$_3$ (top) and Scenario$_4$ (bottom).

only voltage regulation and feeder load variance minimization. Considering the results in Fig. 7.10, Scenario$_1$, Scenario$_2$, and Scenario$_4$ lead to 18.1%, 22.1%, and 17.9% aggregated charging cost reduction comparing with sCC mode where there is no control on EV charging load. As discussed in [KT05], it is expected that the charging cost reduction improves by compensating the EV owners for providing the spinning reserve capacity.

7.5 Conclusion

In this chapter, the scalability issues in optimal EV charging coordination to mitigate the negative effects of EV charging load on the distribution grid has been addressed. Using the relaxed power flow model, the EV charging coordination problem has been written in the form of the *consensus problem*, so that it is solved by ADMM in a distributed manner between DSO and EV load aggregators. The *consensus* variables are the aggregated active and reactive

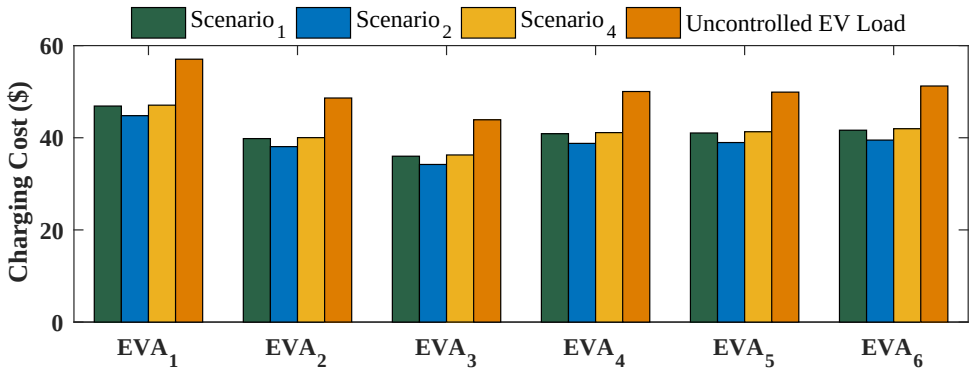

Figure 7.10: EVAs' aggregated electricity cost.

loads of EVAs, which should converge to an equilibrium point satisfying both DSO and EVAs. Using real data and numerical simulations, the performance of the proposed DCEVCS has been validated for different scenarios including V2G and BESS control. The results have revealed the efficacy of DCEVCS in voltage regulation, feeder congestion mitigation, and electricity cost reduction. It has been also shown that the EV owners are not interested in participation in V2G if they are only paid based on the energy they inject in the grid, not the provided energy capacity. One more important result is that BESS integration in the grid without EVCS can not optimize the grid capacity utilization, and EVCS should be integrated in DMS.

CHAPTER 8

Hierarchical Distributed EV and Heat Pump Load Coordination in Distribution Grids

In this chapter, a hierarchical and fully distributed framework is proposed to control EV and HP loads in the residential distribution grids. The framework consists of three layers of entities which are DSO, the residential load aggregators (RLAs), and the residential consumers (ReCs). The purpose of the proposed residential load coordination (RLC) is to minimize the energy loss in the grid, improve the bus voltage profiles, flatten the aggregated load of RLAs, and reduce ReCs' electricity cost. To decrease the computational burden of RLC, the distributed optimization methods, specifically ADMM, is used to solve the coordination problem in a distributed manner between DSO and RLAs, similar to DCEVCS developed in Chapter 7. As the distributed RLC (DRLC) is not computationally efficient for RLAs, and it requires ReCs to share their private information with RLAs, the mathematical properties of DRLC is further exploited, and a hierarchical DRLC (HDRLC) is proposed in the form of the *sharing problem* which is solved efficiently in a distributed manner among the grid entities. To validate the performance of HDRLC, it is applied to the IEEE-13 bus system, and the results are discussed for different scenarios.

8.1 Model Description

A residential distribution grid including a set of RLAs through which ReCs are supplied is assumed. $\mathbb{N}^{ra}$ denotes the set of grid RLAs, which its cardinality is shown by $\mathcal{N}^{ra}$. In addition, the set of ReCs which are supplied through the jth RLA and its cardinality are shown by $\mathbb{N}^{r}_{j}$ and $\mathcal{N}^{r}_{j}$, respectively. $ReC_{i,j}$ denotes the ith ReC supplied by the jth RLA.

In this section, the electricity consumption model of ReC, which is equipped with a solar panel, an EV charger, and an HP, is introduced.

According to Fig. 8.1 showing an ReC, we can write:

$$p_{i,j}^{rec}(t) = p_{i,j}^{uc}(t) + p_{i,j}^{ev}(t) + p_{i,j}^{hp}(t), \tag{8.1}$$

where $p_{i,j}^{rec}(t) \in \mathbb{R}$ is the total electric power of $ReC_{i,j}$. The set of feasible trajectories of $ReC_{i,j}$ is defined as:

$$\mathbb{P}_{i,j}^{rec} = \mathbb{P}_{i,j}^{ev} \cup \mathbb{P}_{i,j}^{hp}, \tag{8.2}$$

in which $\mathbb{P}_{i,j}^{ev}$ and $\mathbb{P}_{i,j}^{hp}$ are already defined in Sections 2.2 and 2.3, respectively.

According to the model defined for ReCs, the active and reactive powers of the jth bus, where the jth RLA is located, are obtained by:

$$P_j^{ra}(t) = p_j^{bs}(t) + p_j^{auc}(t) + \sum_{i \in \mathbb{N}_j^r} (p_{i,j}^{ev}(t) + p_{i,j}^{hp}(t)) \tag{8.3a}$$

$$Q_j^{ra}(t) = q_j^{bs}(t) + q_j^{auc}(t), \tag{8.3b}$$

in which $p_j^{auc}(t) = \sum_{i \in \mathbb{N}_j^r} p_{i,j}^{uc}(t)$ and $q_j^{auc}(t) = \sum_{i \in \mathbb{N}_j^r} q_{i,j}^{uc}(t)$ are the aggregated uncontrollable active and reactive powers. $p_j^{bs}(t)$ and $q_j^{bs}(t) \in \mathbb{R}$ are already defined in Section 2.1.

In addition, we introduce $p_{i,j}^{c}(t) = \left(p_{i,j}^{ev}(t) + p_{i,j}^{hp}(t)\right)$ as the total controllable load of the ith ReC supplied by the jth RLA. Therefore, we can introduce:

$$p_j^{ac}(t) = \sum_{i \in \mathbb{N}_j^r} p_{i,j}^{c}(t), \ j \in \mathbb{N}^{ra}, \tag{8.4}$$

as the aggregated controllable load of the jth RLA, which is also called the *sharing problem* constraint and used in Subsection 8.3.2.

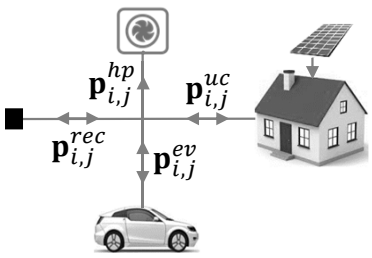

Figure 8.1: ReC model including solar panel, EV charger, and HP.

8.2 Problem Formulation

The distribution grid has a hierarchical trilayer structure including DSO, RLAs, and ReCs. The goal of DSO can be the grid loss minimization or voltage profile improvement while meeting the power flow constraints, RLAs may target load variance minimization on their supplying feeder or only keep their aggregated load less than the feeder capacity, and ReCs aim at electricity cost reduction. Accordingly, the objective function of RLC is threefold which is written as follows:

$$V_{rlc} := \min_{\mathbf{V},\mathbf{I},\mathbf{P},\mathbf{Q}} \mathbf{F}^d(\mathbf{P}) + \sum_{j\in\mathbb{N}^{ra}} \mathbf{F}^{ra}_j(\mathbf{P}^{ra}_j) + \sum_{j\in\mathbb{N}^{ra}} \sum_{i\in\mathbb{N}^r_j} \mathbf{F}^{rec}_{i,j}(\mathbf{p}^c_{i,j})$$
$$\text{s.t. } \mathbb{P}^{rec}_{i,j},\ \mathbb{P}^{bs}_j,\ \text{and (8.3) } \forall i \in \mathbb{N}^r_j,\ j \in \mathbb{N}^{ra},\ (2.15)-(2.16), \tag{8.5}$$

where $\mathbf{F}^d$, $\mathbf{F}^{ra}$, and $\mathbf{F}^{rec}$ are the DSO's, RLAs', and ReCs' optimization objectives, respectively. The grid constraints $(2.15)-(2.16)$ are considered as the DSO's local constraint, the jth RLA's local constraints are indicated by $\mathbb{P}^{bs}_j$, and the local constraints for $ReC_{i,j}$ are included by $\mathbb{P}^{rec}_{i,j}$.

The optimal load coordination (8.5) is relaxed by the similar approach discussed in Section 7.3. For a large-scale distribution grid with significant number of RLAs and ReCs, solving (8.5) centrally is not computationally efficient for DSO. Therefore in the following subsections, a scalable and fully distributed framework is derived to solve (8.5) using the distributed optimization methods.

8.3 Scalable Residential Load Coordination

In this section, DRLC method using the *consensus* ADMM is proposed to solve RLC problem. However, as each RLA has to solve the load scheduling problem for all the ReCs which it supplies, DRLC is not scalable and fully distributed, and ReCs have to share their private information with their RLA. Therefore, HDRLC method is proposed where the RLAs' optimization problem is rewritten as the *sharing problem* in a fully distributed and scalable manner which is solved by ADMM.

8.3.1 Distributed Residential Load Coordination

In this subsection, ADMM is used to solve the optimization problem (8.5) in a distributed manner through an iterative procedure between DSO and RLAs. Similar to the discussion in 7.3, (2.15d) should be replaced by (7.6) in (8.5) to write the RLC optimization problem in the form of the *consensus problem* [BPE11, Chapter 7.1] as follows:

$$V_{rlc} := \min_{\mathbf{P},\mathbf{Q}} \mathbf{F}^d(\mathbf{P}) + \sum_{j\in\mathbb{N}^{ra}} \Big(\mathbf{F}_j^{ra}(\mathbf{P}_j^{ra}) + \sum_{i\in\mathbb{N}_j^r} \mathbf{F}_{i,j}^{rec}(\mathbf{p}_{i,j}^c)\Big)$$
$$\text{s.t. } \begin{cases} \mathbf{P}_j = \mathbf{P}_j^{ra} \\ \mathbf{Q}_j = \mathbf{Q}_j^{ra} \end{cases} \quad \forall j \in \mathbb{N}^{ra}, \tag{8.6}$$

where only the *consensus* constraint between DSO and RLAs is shown. Therefore, 8.5 can be solved efficiently by ADMM in an iterative procedure between DSO and RLAs as follows:

$$(\mathbf{P}_j^{ra^{k+1}}, \mathbf{Q}_j^{ra^{k+1}}) := \underset{\mathbf{P}_j^{ra},\mathbf{Q}_j^{ra}}{\operatorname{argmin}} \Big(\mathbf{F}_j^{ra}(\mathbf{P}_j^{ra}) + \sum_{i\in\mathbb{N}_j^r} \mathbf{F}_{i,j}^{rec}(\mathbf{p}_{i,j}^c)$$
$$+\tfrac{\rho}{2}\left\|\mathbf{P}_j^{ra} - \mathbf{P}_j^k + \mathbf{v}_j^k\right\|_2^2 + \tfrac{\rho}{2}\left\|\mathbf{Q}_j^{ra} - \mathbf{Q}_j^k + \mathbf{u}_j^k\right\|_2^2\Big)$$
$$\text{s.t. } \mathbb{P}_{i,j}^{rec},\ \mathbb{P}_j^{bs},\ \text{and (8.3)},\ \forall i \in \mathbb{N}_j^r,\ j \in \mathbb{N}^{ra} \tag{8.7}$$

$$(\mathbf{P}_j^{k+1}, \mathbf{Q}_j^{k+1}) := \underset{\mathbf{P},\mathbf{Q},\mathbf{V},\mathbf{I}}{\operatorname{argmin}} \Big(\mathbf{F}^d(\mathbf{P})$$
$$+\tfrac{\rho}{2}\sum_{j\in\mathbb{N}^{ra}}\left\|\mathbf{P}_j^{ra^{k+1}} - \mathbf{P}_j + \mathbf{v}_j^k\right\|_2^2 + \tfrac{\rho}{2}\sum_{j\in\mathbb{N}^{ra}}\left\|\mathbf{Q}_j^{ra^{k+1}} - \mathbf{Q}_j + \mathbf{u}_j^k\right\|_2^2\Big)$$
$$\text{s.t. (2.15a)} - \text{(2.15c)},\ \text{(2.16) and (7.6)} \tag{8.8}$$

$$\begin{cases} \mathbf{v}_j^{k+1} = \mathbf{v}_j^k + \mathbf{P}_j^{ra^{k+1}} - \mathbf{P}_j^{k+1} \\ \mathbf{u}_j^{k+1} = \mathbf{u}_j^k + \mathbf{Q}_j^{ra^{k+1}} - \mathbf{Q}_j^{k+1} \end{cases} \quad \forall j \in \mathbb{N}^{ra}, \tag{8.9}$$

where k is the iteration index, ρ is the penalty factors, and $\mathbf{v}_j$ and $\mathbf{u}_j$ are the dual variables relating to the *consensus* constraints on active and reactive powers of the jth RLA, respectively. RLAs solve (8.7) in parallel and send the pair of $(\mathbf{P}_j^{ra^{k+1}}, \mathbf{Q}_j^{ra^{k+1}})$ to DSO. DSO solves (8.8)-(8.9) and sends the pairs of $(\mathbf{P}_j^{k+1}, \mathbf{Q}_j^{k+1})$ and $(\mathbf{v}_j^{k+1}, \mathbf{u}_j^{k+1})$ to RLAs. This procedure is repeated until the stopping criteria are satisfied [BPE11, Chapter 7.1].

8.3.2 Hierarchical Distributed Residential Load Coordination

Considering the first step of ADMM (8.7), each RLA has to solve the optimal load coordination problem for all the ReCs which it is supplying. If the number of ReCs is considerable, the computational burden for RLAs will be substantial. Also, ReCs have to share their sensitive information such as the arrival/departure time, required charging energy, maximum/minimum desired room temperature, etc. with RLAs. By exploiting the mathematical formulation, the *sharing problem* form is derived for (8.7) [BPE11, Chapter 7.3], which is solved efficiently by ADMM in a distributed manner between each RLA and its ReCs. For details on the *sharing problem* and how it is derived, refer to Subsections 5.2.3 and 5.2.4.

To make it clear how (8.7) is the *sharing problem*, the objective functions of RLAs and ReCs are shown as the functions of the *sharing* variables, i.e. $\mathbf{p}_j^{ac}$ and $\mathbf{p}_{i,j}^{c}$. Using (8.3) and (8.4), (8.7) is rewritten as:

$$\begin{aligned}
&\min\Big(\mathbf{F}_j^{ra}(\mathbf{p}_j^{ac}) + \sum_{i\in\mathbb{N}_j^r}\mathbf{F}_{j,i}^{rec}(\mathbf{p}_{i,j}^{c}) \\
&+\tfrac{\rho}{2}\left\|\sum_{i\in\mathbb{N}_j^r}\mathbf{p}_{j,i}^{c} + \mathbf{p}_j^{uc} + \mathbf{p}_j^{bs} - \mathbf{P}_j^{k} + \mathbf{v}_j^{k}\right\|_2^2 + \tfrac{\rho}{2}\left\|\mathbf{q}_j^{uc} + \mathbf{q}_j^{bs} - \mathbf{Q}_j^{k} + \mathbf{u}_j^{k}\right\|_2^2\Big) \\
&\text{s.t. } \mathbb{P}_{i,j}^{rec},\ \mathbb{P}_j^{bs},\ (8.3),\ \text{and } (8.4)\ \forall i\in\mathbb{N}_j^r,\ j\in\mathbb{N}^{ra},
\end{aligned} \tag{8.10}$$

in which the aggregation of the first and third expressions is a function of $\mathbf{p}_j^c$ which is also called the shared objective, the second part of the objective is a function of $\mathbf{p}_{j,i}^c$, the first constraint ($\mathbb{P}_{j,i}^c$) is local for $ReC_{j,i}$, RLA_j's local constraints are $\mathbb{P}_j^{bs}$ and (8.3), and (8.4) is the shared constraint. Therefore, (8.10) is the *sharing problem* that involves the entities adjusting their variable to minimize their individual as well as the shared objectives. The *sharing problem* (8.10) is solved by ADMM in a distributed manner as follows:

$$\begin{aligned}
\mathbf{p}_{i,j}^{c^{l+1}} := \underset{\mathbf{p}_{i,j}^{c}}{\operatorname{argmin}}&\Big(\mathbf{F}_{i,j}^{rec}(\mathbf{p}_{i,j}^{c}) + \frac{\rho_j}{2}\left\|\mathbf{p}_{i,j}^{c} - \mathbf{p}_{i,j}^{c^l} + \overline{\mathbf{p}}_j^{c^l} - \mathbf{p}_j^{ac^l} + \boldsymbol{\lambda}_j^{l}\right\|_2^2\Big) \\
&\text{s.t. } \mathbb{P}_{i,j}^{rec},\ \forall i\in\mathbb{N}_j^r
\end{aligned} \tag{8.11}$$

$$\mathbf{p}_j^{ac^{l+1}} := \underset{\mathbf{p}_j^{bs},\mathbf{q}_j^{bs},\mathbf{p}_j^{ac}}{\operatorname{argmin}} \Big(\mathbf{F}_j^{ra}(\mathcal{N}_j^r.\mathbf{p}_j^{ac}) + \frac{\rho}{2} \left\| \mathcal{N}_j^r.\mathbf{p}_j^{ac} + \mathbf{p}_j^{uc} + \mathbf{p}_j^{bs} - \mathbf{P}_j^k + \mathbf{v}_j^k \right\|_2^2 + \frac{\rho}{2} \left\| \mathbf{q}_j^{uc} + \mathbf{q}_j^{bs} - \mathbf{Q}_j^k + \mathbf{u}_j^k \right\|_2^2 + (\tfrac{\mathcal{N}_j^r.\rho_j}{2}) \left\| \mathbf{p}_j^{ac} - \overline{\mathbf{p}}_j^{c^{l+1}} - \boldsymbol{\lambda}_j^l \right\|_2^2 \Big)$$
$$\text{s.t. } \mathbb{P}_j^{bs} \text{ and } (8.3) \tag{8.12}$$

$$\boldsymbol{\lambda}_j^{l+1} = \boldsymbol{\lambda}_j^l + \overline{\mathbf{p}}_j^{c^{l+1}} - \mathbf{p}_j^{ac^{l+1}}. \tag{8.13}$$

where l is the iteration index, ρ_j is the penalty factor, $\boldsymbol{\lambda}_j$ is the dual variable, and $\overline{\mathbf{p}}_j^{c^l}$ is defined as:

$$\overline{\mathbf{p}}_j^{c^l} = \frac{1}{\mathcal{N}_j^r} \sum_{i \in \mathbb{N}_j^r} \mathbf{p}_{i,j}^{c^l}. \tag{8.14}$$

ReCs solve (8.11) in parallel, and RLAs solve (8.12) and update the dual variable by (8.13). It is worthwhile to note that the size of the optimization problem solved by RLAs (8.12) does not depend on the number of ReCs which they supply. To decrease the communication overhead, we define $\boldsymbol{\Lambda}_j^{l+1} = \boldsymbol{\lambda}_j^{l+1} + \overline{\mathbf{p}}_j^{c^{l+1}} - \overline{\mathbf{p}}_j^{ac^{l+1}}$. Thus, at each *sharing problem* iteration after the third step (8.13), the jth RLA broadcasts $\boldsymbol{\Lambda}_j^{l+1}$ to all $ReC_{i,j}$, $\forall i \in \mathbb{N}_j^r$. For more details, we refer the reader to Subsection 5.2.4.

The whole procedure of the proposed HDRLC is shown in Algorithm 9, and the communication links among the entities are shown in Fig. 8.2. The iterative procedure between DSO and RLAs (8.7)-(8.9) is called $ADMM_1$, and the *sharing problem* between each RLA and its ReCs (8.11)-(8.13) is called $ADMM_2$. Err_1 and Err_2 are the primal and dual residuals, respectively, for $ADMM_1$ and $ADMM_2$, and Th_1 and Th_2 are the feasibility tolerances for the primal and dual residuals in $ADMM_1$ and $ADMM_2$, respectively. For more details about residual calculation and stopping criteria, we refer the reader to [BPE11, Chapter 3.3].

8.4 Numerical Simulations and Discussion

In this section, the performance of HDRLC is evaluated for the modified IEEE-13 bus system. The single-phase balanced IEEE-13 bus system is considered with six RLAs which are located at bus# 634, 646, 675, 680, 652 and 611. The performance of HDRLC for different

Algorithm 9: HDRLC.

Initialization: Set initial values for $\mathbf{P}^0$, $\mathbf{p}^{ac^0}$, $\mathbf{p}^{bs^0}$, $\mathbf{q}^{bs^0}$, $\mathbf{p}^{ev^0}$, $\mathbf{p}^{hp^0}$, $\mathbf{v}^0$, $\mathbf{u}^0$, and $\boldsymbol{\lambda}^0$.
$k \leftarrow 0$.
$l \leftarrow 0$.
while $Err_1 < Th_1$ **do**
  for $j = 1 : \mathcal{N}^{ra}$ **do**
    while $Err_2 < Th_2$ **do**
      for $i = 1 : \mathcal{N}_j^r$ **do**
        calculate $\mathbf{p}_{i,j}^{c^{l+1}}$ by (8.11) & send to RLA_j.
      end
      Update $\overline{\mathbf{p}}_j^{c^{l+1}} = \frac{1}{\mathcal{N}_j^r} \sum_{i \in \mathbb{N}_j^r} \mathbf{p}_{i,j}^{c^{l+1}}$.
      Calculate $\mathbf{p}_j^{ac^{l+1}}$, $\mathbf{p}_j^{bs^{l+1}}$ and $\mathbf{q}_j^{bs^{l+1}}$ by (8.12).
      Update $\boldsymbol{\lambda}_j^{l+1}$ by (8.13).
      Update & broadcast $\boldsymbol{\Lambda}_j^{l+1}$ to $\forall i \in \mathbb{N}_j^r$.
      Update Err_2.
    end
    Send $(\mathbf{P}_j^{ra}, \mathbf{Q}_j^{ra})$ to DSO.
    $l \leftarrow l + 1$.
  end
  Calculate $(\mathbf{P}_j, \mathbf{Q}_j)$, $\forall j \in \mathbb{N}^{ra}$ by (8.8).
  Update $(\mathbf{v}_j, \mathbf{u}_j)$, $\forall j \in \mathbb{N}^{ra}$ by (8.9).
  Broadcast $(\mathbf{P}_j, \mathbf{Q}_j)$ and $(\mathbf{v}_j, \mathbf{u}_j)$ to RLA_j, $\forall j \in \mathbb{N}^{ra}$.
  Update Err_1.
  $k \leftarrow k + 1$.
end

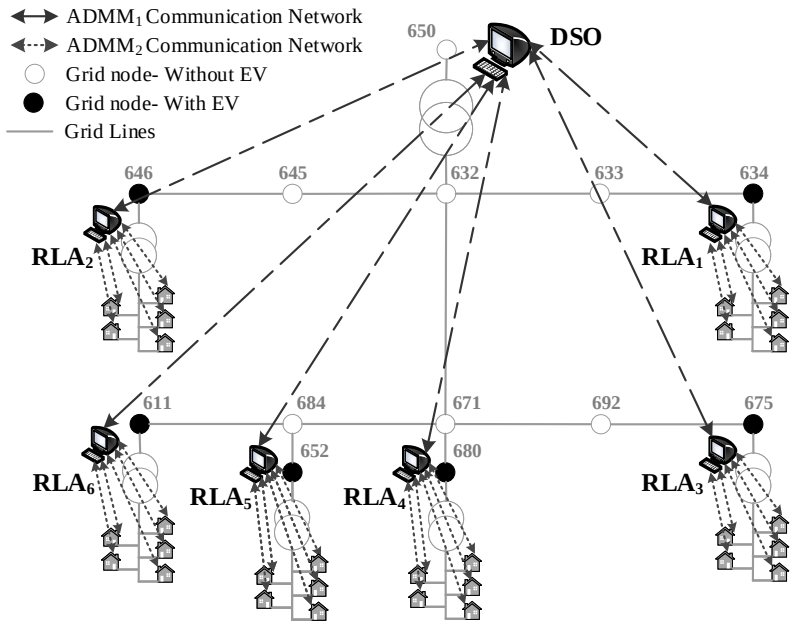

Figure 8.2: IEEE-13 bus system with the communication layers of HDRLC.

RLAs' objective functions are compared with the case where EVs and HPs are not controlled, in which EVs start charging with the maximum power rating (i.e. $\overline{\mathbf{p}}_{i,j}^{ev}$) as soon as they are plugged in, and HPs keep the zone temperature at a specific desired level. The netload dataset of ReCs is collected from [Aus], and the wholesale electricity price is available from the California Independent System Operator-CAISO [CAI]. More details about the simulation parameters are found in Table 8.1. All the simulations are executed by MATLAB on a PC with Intel® Core™ i7 − 4770 3.40 GHz CPU, 4 cores and 8 GB RAM, and the convex optimization problems are solved by CVX [GB14].

Table 8.1: EV, HP, BESS and HDRLC simulation parameters.

Parameter	**Value**	**Parameter**	**Value**	**Parameter**	**Value**
$\overline{\mathbf{p}}^{ev}$, $\underline{\mathbf{p}}^{ev}$	4, −4 [kW]	$\overline{\mathbf{C}}_{bs}$	55 [kWh]	$C(t_0)^{ev}$	$\{8, 9, 10\}$ [kWh]
$\underline{\mathbf{C}}_{bs}$	11 [kWh]	$C(t_f)^{ev}$	$\{23, 24, 25\}$ [kWh]	$\overline{\mathbf{s}}_{bs}$	50 [kVA]
$\underline{\mathbf{T}}^{z}$	$\{17, 18, 19\}$ ^{o}C	$(\overline{\mathbf{v}}, \underline{\mathbf{v}})$	(0.95, 1.05) [p.u.]	$\overline{\mathbf{T}}^{z}$	$\{23, 24, 25\}$ ^{o}C
$\mathbf{v}_{ref}$	1.0 [p.u.]	$\mathbf{T}^{des}$	$\{21, 22\}$ ^{o}C	N	48
$(\alpha, \eta^{+}, \eta^{-})$	$(0.99, 0.95, 095)$	(ρ_p, ρ_q)	$(0.1, 0.1)$	ρ_j	1

In order to compare the performance of HDRLC on the grid operation, four different

scenarios are simulated. For all scenarios except Scenario$_4$, the DSO's objective function is the grid loss reduction, however, RLAs' and ReCs' objectives are defined as listed below.

Scenario$_1$: RLAs' objective function is to keep their feeder load less than the capacity constraint [KCG19], and ReCs' objective function is the cost reduction by EV and HP control.

Scenario$_2$: RLAs' objective function is to flatten their total aggregated power [KCG19], and ReCs' objective function is the cost reduction by EV and HP control.

Scenario$_3$: RLAs' objective function is to keep their feeder load less than the capacity constraint, and ReCs' objective function is the cost reduction by only EV charging control.

Scenario$_4$: There is no control on the loads, i.e. EVs are charge with the maximum charger's power rating, and HPs keep the zone temperature at a specific desired level.

Regarding DSO's objective function, the results obtained from the defined scenarios are shown in Table 8.2. Comparing the results, the loss decreases significantly in Scenario$_1$ and Scenario$_2$, where ReCs respond to RLAs' commands by controlling both EV and HP loads. Considering Line$_{(650,632)}$ which is the HV/MV transformer, the energy loss is reduced 76%, 78% and 40% in the first three scenarios, respectively, in comparison with Scenario$_4$.

The obtained voltage profiles for the simulated scenarios are shown in Fig. 8.3. As it is expected, the best voltage profiles are achieved in Scenario$_1$, followed by Scenario$_2$, and Scenario$_3$, respectively. Obviously, not participating in HDRLC (Scenario$_4$) leads to the voltage reduction below the minimum allowable constraint (0.95 pu). For better clarification, showing the minimum and maximum voltage by $(\mathbf{v}_{min}, \mathbf{v}_{max})_x$, in which x is the scenario number, the obtained results are $(0.99, 1.016)_1$, $(0.981, 1.011)_2$, $(0.977, 1.016)_3$, and $(0.924, 1.019)_4$, where the deviation of voltage from the reference value ($\mathbf{v}_{ref}$) in Scenario$_1$ is less than the others. It should be noted how HP load results in the voltage drop when ReCs selfishly want to keep their zone temperature at a specific level and respond to DSO's and RLA's request by only EV load control.

Table 8.2: Loss reduction by the proposed HDRLC.

	Line	(650, 632)	(632, 633)	(633, 634)	(632, 645)	(645, 646)	(632, 671)	(671, 675)	(671, 684)	(684, 611)	(671, 680)	(684, 652)
kWh	**Scenario$_1$**	292	3.1	8.3	121	2.1	2.6	11.9	15.6	1.9	5.4	6.0
	Scenario$_2$	272	3.4	8.8	100	1.6	2.2	8.8	14.3	1.8	3.9	6.1
	Scenario$_3$	733	6.9	20.9	300	6.3	8.4	16.9	43.3	6.6	11.5	21.9
	Scenario$_4$	1214	22.7	30.5	426	24.7	12.2	17.1	66.3	10.6	15.1	37.1
kVarh	**Scenario$_1$**	945	4.9	8.5	367	0.4	2.6	6.7	15.9	5.7	5.5	2.3
	Scenario$_2$	892	5.4	9.0	304	0.3	2.3	4.9	14.6	5.6	3.9	2.3
	Scenario$_3$	2366	11.1	21.4	909	1.1	8.6	9.5	44.4	19.9	11.6	8.4
	Scenario$_4$	4065	36.4	31.3	1154	4.5	12.5	9.5	67.9	32.1	15.3	14.2

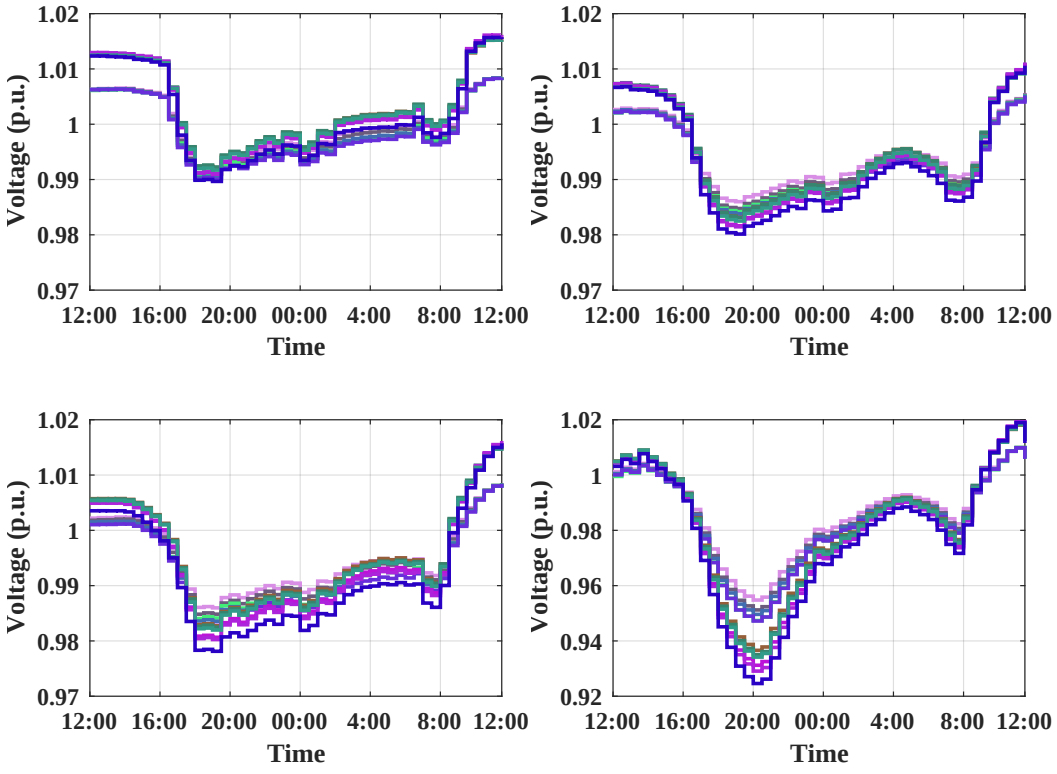

Figure 8.3: Voltage profiles of the grid buses for Scenario$_1$ (top-left), Scenario$_2$ (top-right), Scenario$_3$ (bottom-left), and Scenario$_4$ (bottom-right).

Comparing the loading profiles of the grid lines in Fig. 8.4 reveals that in Scenario_3 and Scenario_4 the lines' peak power increases considerably, specially on $\text{Line}_{(650,632)}$ where the peak power is 1.72 MVA and 3.45 MVA, while it is 1.15 MVA and 1.14 MVA in Scenario_1 and Scenario_2, respectively. Consequently, the last two scenarios overload the HV/MV transformer and may lead to Blackout in the distribution grid.

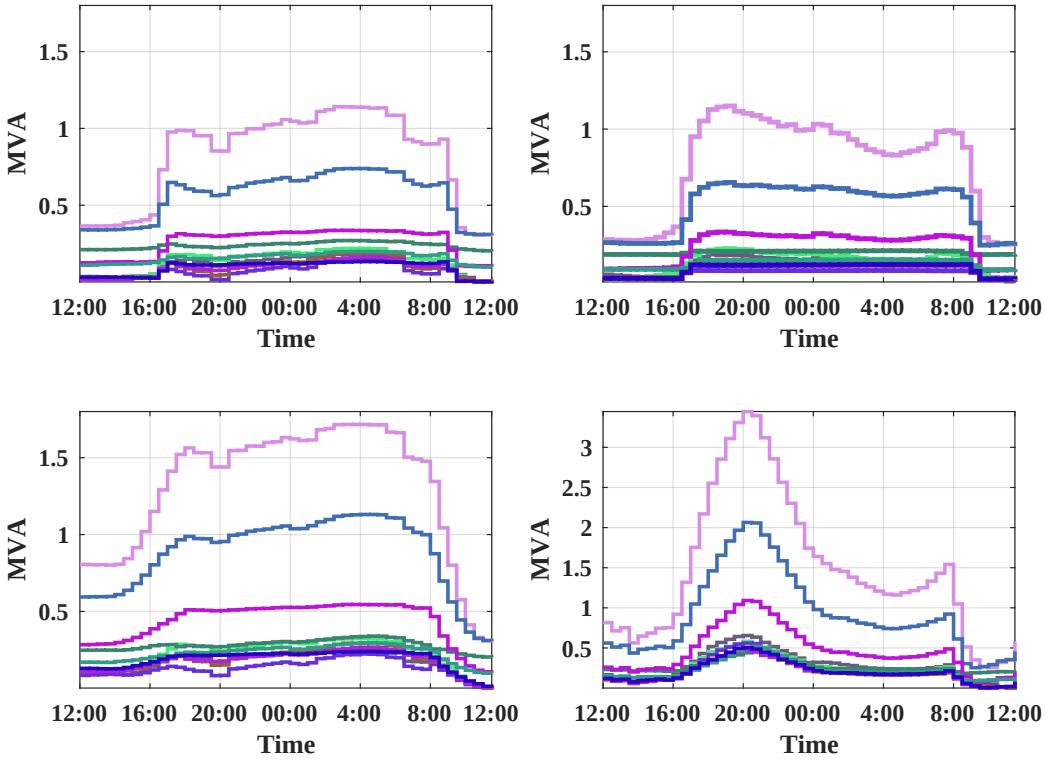

Figure 8.4: Loading profile of the grid lines for Scenario_1 (top-left), Scenario_2 (top-right), Scenario_3 (bottom-left), and Scenario_4 (bottom-right).

To more effectively compare the results obtained for the loading profile of the lines which directly supply RLAs, PTP, PTA, and RMS defined by (5.31), (5.32), and (5.33) are calculated and shown in Fig. 8.5, Fig. 8.6, Fig. 8.7, respectively. Considering RLAs' objective function which is to flatten the loading profile of the supplying feeder, Scenario_2 outperforms the others, and it is followed by Scenario_1 and Scenario_3. The figures clarify that Scenario_4 has significantly high values for all three criteria as there is no control on the loads.

It is also worthwhile to look at the charging/discharging of BESS, shown in Fig. 8.8,

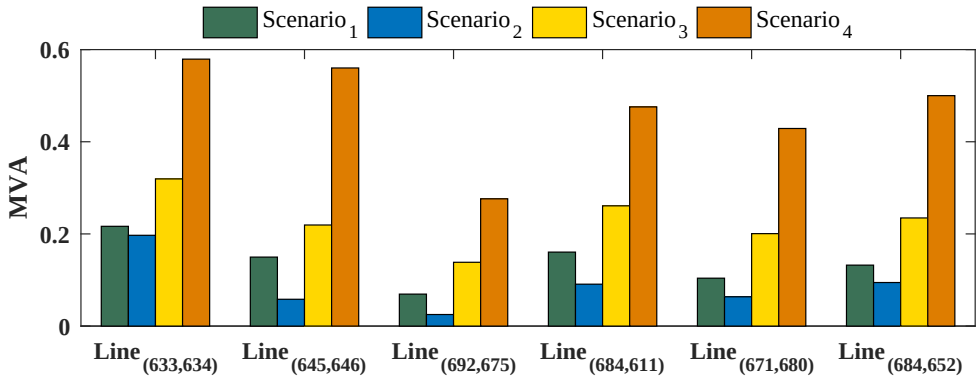

Figure 8.5: PTP of the RLAs' power profile obtained from the defined scenarios.

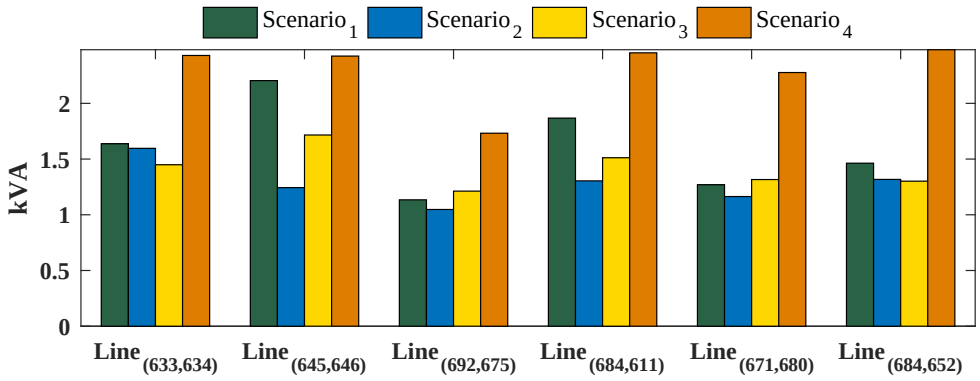

Figure 8.6: PTA of the RLAs' power profile obtained from the defined scenarios.

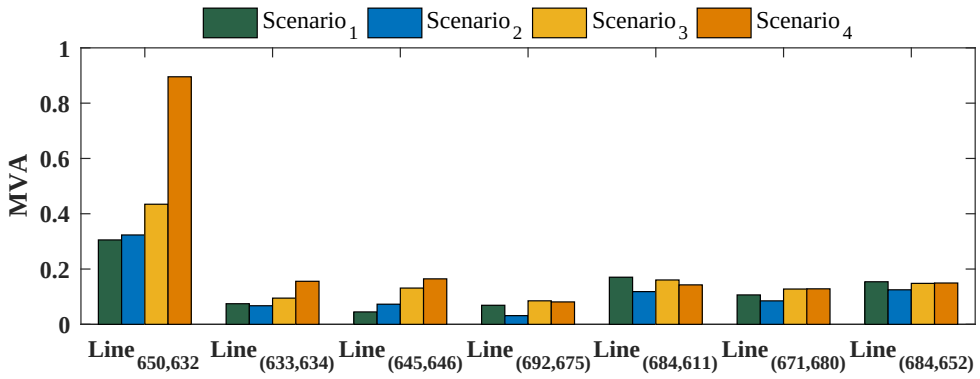

Figure 8.7: RMS of the RLAs' power profile obtained from the defined scenarios.

for the defined scenarios. In Scenario$_1$ and Scenario$_3$ where RLAs' objective is an indicator function, and so they just try to match DSO's desired active and reactive loads with ReCs, the active and reactive power profiles of BESS are fairly similar. Also, in these two scenarios,

BESS mostly contributes to the reactive power compensation over the time period $16:00-8:00$. However in Scenario$_2$, as the RLAs not only try to match DSO's request with ReCs', but also have their own objective function which is power profile flattening, BESS charges and discharges more frequently.

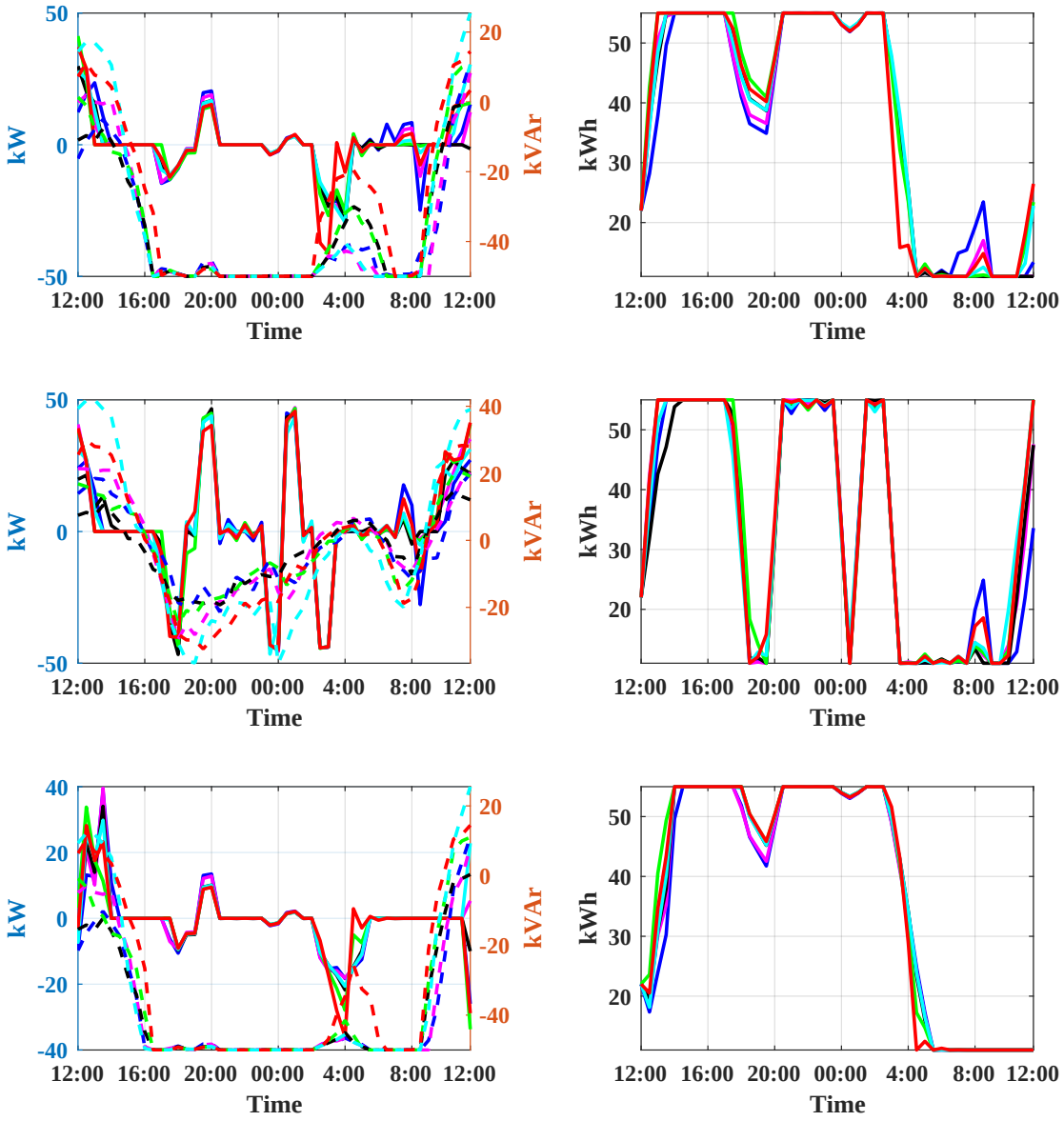

Figure 8.8: Active (solid line) and reactive (dashed line) powers (left) and energy (right) of BESS for Scenario$_1$ (top), Scenario$_2$ (middle), and Scenario$_3$ (bottom).

Finally, as the objective of ReCs is the cost reduction, the corresponding results obtained

from the scenarios are compared. Since ReCs control both EV and HP loads in the first two scenarios, obviously their electricity cost is considerably less than when they only participate in HDRLC by controlling the EV charging demand. This is shown in Fig. 8.9, where the aggregated ReCs' electricity cost is shown. Comparing to Scenario_4, the total aggregated cost reduction is 69.5%, 68.8%, and 19.2% in the first three scenarios, respectively.

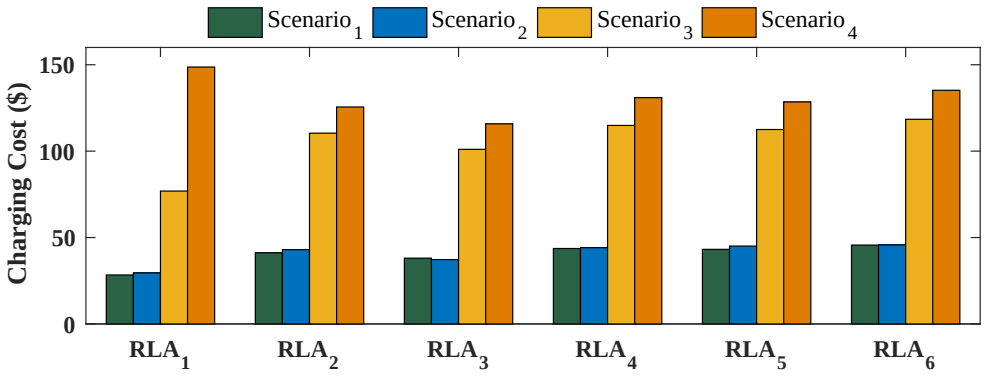

Figure 8.9: RLAs' aggregated electricity cost.

8.5 Conclusion

In this chapter, a fully distributed and hierarchical framework has been proposed for optimal EV and HP load coordination in the residential grids with the consideration of distribution grid model including voltage and feeder loading constraints. The proposed framework consists of two iterative layers, the first of which is executed between DSO and RLAs, and the second one is carried out between each RLA and the consumers which it supplies. The proposed framework, HDRLC, reduces the computation burden of RLAs comparing to the other methods introduced in the literature and DCEVCS developed in Chapter 7 since the load coordination is distributed between ReCs and RLA. Moreover, the size of the optimization problem solved by RLAs does not depend on the number of ReCs which they supply. To evaluate the performance of HDRLC, it was applied to the IEEE-13 bus system and various scenarios were simulated. The results have revealed that when ReCs participate in HDRLC with controlling both EV and HP loads in response to RLAs' and DSO's commands, the

distribution grid experiences considerable voltage profile improvement and energy loss reduction. This also leads to less loading stress on the grid lines meaning that the grid can operate safely in the presence of large EV and HP populations without any requirement for investment in the grid expansion.

CHAPTER 9

Conclusion & Future Work

To have a sustainable and clean energy infrastructure, two objectives have been followed by the governments and utilities: integration of renewable energy resources in the generation system, and electrification on the energy consumption side. Renewable resources of energy, e.g. solar energy, are inherently intermittent and non-dispatchable. To address this issue, the energy storage deployment is unavoidable, which its efficient utilization requires accurate modeling of the energy resource availability and optimal coordination and operation. On the consumer side, the electrification in two sectors, transportation and building, is the trend. The reliance of the transportation system on the fossil fuels and the percentage of the energy consumed for heating and cooling in the buildings reveal the capacity of these sectors to reduce the greenhouse gas emission and improve the energy efficiency.

To facilitate the integration of solar energy and EVs in the power grids, a new method based on non-parametric kernel density estimation has been proposed which can accurately model the stochastic behavior of solar generation profile, netload demand, aggregated EV load, and individual EV charging demand, namely arrival time, required energy, and departure time. The method has been used to design an optimal coordination algorithm for BESS control which is able to reduce the charging cost of EVs and provide load leveling.

To validate the performance of BESS for the EV charging system, a mobile BESS has been prototyped. The operation of the setup has been verified by its integration in a real EV charging system in the City of Santa Monica. Through numerous experiments, it has been shown that the mobile BESS not only reduces the charging cost and peak load demand, but also provides the emergency power to the charging system if no electricity is available from the grid.

As the large penetration of EVs in the distribution system can push the grid toward its capacity boundaries and lower the power quality, four frameworks have been developed in this dissertation. The features of the proposed frameworks are their scalability and customers' privacy-preserving. Two developed frameworks can be utilized in the distribution management system as the separate network applications, and the others can be integrated with the distribution management system.

The first proposed EV management framework is designed based on a trilayer hierarchical structure where the grid entities solve their problem locally and sequentially. In this method called hierarchical ADMM, the EVCS problem is formulated as the sharing problem. The simulation results show 25% charging cost reduction and $\approx 30\%$ peak-to-average decrease in the aggregated load profile comparing to the uncontrolled EV charging load. By exploiting the mathematical properties of the trilayer EV charging problem, a new hierarchical method called HDEVCS has been developed where all the entities solve their problem simultaneously, therefore it shows faster convergence and lower communication overhead ($\approx 98\%$) comparing to the hierarchical ADMM. Using real data, the numerical simulation results show $\approx 16.5\%$ charging cost reduction and 35% peak-to-average decrease in the aggregated load profile for a very large-scale system

In the last two proposed EVMS methods as the DMS integrated applications, the power flow model of the grid including the nodal voltage constraints are also included directly in the EV load coordination problem. In these methods, the system operator negotiates with the load aggregators on the load demand to regulate the voltage and decrease the energy loss, and each load aggregator negotiates with its customers to keep the total load demand less than the grid feeder capacity, minimize its load profile variance, and reduce the charging cost. The numerical simulation results using real data show the efficacy of the proposed EVMS methods in reducing the EV charging cost, avoiding feeder overloading conditions, improving the voltage profiles, and decreasing the energy loss in the grid. Using comprehensive numerical simulations, improving the voltage profile from 45% up to 93% and reducing the peak load from 50% up to 66% have been verified. The developed methods also reveal the capability of EVMS in accommodating the large EV penetration without any

investment on the grid capacity expansion. Last but not least, the designed frameworks preserve the privacy of the EV owners and other involved entities as they are not required to share their sensitive information with others.

The contributions of this dissertation, however, can be further developed as follows:

- The stochastic optimal BESS control proposed in Chapter 4 can be manipulated to formulate a chance-constraint problem. Comparing to the MCS-based method used in this dissertation, chance-constraint optimization has less computation burden without compromising the accuracy. It is also interesting to consider the individual EV charging control as well as the optimal BESS sizing by including the battery degradation cost in the optimization problem.

- Recently, several methods have been proposed to accelerate the convergence rate of ADMM. Implementing those methods in the proposed EVMS frameworks in Chapter 5- Chapter 8 is recommended as a possible future work so that the agents reach the equilibrium point faster. This helps include the proposed framework in a real-time control system.

- Package loss, network congestion, and latency are very common in the communication networks. To make the proposed frameworks in Chapter 5- Chapter 8 practical, it is suggested to investigate the communication loss and delay effects on the convergence of the proposed algorithms and the optimality of their results.

- In Chapter 5- Chapter 8, the agents negotiate the power demand only. It is interesting that the pricing models based on the agents' criteria are developed, and the price negotiation is also included in the proposed frameworks [ANK19]. This will be especially important if the EV owners are expected to participate in V2G.

- The dynamic electricity price, which is used as an input parameter in this dissertation, is designed according to the customers' load demand by the distribution system operator. That is, the total load profile of the grid is analyzed by the system operator to design an effective dynamic price which motivates the customers to shift their

loads from peak-load hours to the off-peak time. Accordingly, EV load management results can affect the dynamic price design, which is not investigated in this research. It is practical that a mechanism for electricity price determination considering EV load demand is integrated with the developed load management system.

- As it is shown, the participation of the EV owners in V2G is not significant by current electricity price. As V2G can provide spinning reserve for the grid, the price mechanism based on only the power that V2G can contribute to the grid is not compelling enough for the EV owners [KT05]. Therefore, it is required that the stay duration of EVs is considered in designing the compensation for the EV owners for their participation in V2G.

REFERENCES

[AGK18] X. G. Agoua, R. Girard, and G. Kariniotakis. "Short-Term Spatio-Temporal Forecasting of Photovoltaic Power Production." *IEEE Transactions on Sustainable Energy*, **9**(2):538–546, April 2018.

[AGK19] X. G. Agoua, R. Girard, and G. Kariniotakis. "Probabilistic Models for Spatio-Temporal Photovoltaic Power Forecasting." *IEEE Transactions on Sustainable Energy*, **10**(2):780–789, April 2019.

[ANK19] A. G. Azar, H. Nazaripouya, B. Khaki, C. Chu, R. Gadh, and R. H. Jacobsen. "A Non-Cooperative Framework for Coordinating a Neighborhood of Distributed Prosumers." *IEEE Transactions on Industrial Informatics*, **15**(5):2523–2534, May 2019.

[ASD14] M. Alizadeh, A. Scaglione, J. Davies, and K. S. Kurani. "A Scalable Stochastic Model for the Electricity Demand of Electric and Plug-In Hybrid Vehicles." *IEEE Transactions on Smart Grid*, **5**(2):848–860, March 2014.

[Aus] "Ausgrid Dataset." `http://www.ausgrid.com.au`.

[AV07] David Arthur and Sergei Vassilvitskii. "k-means++: The advantages of careful seeding." In *Proceedings of the eighteenth annual ACM-SIAM symposium on Discrete algorithms*, pp. 1027–1035. Society for Industrial and Applied Mathematics, 2007.

[BCD17] A. Bracale, G. Carpinelli, and P. De Falco. "A Probabilistic Competitive Ensemble Method for Short-Term Photovoltaic Power Forecasting." *IEEE Transactions on Sustainable Energy*, **8**(2):551–560, April 2017.

[BFG18] P. Braun, T. Faulwasser, L. Grüne, C. M. Kellett, S. R. Weller, , and K. Worthmann. "Hierarchical distributed ADMM for predictive control with applications in power networks." *IFAC Journal of Systems and Control*, **2**:10–22, 2018.

[BGK10] Z. I. Botev, J. F. Grotowski, and D. P. Kroese. "Kernel density estimation via diffusion." *The annals of Statistics*, **38**(5):2916–2957, 2010.

[BNE18] A. Bilh, K. Naik, and R. El-shatshat. "A Novel Online Charging Algorithm for Electric Vehicles Under Stochastic Net-Load." *IEEE Transactions on Smart Grid*, **9**(3):1787–1799, 2018.

[Bot07] Z. I. Botev. "Nonparametric density estimation via diffusion mixing." `http://espace.library.uq.edu.au`, 2007.

[BPE11] S. Boyd, N. Parikh, B. Peleato E. Chu, , and J. Eckstein. "Distributed optimization and statistical learning via the alternating direction method of multipliers." *Foundations and Trends® in Machine Learning*, **3**(1):1–122, 2011.

[CAD] "California Duck Curve." https://www.caiso.com/.

[CAI] "California Independent System Operator- Locational Marginal Price." http://oasis.caiso.com.

[CCY09] Haisheng Chen, Thang Ngoc Cong, Wei Yang, Chunqing Tan, Yongliang Li, and Yulong Ding. "Progress in electrical energy storage system: A critical review." *Progress in Natural Science*, **19**(3):291 – 312, 2009.

[CHD10] K. Clement-Nyns, E. Haesen, and J. Driesen. "The impact of charging plug-in hybrid electric vehicles on a residential distribution grid." *IEEE transactions on power systems*, **25**(1):371–380, 2010.

[CLL18] X. Chen, K. Leung, A. Y. S. Lam, and D. Hill. "Online Scheduling for Hierarchical Vehicle-to-Grid System: Design, Formulation, and Algorithm." pp. 1–1, 2018.

[CLY18] H Chung, W Li, C Yuen, C Wen, and N Crespi. "Electric Vehicle Charge Scheduling Mechanism to Maximize Cost Efficiency and User Convenience." *IEEE transactions smart grid*, 2018.

[Cri16] M. B. Cristopher. *Pattern Recognition and Machine Learning*. Springer-Verlag, New York, 2016.

[CTL12] Y. Cao, S. Tang, C. Li, P. Zhang, Y. Tan, Z. Zhang, and J. Li. "An Optimized EV Charging Model Considering TOU Price and SOC Curve." *IEEE Transactions on Smart Grid*, **3**(1):388–393, March 2012.

[DDL13] Maimouna Diagne, Mathieu David, Philippe Lauret, John Boland, and Nicolas Schmutz. "Review of solar irradiance forecasting methods and a proposition for small-scale insular grids." *Renewable and Sustainable Energy Reviews*, **27**:65–76, 2013.

[doe] "U.S. Department of Energy- Energy Efficiency & Renewable Energy.".

[DPM18] M. Diekerhof, F. Peterssen, and A. Monti. "Hierarchical Distributed Robust Optimization for Demand Response Services." *IEEE Transactions on Smart Grid*, **9**(6):6018–6029, Nov 2018.

[eia] "U.S. Energy Information Administration.".

[GB14] Michael Grant and Stephen Boyd. "CVX: Matlab Software for Disciplined Convex Programming, version 2.1." http://cvxr.com/cvx, March 2014.

[GLT15] L. Gan, N. Li, U. Topcu, and S. H. Low. "Exact convex relaxation of optimal power flow in radial networks." *IEEE Transactions on Autommatic Control*, **60**(1):72–87, 2015.

[GPG16] F. Golestaneh, P. Pinson, and H. B. Gooi. "Very Short-Term Nonparametric Probabilistic Forecasting of Renewable Energy Generation— With Application to Solar Energy." *IEEE Transactions on Power Systems*, **31**(5):3850–3863, Sep. 2016.

[gre] "Green Car Congree.".

[GTL13] L. Gan, U. Topcu, and S. H. Low. "Optimal decentralized protocol for electric vehicle charging." *IEEE Transactions on Power Systems*, **28**(2):940–951, May 2013.

[HMC18] A. Hassan, R. Mieth, M. Chertkov, D. Deka, and Y. Dvorkin. "Optimal Load Ensemble Control in Chance-Constrained Optimal Power Flow." *IEEE Transactions on Smart Grid*, pp. 1–1, 2018.

[HST19] B. Hashemi, M. Shahabi, and P. Teimourzadeh-Baboli. "Stochastic-Based Optimal Charging Strategy for Plug-In Electric Vehicles Aggregator Under Incentive and Regulatory Policies of DSO." *IEEE Transactions on Vehicular Technology*, **68**(4):3234–3245, April 2019.

[HW18] S. Huang and Q. Wu. "Dynamic Subsidy Method for Congestion Management in Distribution Networks." *IEEE Transactions on Smart Grid*, **9**(3):2140–2151, May 2018.

[ins] "INSIDEEVs.".

[IPC13] Rich H Inman, Hugo TC Pedro, and Carlos FM Coimbra. "Solar forecasting methods for renewable energy integration." *Progress in energy and combustion science*, **39**(6):535–576, 2013.

[KCG19] Behnam Khaki, Chicheng Chu, and Rajit Gadh. "Hierarchical distributed framework for EV charging scheduling using exchange problem." *Applied Energy*, **241**:461 – 471, 2019.

[KJC17] M. Kramer, A. Jambagi, and V. Cheng. "Bottom-up Modeling of Residential Heating Systems for Demand Side Management in District Energy System Analysis and Distribution Grid Planning." In *The 15th International Conference of International Building Performance Association (IBPSA)*, San Francisco, CA, USA, August 2017.

[KMY19] H. Kikusato, K. Mori, S. Yoshizawa, Y. Fujimoto, H. Asano, Y. Hayashi, A. Kawashima, S. Inagaki, and T. Suzuki. "Electric Vehicle Charge–Discharge Management for Utilization of Photovoltaic by Coordination Between Home and Grid Energy Management Systems." *IEEE Transactions on Smart Grid*, **10**(3):3186–3197, May 2019.

[KT05] Willett Kempton and Jasna Tomić. "Vehicle-to-grid power fundamentals: Calculating capacity and net revenue." *Journal of Power Sources*, **144**(1):268 – 279, 2005.

[LBM16] C. Le Floch, F. Belletti, and S. Moura. "Optimal Charging of Electric Vehicles for Load Shaping: A Dual-Splitting Framework With Explicit Convergence Bounds." *IEEE Transactions on Transportation Electrification*, **2**(2):190–199, June 2016.

[LLa14] J Lin, K Leung, and and V. O. K. Li. "Optimal Scheduling With Vehicle-to-Grid Regulation Service." *IEEE Internet of Things Journal*, **1**(6):556–569, 2014.

[LLL19] Zachary J. Lee, Tongxin Li, and Steven H. Low. "ACN-Data: Analysis and Applications of an Open EV Charging Dataset." In *Proceedings of the Tenth ACM International Conference on Future Energy Systems*, e-Energy '19, pp. 139–149, New York, NY, USA, 2019. ACM.

[LLY15] M. Liang, W. Li, J. Yu, and L. Shi. "Kernel-based electric vehicle charging load modeling with improved latin hypercube sampling." In *2015 IEEE Power Energy Society General Meeting*, pp. 1–5, July 2015.

[Low14a] S. H. Low. "Convex Relaxation of Optimal Power Flow—Part I: Formulations and Equivalence." *IEEE Transactions on Control of Network Systems*, **1**(1):15–27, March 2014.

[Low14b] S. H. Low. "Convex Relaxation of Optimal Power Flow—Part II: Exactness." *IEEE Transactions on Control of Network Systems*, **1**(2):177–189, June 2014.

[LPS19] M. Liu, P. K. Phanivong, Y. Shi, and D. S. Callaway. "Decentralized Charging Control of Electric Vehicles in Residential Distribution Networks." *IEEE Transactions on Control Systems Technology*, **27**(1):266–281, Jan 2019.

[LRK19] M. Latifi, A. Rastegarnia, A. Khalili, and S. Sanei. "Agent-Based Decentralized Optimal Charging Strategy for Plug-in Electric Vehicles." *IEEE Transactions on Industrial Electronics*, **66**(5):3668–3680, May 2019.

[LWS18] Z. Liu, Q. Wu, M. Shahidehpour, C. Li, S. Huang, and W. Wei. "Transactive Real-time Electric Vehicle Charging Management for Commercial Buildings with PV On-site Generation." *IEEE Transactions on Smart Grid*, pp. 1–1, 2018.

[LZC18] Luyao Liu, Yi Zhao, Dongliang Chang, Jiyang Xie, Zhanyu Ma, Qie Sun, Hongyi Yin, and Ronald Wennersten. "Prediction of short-term PV power output and uncertainty analysis." *Applied energy*, **228**:700–711, 2018.

[MGT14] W. J. Ma, V. Gupta, and U. Topcu. "On distributed charging control of electric vehicles with power network capacity constraints." In *American control conference*, pp. 4306–4311, Portland, OR, 2014. IEEE.

[MJL18] Trieu T Mai, Paige Jadun, Jeffrey S Logan, Colin A McMillan, Matteo Muratori, Daniel C Steinberg, Laura J Vimmerstedt, Benjamin Haley, Ryan Jones, and Brent Nelson. "Electrification Futures Study: Scenarios of Electric Technology Adoption and Power Consumption for the United States." Technical report, National Renewable Energy Lab.(NREL), Golden, CO (United States), 2018.

[MML19] Maryam Mohiti, Hassan Monsef, and Hamid Lesani. "A decentralized robust model for coordinated operation of smart distribution network and electric vehicle aggregators." *International Journal of Electrical Power & Energy Systems*, **104**:853 – 867, 2019.

[MQC15] M. Majidpour, C. Qiu, P. Chu, R. Gadh, and H. R. Pota. "Fast Prediction for Sparse Time Series: Demand Forecast of EV Charging Stations for Cell Phone Applications." *IEEE Transactions on Industrial Informatics*, **11**(1):242–250, Feb 2015.

[MSF13] S. J. Moura, J. L. Stein, and H. K. Fathy. "Battery-Health Conscious Power Management in Plug-In Hybrid Electric Vehicles via Electrochemical Modeling and Stochastic Control." *IEEE Transactions on Control Systems Technology*, **21**(3):679–694, May 2013.

[MSK18] R. Mehta, D. Srinivasan, A. M. Khambadkone, J. Yang, and A. Trivedi. "Smart Charging Strategies for Optimal Integration of Plug-In Electric Vehicles Within Existing Distribution System Infrastructure." *IEEE Transactions on Smart Grid*, **9**(1):299–312, Jan 2018.

[MVS19] R. Mehta, P. Verma, D. Srinivasan, and Jing Yang. "Double-layered intelligent energy management for optimal integration of plug-in electric vehicles into distribution systems." *Applied Energy*, **233-234**:146 – 155, 2019.

[MZL15] Z Ma, S Zou, and X Liu. "A Distributed Charging Coordination for Large-Scale Plug-In Electric Vehicles Considering Battery Degradation Cost." *IEEE Transactions on Control Systems Technology*, **23**(5):2044–2052, 2015.

[NRF93] M Noia, CF Ratto, and R Festa. "Solar irradiance estimation from geostationary satellite data: I. Statistical models." *Solar Energy*, **51**(6):449–456, 1993.

[PGM18] Alvaro Perez-Diaz, Enrico Gerding, and Frank McGroarty. "Coordination and payment mechanisms for electric vehicle aggregators." *Applied Energy*, **212**:185 – 195, 2018.

[PZL17] Chao Peng, Jianxiao Zou, Lian Lian, and Liying Li. "An optimal dispatching strategy for V2G aggregator participating in supplementary frequency regulation considering EV driving demand and aggregator's benefits." *Applied Energy*, **190**:591 – 599, 2017.

[QXS14] W Qi, Z Xu, Z M Shen, Z Hu, and Y Song. "Hierarchical Coordinated Control of Plug-in Electric Vehicles Charging in Multifamily Dwellings." *IEEE transactions smart grid*, **5**(3):1465–1474, 2014.

[RGJ17] J. Rivera, C. Goebel, and H. Jacobsen. "Distributed Convex Optimization for Electric Vehicle Aggregators." *IEEE Transactions on Smart Grid*, **8**(4):1852–1863, July 2017.

[RM09] James Blake Rawlings and David Q Mayne. *Model predictive control: Theory and design*. Nob Hill Pub. Madison, Wisconsin, 2009.

[SDR09] Alexander Shapiro, Darinka Dentcheva, and Andrzej Ruszczyński. *Lectures on stochastic programming: modeling and theory*. SIAM, 2009.

[SHM11] E. Sortomme, M. M. Hindi, S. D. J. MacPherson, and S. S. Venkata. "Coordinated Charging of Plug-In Hybrid Electric Vehicles to Minimize Distribution System Losses." *IEEE Transactions on Smart Grid*, **2**(1):198–205, March 2011.

[Sil86] B. W. Silverman. *Density estimation for statistics and data analysis*. CRC press, 1986.

[SK19] M. Shokri and H. Kebriaei. "Mean Field Optimal Energy Management of Plug-In Hybrid Electric Vehicles." *IEEE Transactions on Vehicular Technology*, **68**(1):113–120, Jan 2019.

[SKR18] Sobrina Sobri, Sam Koohi-Kamali, and Nasrudin Abd Rahim. "Solar photovoltaic generation forecasting methods: A review." *Energy Conversion and Management*, **156**:459–497, 2018.

[SMN17] Adella Santos, Nancy McGuckin, Hikari Yukiko Nakamoto, Danielle Gray, and Susan Liss. "Summary of travel trends: 2017 national household travel survey." Technical report, 2017.

[SSG18] Philipp Staudt, Marc Schmidt, Johannes Gärttner, and Christof Weinhardt. "A decentralized approach towards resolving transmission grid congestion in Germany using vehicle-to-grid technology." *Applied Energy*, **230**:1435 – 1446, 2018.

[STS19] Y. Shi, H. D. Tuan, A. V. Savkin, T. Q. Duong, and H. V. Poor. "Model Predictive Control for Smart Grids With Multiple Electric-Vehicle Charging Stations." *IEEE Transactions on Smart Grid*, **10**(2):2127–2136, March 2019.

[SWW16] C Shao, X Wang, X Wang, C Du, and B Wang. "Hierarchical Charge Control of Large Populations of EVs." *IEEE transactions smart grid*, **7**(2):1147–1155, 2016.

[TK18] M. A. Tajeddini and H. Kebriaei. "A Mean-Field Game Method for Decentralized Charging Coordination of a Large Population of Plug-in Electric Vehicles." *IEEE Systems Journal*, pp. 1–10, 2018.

[TZ17] W Tang and Y J Zhang. "A Model Predictive Control Approach for Low-Complexity Electric Vehicle Charging Scheduling: Optimality and Scalability." *IEEE transactions on power systems*, **32**(2):1050–1063, 2017.

[WAM19] Y. Wen, D. AlHakeem, P. Mandal, S. Chakraborty, Y. Wu, T. Senjyu, S. Paudyal, and T. Tseng. "Performance Evaluation of Probabilistic Methods Based on Bootstrap and Quantile Regression to Quantify PV Power Point Forecast Uncertainty." *IEEE Transactions on Neural Networks and Learning Systems*, pp. 1–11, 2019.

[WBP19] J. Wang, G. R. Bharati, S. Paudyal, O. Ceylan, B. P. Bhattarai, and K. S. Myers. "Coordinated Electric Vehicle Charging With Reactive Power Support to Distribution Grids." *IEEE Transactions on Industrial Informatics*, **15**(1):54–63, Jan 2019.

[WCC15] Joakim Widén, Nicole Carpman, Valeria Castellucci, David Lingfors, Jon Olauson, Flore Remouit, Mikael Bergkvist, Mårten Grabbe, and Rafael Waters. "Variability assessment and forecasting of renewables: A review for solar, wind, wave and tidal resources." *Renewable and Sustainable Energy Reviews*, **44**:356–375, 2015.

[WCL15] Jianhui Wang, Chen Chen, and Xiaonan Lu. "Guidelines for Implementing Advanced Distribution Management Systems-Requirements for DMS Integration with DERMS and Microgrids." Technical report, Argonne National Lab.(ANL), Argonne, IL (United States), 2015.

[WCT12] C Wen, J Chen, J Teng, and P Ting. "Decentralized Plug-in Electric Vehicle Charging Selection Algorithm in Power Systems." *IEEE transactions smart grid*, **3**(4):1779–1789, 2012.

[WHQ15] B. Wang, B. Hu, C. Qiu, P. Chu, and R. Gadh. "EV charging algorithm implementation with user price preference." In *2015 IEEE Power Energy Society Innovative Smart Grid Technologies Conference (ISGT)*, pp. 1–5, Feb 2015.

[WHW16] Bin Wang, Rui Huang, Yubo Wang, Hamidreza Nazaripouya, Charlie Qiu, Chi-Cheng Chu, and Rajit Gadh. "Predictive scheduling for Electric Vehicles considering uncertainty of load and user behaviors." In *IEEE/PES Transmission and Distribution Conference and Exposition (T&D)*, pp. 1–5, Dallas, TX, USA, May 2016.

[WSW17] Yubo Wang, Wenbo Shi, Bin Wang, Chi-Cheng Chu, and Rajit Gadh. "Optimal operation of stationary and mobile batteries in distribution grids." *Applied Energy*, **190**:1289 – 1301, 2017.

[WWN17] B. Wang, Y. Wang, H. Nazaripouya, C. Qiu, C. Chu, and R. Gadh. "Predictive Scheduling Framework for Electric Vehicles With Uncertainties of User Behaviors." *IEEE Internet of Things Journal*, **4**(1):52–63, Feb 2017.

[WYP17] Huaizhi Wang, Haiyan Yi, Jianchun Peng, Guibin Wang, Yitao Liu, Hui Jiang, and Wenxin Liu. "Deterministic and probabilistic forecasting of photovoltaic power based on deep convolutional neural network." *Energy conversion and management*, **153**:409–422, 2017.

[Xana] "Xanbus.".

[Xanb] "Xantrex.".

[XFG16] Zheng Xu, Mário AT Figueiredo, and Tom Goldstein. "Adaptive ADMM with spectral penalty parameter selection." *arXiv preprint arXiv:1605.07246*, 2016.

[XLL17] Yi Xu, Mingrui Liu, Qihang Lin, and Tianbao Yang. "ADMM without a fixed penalty parameter: faster convergence with new adaptive penalization." In *Advances in Neural Information Processing Systems*, pp. 1267–1277, 2017.

[XWC18] Yingqi Xiong, Bin Wang, Chi cheng Chu, and Rajit Gadh. "Vehicle grid integration for demand response with mixture user model and decentralized optimization." *Applied Energy*, **231**:481 – 493, 2018.

[XYF19] Shaolun Xu, Zheng Yan, Donghan Feng, and Xiaobo Zhao. "Decentralized charging control strategy of the electric vehicle aggregator based on augmented Lagrangian method." *International Journal of Electrical Power & Energy Systems*, **104**:673 – 679, 2019.

[XYX15] X. Xu, Z. Yan, and S. Xu. "Estimating wind speed probability distribution by diffusion-based kernel density method." *Electric Power Systems Research*, **121**:28–37, 2015.

[YJD18] Y. Yang, Q. Jia, G. Deconinck, X. Guan, Z. Qiu, and Z. Hu. "Distributed Coordination of EV Charging With Renewable Energy in a Microgrid of Buildings." *IEEE Transactions on Smart Grid*, **9**(6):6253–6264, Nov 2018.

[YZW13] W. Yao, J. Zhao, F. Wen, Y. Xue, and G. Ledwich. "A Hierarchical Decomposition Approach for Coordinated Dispatch of Plug-in Electric Vehicles." *IEEE Transactions on Power Systems*, **28**(3):2768–2778, Aug 2013.

[ZHM18] Suli Zou, Ian Hiskens, and Zhongjing Ma. "Consensus-based coordination of electric vehicle charging considering transformer hierarchy." *Control Engineering Practice*, **80**:138 – 145, 2018.

[ZKG17] L. Zhang, V. Kekatos, and G. B. Giannakis. "Scalable Electric Vehicle Charging Protocols." *IEEE Transactions on Power Systems*, **32**(2):1451–1462, March 2017.

[ZLL19] X. Zhang, Y. Li, S. Lu, H. F. Hamann, B. Hodge, and B. Lehman. "A Solar Time Based Analog Ensemble Method for Regional Solar Power Forecasting." *IEEE Transactions on Sustainable Energy*, **10**(1):268–279, Jan 2019.

[ZRF19] R. Zafar, J. Ravishankar, J. E. Fletcher, and H. R. Pota. "Optimal Dispatch of Battery Energy Storage System using Convex Relaxations in Unbalanced Distribution Grids." *IEEE Transactions on Industrial Informatics*, pp. 1–1, 2019.

[ZSS18] Yanchong Zheng, Yitong Shang, Ziyun Shao, and Linni Jian. "A novel real-time scheduling strategy with near-linear complexity for integrating large-scale electric vehicles into smart grid." *Applied Energy*, **217**:1 – 13, 2018.

[ZW15] Y. Zhang and J. Wang. "GEFCom2014 probabilistic solar power forecasting based on k-nearest neighbor and kernel density estimator." In *2015 IEEE Power Energy Society General Meeting*, pp. 1–5, July 2015.